Journal of Science & Technology in the Tropics

Volume 5 Number 1 June 2009

JOSTT

DEDICATED TO THE ADVANCEMENT OF SCIENCE AND TECHNOLOGY RELATED TO THE TROPICS

Journal of Science & Technology in the Tropics

AKADEMI SAINS MALAYSIA

COSTAM

Volume 5 Number 1
June 2009
ISSN 1823-5034

9 771823 503009

Journal of Science & Technology in the Tropics Volume 5 Number 1 June 2009

CONTENTS

Journal of Science and Technology in the Tropics (2009) **5**: 11-12

Neoscona vigilans (Arachnida: Araneae, Araneidae): a new record of orb-web spider from Peninsular Malaysia

Yong Hoi Sen
Institute of Biological Sciences, University of Malaya, 50603 Kuala Lumpur, Malaysia
(Email: yong@um.edu.my)

Received 08-02-2009; accepted 22-02-2009

Abstract A single female specimen of the Brown-legged Spider *Neoscona vigilans* (Blackwall, 1865) was collected in the University of Malaya campus on 20 July 2008. This orb-web spider is a new record for Peninsular Malaysia. It was found inside a rolled green leaf and does not appear to be common.

Keywords fauna – orb-web spider – *Neoscona vigilans* – Malaysia – new record

INTRODUCTION

There are some 40,700 species of spiders (Arachnida: Araneae) in the world, grouped into some 3733 genera in 109 families [1]. A recent count for Malaysia indicated 463 species in 181 genera and 42 families [2]. The actual number certainly far outnumbers this. For example, a new genus (*Malayozodaria*) and four new species (*Mallinella gombakensis*, *Mallinella maruyamai*, *Mallinella tunidifemoris* and *Malayozodaria hoiseni*) of the Family Zodariidae were recently added to Peninsular Malaysia [3]. New records of jumping spiders (Family Salticidae) have also been reported [4]. Indeed many specimens at hand are believed to be unnamed species or new records [4-6]. This paper reports a new record of orb-web spider (*Neoscona vigilans*) for Peninsular Malaysia.

MATERIALS AND METHODS

In the course of a long-term study of the fauna of the University of Malaya campus, spiders were observed, photographed and collected when needed for further taxonomic confirmation. On 20 July 2008, a female orb-web spider was sighted inside a rolled green leaf at the upper part of a shrub by the drain next to a building of the Institute of Biological Sciences. It was collected and brought back to the lab for identification and observation. The specimen was identified with existing literature [e.g. 7].

RESULTS AND DISCUSSION

The single female specimen (Figs. 1-3) found in the University of Malaya campus was *Neoscona vigilans* (Blackwall, 1865). It is known commonly as the Brown-legged Spider. When first described, it was named as *Epeira vigilans* Blackwall, 1865. It has not been recorded in Malaysia [1, 2, 7, 8]. Its distribution has been reported to be Africa to Philippines and New Guinea [1]. More specifically, it has been recorded in Singapore in addition to India, Sri Lanka, Pakistan, Myanmar, Hong Kong, Southern Japan, Indonesia, and Papua New Guinea [7]. In earlier literature it was referred to as *Neoscona rufofemorata* (Simon, 1884) [1, 7].

Female *N. vigilans* measures 12-18 mm, the male 9-11 mm [7]. The spider is brownish in colour. Dorsally the abdomen is generally patterned with light and dark markings but it may be uniformly darkish brown. Ventrally the abdomen of the specimen at hand has paired pale yellow spots (Fig. 3). The legs are marked with dark and paler bands.

During the day, this orb-web spider hides in a rolled or curled green leaf. It does not appear to be common as several attempts to look for it in various places have been unsuccessful. Its habitat has been reported to be "trees and scrubs in shady parts of garden, waste-land and secondary forests", and the egg-sacs are woolly in appearance [7].

Members of the Family Araneidae Dahl, 1912 are small to large orb-web spiders, measuring 3-30 mm.

It is a large family comprising some 2985 species in 167 genera worldwide [1]. The genus *Neoscona* Simon, 1864 is represented by about 91 species [1]. Members of the genus have a longitudinal thoracic groove in the cephalothorax.

Figure 1. Female *Neoscona vigilans* on its day-time abode (exposed).

Figure 2. Female *Neoscona vigilans* from University of Malaya campus.

Figure 3. Ventral view of female *Neoscona vigilans* showing characteristic spots on the abdomen.

In Malaysia, only one species *Neoscona theisi triangulifera* (Thorell, 1878) has been explicitly stated to be present [8]. This spider has been observed and photographed in Clearwater Sanctuary, Perak, Peninsular Malaysia on 11 April 2001, and more recently (January 2009) in Bukit Rengit, Pahang. It constructs a usual orb-web.

Four species of *Neoscona* have been recorded in neighbouring Singapore – *N. bengalensis* Tikader & Bal, 1981; *N. nautica* (L. Koch, 1875); *N. punctigera* (Doleschall, 1857); and *N. vigilans* [2]. Of these, *N. nautica* has a cosmotropical distribution [1] and has been observed in the University of Malaya campus (22 December 2002). As *N. vigilans* has been found in Peninsular Malaysia, the occurrence of *N. bengalensis* and *N. punctigera* in this country is to be expected. Likewise, the possibility of finding *N. theisi* (Walckenaer, 1841) in Singapore should be fairly good.

REFERENCES

1. Platnick N.I. (2009) *The world spider catalog, version 9.5*. American Museum of Natural History, online at http:/research.amnh.org/entomology/spiders/catalog/index.html.
2. Song D.X., Zhang J.X. and Li D. (2002) A checklist of spiders from Singapore (Arachnida: Araneae). *Raffles Bulletin of Zoology* **50**: 359-388.
3. Ono H. and Hashim R. (2008) Four new species of the Family Zodariidae (Araneae) from Malaysia. *Memoirs of the National Museum of Nature and Science, Tokyo* (45): 41-51.
4. Yong H.S. (2008) *Telamonia dimidiata* and *Phintella versicolor* (Arachnida: Salticidae): two new records for Peninsular Malaysia. *Journal of Science and Technology in the Tropics* **4**: 97-98.
5. Yong H.S. (1998) Spiders. In Yong H.S. (Ed.) *The Encyclopedia of Malaysia Vol. 3 Animals* pp 94-95. Editions Didier Millet, Singapore.
6. Yong H.S. (2004) Arachnida: Araneae. In Yule C.M. and Yong H.S. (Eds.) *Freshwater Invertebrates of the Malaysian Region*. Academy of Sciences Malaysia, Kuala Lumpur.
7. Koh J.K.H. (1989) *A guide to common Singapore spiders*. Singapore Science Centre, Singapore.
8. Murphy F. and Murphy J. (2000) *An introduction to the spiders of South East Asia*. Malaysian Nature Society, Kuala Lumpur.

Journal of Science and Technology in the Tropics (2009) **5**: 13-17

Effective and maximum quantum yield of the lace coral *Pocillopora damicornis* (Anthozoa: Scleractinia: Pocilloporidae) in Pulau Tioman, Malaysia

Kee Alfian Abdul Adzis[1], Affendi Yang Amri[2], Jamie Oliver[3] and Che Abd. Rahim Mohamed[1]
[1]Marine Ecosystem Research Centre (EKOMAR), Faculty of Science & Technology,
National University of Malaysia, 43000 Bangi, Selangor D.E., Malaysia
(Email: alfian@ukm.My / keealf@hotmail,com)
[2]Institute of Biological Sciences, Faculty of Science, University of Malaya,
50603 Kuala Lumpur, Malaysia
[3]The World Fish Centre, Jalan Batu Maung, 11960 Bayan Lepas, Penang, Malaysia

Received 18-03-2009; accepted 02-04-2009

Abstract Effective and Maximum quantum yield is important in assessing the photosynthetic ability of the lace coral *Pocillopora damicornis*. The changes of its photosynthetic ability can reflect its current health status. A pulse amplitude modulation (PAM) chlorophyll fluorescence technique was used and measurements were taken *in situ* and in real time using a submersible PAM fluorometer or Diving-PAM. Two colonies of *P. damicornis* were chosen and their effective quantum yield (light-adapted) ($\Delta F/F_m$) was measured for 21 days with an average yield value of 0.70±0.05 and 0.72±0.03 for colony 1 and 2 respectively. Maximum quantum yield (dark-adapted) (F_v/F_m) reading was taken at dawn between 06:00-07:00 hour with an average yield value of 0.70±0.02 for each colony. The diurnal variation showed that *P. damicornis* was most vulnerable during noontime. Under 'normal' conditions, the light and dark adapted corals gave almost similar yield values. This information could be used as the baseline standard of *P. damicornis* yield value in its 'normal' state in Pulau Tioman and generally for the east coast of Peninsular Malaysia.

Keywords effective quantum yield – maximum quantum yield – *Pocillopora damicornis* – Diving-PAM – Pulau Tioman

INTRODUCTION

Corals contain symbiotic, unicellular dinoflagellate microalgae which are known as zooxanthellae. They are responsible for converting light energy into chemical energy that is used for CO_2 fixation and other assimilatory reactions. The process is also known as photosynthesis [1]. These dinoflagellates provide an energy source for the coral host but this symbiosis relationship is highly susceptible to extreme environmental condition changes [1]. The photosynthetic ability of the corals has been used for assessing changes of its physiology process in a stressful environment [2-6]. It has also been used to assess the health of the corals towards introduced foreign substances in the coral reef environment [7-10].

The lace coral *Pocillopora damicornis* (Linnaeus) forms an integral part of the coral reef ecosystems in the Indo-Pacific region and it is known to provide essential habitat for a range of fishes and invertebrates [10]. It is one of the dominant species in the shallower waters in Pulau Tioman [11] which is the focused area of most recreational activities (SCUBA diving and Snorkeling). Therefore it is exposed to potential physical damage from unsupervised recreational activities. *In situ* photosynthetic performance of *P. damicornis* is a potential indicator to help assess the current condition of the waters around Malaysia's coral reefs as it is one of the dominant species and also has been widely used globally for ecotoxicology experiments.

At present there is no known baseline standard for the effective and maximum quantum photosynthetic yield of any scleractinian coral in a 'normal' state in Malaysian waters. This is extremely important to document so that we can monitor any changes due to stress events in the future.

METHODOLOGY

The *in-situ* photosynthetic yield value of *P. damicornis* (Fig.1) was measured in waters with depths ranging from 8-10 meters. Two colonies of *P. damicornis* (Fig. 2) of similar size 30cm diameter in similar environment states with natural light and temperature regimes were chosen. The measurements were all taken whilst SCUBA diving. Due to the *in-situ* and real time measurements needed, the colonies that were chosen were located off the beach of the Pulau Tioman Marine Park Centre in Tg Mesoh. Therefore they were logistically accessible throughout the day, especially for diurnal data measurements. Measurements of the photosynthetic capacity of the coral tissue were performed by using a submersible pulse amplitude modulator (PAM) or Diving-PAM (Walz, Germany) with a 1.5 m acrylic fibre optic cable (Fig. 3).

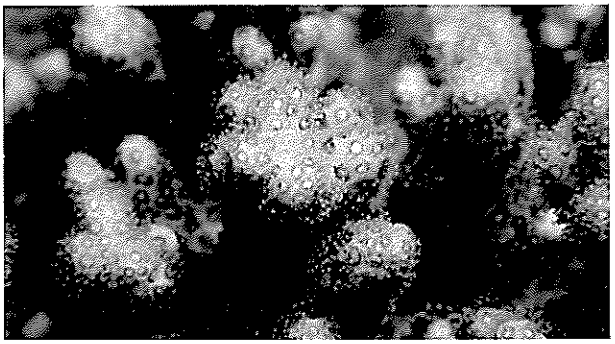

Figure 1. The lace coral *Pocillopora damicornis* in Pulau Tioman, Pahang, Malaysia. The coral tentacles are extended and feeding.

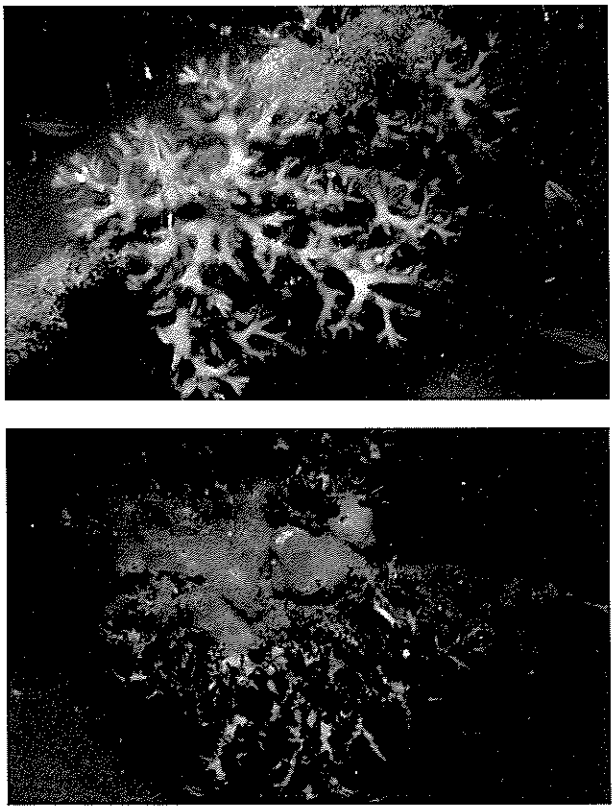

Figure 2. Colony 1 (top) and colony 2 (bottom) of *Pocillopora damicornis* in similar environment, depth (9-12 m) and size (30 cm diameter).

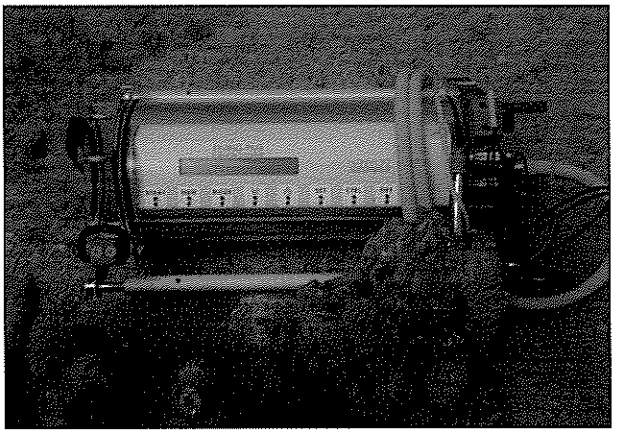

Figure 3. The submersible pulse modulator (PAM) or Diving-PAM (Walz, Germany) used for photosynthetic measurements of coral colony.

Effective Quantum Yield (Light Adapted)

To obtain effective quantum yield readings, *P. damicornis* maximum fluorescence (F_m) was measured using a saturating light pulse (0.8 s, >2000 µmol quanta $m^{-2}s^{-1}$), and the changes in fluorescence ($\Delta F = F_m - F_o$) was then used to calculate effective quantum yield ($\Delta F/F_m$) for light-adapted corals [7]. This reading was taken for 21 days between 1000-1200 hours, and each daily reading is a mean value of eight replicates.

Statistical analysis was done using Microsoft Excel software with data analysis toolpack and ANOVA test was conducted to determine the significant difference between sets of data.

Maximum Quantum Yield (Dark-adapted)

For dark-adapted measurements, the effective quantum yield is the same as the maximum quantum yield ($F_m - F_o/F_m = F_v/F_m$). To obtain maximum quantum yield, the colonies needed to be dark-adapted and measurements were only taken at dawn between 0600-0700 hours to allow maximum recovery of the photosystem and an optimum reading could be recorded. This reading was taken for 9 days, and each daily reading is a mean value of eight replicates.

Diurnal Photosynthetic Performance

Diurnal variations in photosynthetic performance of its effective quantum yield ($\Delta F/F_m$) were also measured over three days (as replicates) for each colony at 0600, 0900, 1200, 1500 and 1800 hours. Concurrently photosynthetic active radiation (PAR) adjacent to the coral colonies were measured using the micro-quantum sensor on the Diving PAM.

RESULTS AND DISCUSSION

The effective and maximum potential yield of *P. damicornis*

The average (n=21days) effective quantum yield value ($\Delta F/F_m$) of *P. damicornis* was 0.70±0.05 and 0.72±0.03 for colony 1 and 2 respectively (ANOVA $p>0.05$; Table 1). The average (n=9days) maximum potential quantum yield value (F_v/F_m) for these colonies was 0.70±0.02 and 0.70±0.02 respectively (ANOVA $p>0.05$; Table 1). The yield value recorded is considered the first documented measurement for Malaysia, and it is higher compared to the yield value reported by Winters [12] of 0.40-0.50 in Red Sea and Ralph [6] of 0.40-0.60 in Heron Island Lagoon, Australia of the same species. It is important to understand and know the yield value in 'normal' conditions; a stressful change in many environmental conditions has been shown to reduce both the effective and maximum quantum yields [2-6], and it is also used to assess stressful levels of introduced substances to the corals [7-9]. Therefore, the data from this study can be used as the standard value for photosynthetic capacity of *P. damicornis* and also to be used as comparison to assess the health of *P. damicornis* in Malaysian waters.

The effective quantum yield diurnal cycle of *P. damicornis*

P. damicornis showed a significant diurnal variation for both colonies with the highest value at 0900 hours (ANOVA $p<0.05$; Fig. 4a). With the start of photosynthetic active radiation (PAR) light penetration, a pronounced noontime depression of ($\Delta F/F_m$) was observed for both colonies (Fig. 4a) when the highest PAR intensity were recorded at noontime (Fig. 4b). It was later followed by a gradual rise towards dusk and recovering to almost the initial values at 1800 hrs (Fig. 4a). The data showed that *P. damicornis* is at its weakest photosynthetic condition between 1200–1500 hours (Fig. 4a). Any further stress inflicted to *P. damicornis* during this time period could be more damaging. It is known that recreational activities such as SCUBA diving and snorkeling contribute to the increase of injured corals [13-15]. According to Toda [15], the coral coverage for Pulau Tioman is only 30% and the low percentage is contributed to the increase and unsupervised recreational SCUBA and snorkeling activities. Unfortunately, the peak hour for tourist activities is between 1100-1600 hours (personal observation). This observation supports the report by Toda [15] that recreational activities on the reef could be the main factor in coral cover decline in Pulau Tioman. With this knowledge, a proper time management plan on tourist activities on certain reefs in order to minimise stress and damage shall be proposed to the Marine Parks Department of Malaysia.

CONCLUSION

The present findings offer the baseline data for effective and maximum quantum yield of *P. damicornis*, especially for Pulau Tioman and generally for the east coast of Peninsular Malaysia. The diurnal

variations gave an insight to the vulnerability period of *P. damicornis* during 1200-1500 hours, which potentially could help managers of the Marine Parks Department to further improve the existing time management plans for tourist activities.

Acknowledgement – This study was funded by Science Fund Grant: 04-01-02-8F0117 to Che Abd. Rahim Mohamed. The authors would like to acknowledge the Marine Park Department, Malaysia for logistics support. We acknowledge the volunteer and diving assistance provided by '*SEABUDS*'.

Table 1. Differences between the effective quantum yield (light-adapted) ($\Delta F/F_m$) and maximum potential quantum yield (dark-adapted) (F_v/F_m) of *Pocillopora damicornis* – standard deviations in parenthesis.

P. damicornis colony	Colony 1	Colony 2
Type of quantum yield process		
Light-adapted (n = 21 days)	0.67(0.06)	0.72(0.08)
	0.69(0.04)	0.72(0.05)
	0.73(0.03)	0.74(0.04)
	0.66(0.06)	0.67(0.07)
	0.68(0.04)	0.71(0.06)
	0.65(0.06)	0.66(0.06)
	0.68(0.05)	0.73(0.05)
	0.72(0.06)	0.74(0.08)
	0.74(0.05)	0.75(0.05)
	0.61(0.06)	0.67(0.06)
	0.67(0.03)	0.67(0.05)
	0.77(0.04)	0.74(0.05)
	0.76(0.04)	0.74(0.04)
	0.72(0.05)	0.76(0.04)
	0.77(0.03)	0.77(0.05)
	0.74(0.05)	0.75(0.05)
	0.65(0.05)	0.69(0.08)
	0.74(0.03)	0.74(0.03)
	0.67(0.05)	0.70(0.06)
	0.65(0.04)	0.66(0.04)
	0.75(0.06)	0.71(0.04)
	X = 0.70(0.05)	x = 0.72(0.03)
Dark-adapted (Colony 1, n = 9 days; Colony 2, n = 8 days)	0.68((0.03)	0.72(0.03)
	0.71(0.03)	0.71(0.02)
	0.70(0.01)	0.70(0.02)
	0.71(0.02)	0.67(0.02)
	0.67(0.02)	0.70(0.02)
	0.70(0.01)	0.69(0.04)
	0.70(0.02)	0.70(0.01)
	0.71(0.01)	0.71(0.01)
	0.71(0.01)	
	x = 0.70(0.02)	x = 0.70(0.02)

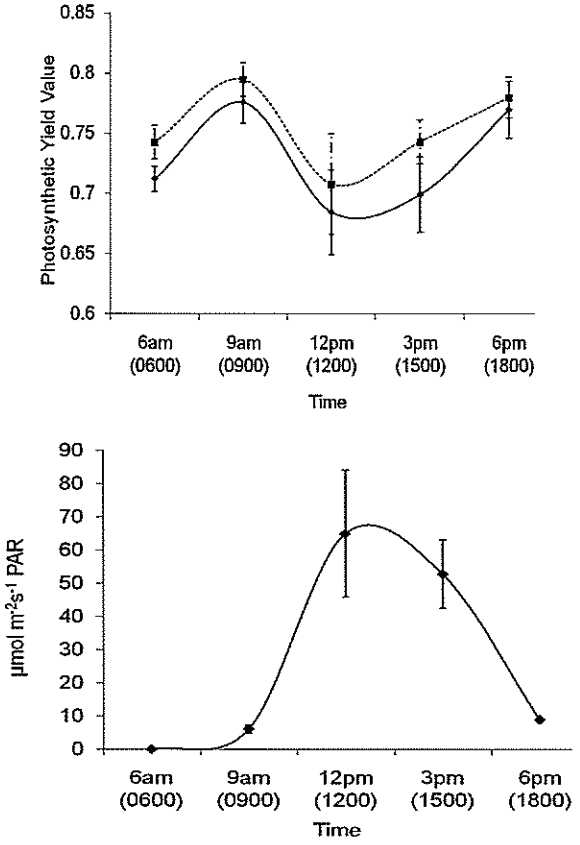

Figure 4. Diurnal measurements for three consecutive days of two colonies of *Pocillopora damicornis*. *Top*: effective quantum yield ($\Delta F/F_m$), -♦- colony 1, -■- colony 2; *Bottom*: PAR measurements.

REFERENCES

1. Hill R., Frankart C. and Ralph P.J. (2005) Impact of bleaching conditions on the components of non-photochemical quenching in the zooxanthellae of a coral. *J. Exp. Mar. Biol. Ecol.* **322**: 83-92.
2. Flores-Ramirez L.A. and Linán-Cabello M.A. (2007) Relationships among thermal stress, bleaching and oxidative damage in the hermatypic coral, *Pocillopora capitata*. *Comp. Biochem. Physiol.* **146C**: 194-202.
3. Hill R., Larkum A.W.D., Frankart C., Kühl M. and Ralph P.J. (2004) Loss of functional Photosystem II reaction centres in zooxanthellae of corals exposed to bleaching conditions: using fluorescence rise kinetics. *Photosynthesis Res.* **82**: 59-72.
4. Jones R.J. (2004) Testing the 'photoinhibition' model of coral bleaching using chemical inhibitors. *Mar. Ecol. Prog. Ser.* **284**: 133-145.
5. Jones R.J., Kildea T. and Hoegh-Guldberg O. (1999) PAM chlorophyll fluorometry: a new in situ technique for stress assessment in scleractinian corals, used to examine the effects of cyanice from cyanice fishing. *Mar. Pollution Bull.* **38**(10): 864-874.
6. Ralph P.J., Larkum A.W.D. and Kühl M. (2005) Temporal patterns in effective quantum yield of individual zooxanthellae expelled during bleaching. *J. Exp. Mar. Biol. Ecol.* **316**: 17-28.
7. Jones R.J., Hoegh-Guldberg O., Larkum A.W.D. and Schreiber U. (1998) Temperature-induced bleaching of corals begins with impairment of the CO_2 fixation mechanism in zooxanthellae. *Plant Cell Environm.* **21**: 1219-1230.
8. Cervino J.M., Hayes R.L., Honovich M., Goreau T.J., Jones S. and Rubec P.J. (2003) Changes in zooxanthellae density, morphology, and mitotic index in hermatypic corals and anemones exposed to cyanide. *Mar. Pollution Bull.* **46**: 573-586.
9. Jones R.J., Ward S., Amri A.Y. and Hoegh-Guldberg O. (2000) Changes in quantum efficiency of Photosystem II of symbiotic dinoflagellates of corals after heat stress, and of bleached corals sampled after the 1998 Great Barrier Reef mass bleaching event. *Mar. Freshwater Res.* **51**: 63-71.
10. Frisch A.J., Ulstrup K.E. and Hobbs J-P.A. (2007) The effects of clove oil on coral: An experimental evaluation using *Pocillopora damicornis* (Linnaeus). *J. Exp. Mar. Biol. Ecol.* **345**: 101-109.
11. Affendi Y.A., Badrul H.T., Lee Y.L., Kee Alfian A.A. and Yusri Y. (2005) Scleractinian coral diversity of Kg. Tekek, Pulau Tioman Marine Park. *Proc. Second Regional Symposium on Environment and Natural Resources, 22-23 March 2005, Kuala Lumpur,* Pp. 20-31.
12. Winters G., Loya Y. and Beer S. (2006) *In situ* measured seasonal variations in F_v/F_m of two common Red Sea corals. *Coral Reefs* **25**: 593-598.
13. Tratalos J.A. and Austin T.J. (2001) Impacts of recreational SCUBA diving on coral communities of the Caribbean island of Grand Cayman. *Biol. Conserv.* **102**: 67-75.
14. Zakai D. and Chadwick-Furman N.E. (2002) Impacts of intensive recreational diving on reef corals at Eilat, northern Red Sea. *Biol. Conserv.* **105**: 179-187.
15. Toda T., Okashita T., Maekawa T., Kee Alfian B.A.A., Mohd. Rajuddin M.K., Nakajima R., Chen W., Takahashi K.T., Othman B.H.R. and Terazaki M. (2007) Community structures of coral reefs around Peninsular Malaysia. *J. Oceanogr.* **63**: 113-123.

Journal of Science and Technology in the Tropics (2009) **5**: 19-21

Nephila antipodiana (Araneae: Nephilidae) from Pahang: a new record for Peninsular Malaysia

Yong Hoi Sen
IKIP International College, 25050 Kuantan, Pahang, Malaysia
Institute of Biological Sciences Malaysia, University of Malaya, 50603 Kuala Lumpur, Malaysia
(E-mail: yong@um.edu.my)

Received 9-3-2009; accepted 3-4-2009

Abstract *Nephila antipodiana* (Batik Golden Web Spider) of the family Nephilidae was found in Teluk Chempedak, Pahang. A single specimen was observed at the forest edge fronting the shore. This constitutes a new record for Peninsular Malaysia. The coloration of the legs and palp as well as the dorsal base colour of the abdomen in the specimen from Teluk Cempedak differs from the 'typical' (commonly reported) form of *N. antipodiana*.

Keywords golden web spider – *Nephila antipodiana* – new record – colour variation – Arachnida

INTRODUCTION

Spiders of the genus *Nephila* Leach 1815 have been previously classified under the family Araneidae and then Tetragnathidae. The genus is now placed in Nephelidae Simon 1894 [1-3]. According to the present classification there are four genera in Nephilidae. Excepting *Clitaetra* Simon 1889, the other three genera – *Herennia* Thorell 1877, *Nephila* and *Nephilengys* L. Koch 1872 – are present in Malaysia. The genus *Nephila* is represented by some 16-22 species in the world. Only two species – *N. kuhlii* Doleschall 1859 and *N. pilipes* (Fabricius 1793) – appear to have been recorded in Malaysia [4]. The present paper reports the occurrence of the Batik (or Asian) Golden Web Spider *Nephila antipodiana* (Walckenaer 1842) in Peninsular Malaysia.

MATERIALS AND METHODS

In the course of duties over the years at IKIP International College, Kuantan, Pahang, I always took the opportunity to visit Teluk Chempedak for observations on natural history and biodiversity. Recently on 28 February 2009, a female Batik Golden Web Spider *N. antipodiana* was sighted at the forest edge fronting the sea shore. This spider was photographed and later confirmed with existing literature [5, 6].

RESULTS AND DISCUSSION

The specimen (Fig. 1) seen at Teluk Chempedak differed from 'typical' (commonly reported) *N. antipodiana* (Fig. 2) in coloration and pattern. The typical form has uniformly black to dark reddish brown cephalothorax; black labium; black chelicerae; black legs; yellow abdomen with six pairs of subovate yellow spots dorsally arranged longitudinally in rows, each spot with a thin black margin; anterior end of abdomen black, posterior end slightly tubercle-like; laterals with five or six yellow spots; and venter black with three transverse chalk-white stripes [5].

A striking difference in the specimen from Teluk Chempedak is the coloration of the legs. Instead of uniformly black [5, 6], the legs are reddish (reddish brown) with black bands. The dorsal base colour of the abdomen is reddish brown, not yellow. In addition the palp is reddish brown instead of black. The pattern on the venter (Fig. 3) is however similar to 'typical' *N. antipodiana*.

Reddish legs and reddish brown dorsal base colour of the abdomen have also been observed in a specimen in Singapore (Fig. 4). This indicates

JOURNAL OF SCIENCE AND TECHNOLOGY IN THE TROPICS

NOTICE TO CONTRIBUTORS

JOSTT is a multi-disciplinary journal. It publishes original research articles and reviews on all aspects of science and technology relating to the tropics. All manuscripts are reviewed by at least two referees, and the editorial decision is based on their evaluations.

Manuscripts are considered on the understanding that their contents have not been previously published, and they are not being considered for publication elsewhere. The authors are presumed to have obtained approval from the responsible authorities, and agreement from all parties involved, for the work to be published.

Submission of a manuscript to JOSTT carries with it the assignment of rights to publish the work. Upon publication, the Publishers (COSTAM and ASM) retain the copyright of the paper.

Manuscript preparation

Manuscript must be in English, normally not exceeding 3500 words. Type double spaced, using MS Word, on one side only of A4 size with at least 2.5 cm marigins all round. Number the pages consecutively and arrange the items in the following order: title page, abstract, key words, text, acknowledgements, references, tables, figure legends.

Title page

Include (i) title, (ii) names, affiliations and addresses of all authors, (iii) running title not exceeding five words, and (iv) email of corresponding author.

Abstract and key words

The abstract, not more than 250 words, should be concise and informative of the contents and conclusions of the work. A list of not more than five key words must immediately follow the abstract.

Text

Original research articles should be organized as follows: Introduction, Materials and Methods, Results, Discussion, Acknowledgement, References. The International System of Units (SI) should be used. Scientific names and mathematical parameters should be in italics.

References

References should be cited in the text as numbers enclosed with square [] brackets. The use of names in the text is discouraged. In the references section, the following examples should be followed:

1 Yong H.S., Dhaliwal S.S. and teh K.L (1989) A female Norway rat, *Rattus norvegicus*, with XO sex chromosome constitution. *Naturwissenschaften* **76**: 387-388.

2 Beveridge W.I.B. (1961) *The Art of Scientific Investigation*. Mercury Book, London.

3 Berryman A.A. (1987) The theory and classification of outbreaks. In Barbosa P. and Schultz J.C. (eds.) *Insect outbreaks* pp. 3-30. Academic Press, San Diego.

Tables

Tables should be typed on separate sheets with short, informative captions, double spacing, numbered consecutively with Arabic numerals, and do not contain any vertical lines. A table should be set up to fit into the text area of at most the entire page of the Journal.

Illustrations

Black-and-white figures (line drawings, graphs and photographs) must be suitable for high-quality reproduction. They must be no bigger than the printed page, kept to a minimum, and numbered consecutively with Arabic numerals. Legends to figures must be typed on a separate sheet. Colour illustrations can only be included at the author's expense.

Proofs and reprints

Authors will receive proofs of their papers before publication. Ten reprints of each paper will be provided free of charge.

Submission

Manuscripts should be submitted in triplicate (including all figures but not original artwork), together with a floppy diskette version of the text, to:

The Chief Editor
Journal of Science and Technology in the Tropics
C-3A-10, 4th Floor Block C, Lift No: 5
No. 1 Jalan SS20/27
47400 Petaling Jaya
Selangor Darul Ehsan
Malaysia

the possible occurrence of polymorphism. How widespread and the extent of polymorphism need to be studied. In addition to coloration, the effect of age and the variability of the number of yellow spots on the abdomen will also yield fruitful investigation.

Nephila antipodiana was originally described as *Epeira antipodiana* Walckenaer 1842. It is distributed in China, Philippines to New Guinea, Solomon Is., and Queensland [1]. In Southeast Asia it has been recorded in Singapore, Indonesia, Thailand and the Philippines [5-7]. The presence of this spider in Peninsular Malaysia is therefore not totally unexpected. Indeed its occurrence in Borneo is to be anticipated.

In Singapore the Red Silver Spider *Argyrodes flavescens* (Pickard-Cambridge 1880) has been observed to inhabit the web of *N. antipodiana* (Yong, unpublished data). This comb-footed spider (Theridiidae) has been reported to inhabit the web of *N. pilipes* [6]. Another species *Argyrodes argentatus* Pickard-Cambridge 1880 (Silver Comb-footed Spider) also lives in the web of *N. antipodiana* [6]. Both *A. flavescens* and *A. argentatus* have been observed to inhabit the web of *Nephila* spiders in Peninsular Malaysia (unpublished data).

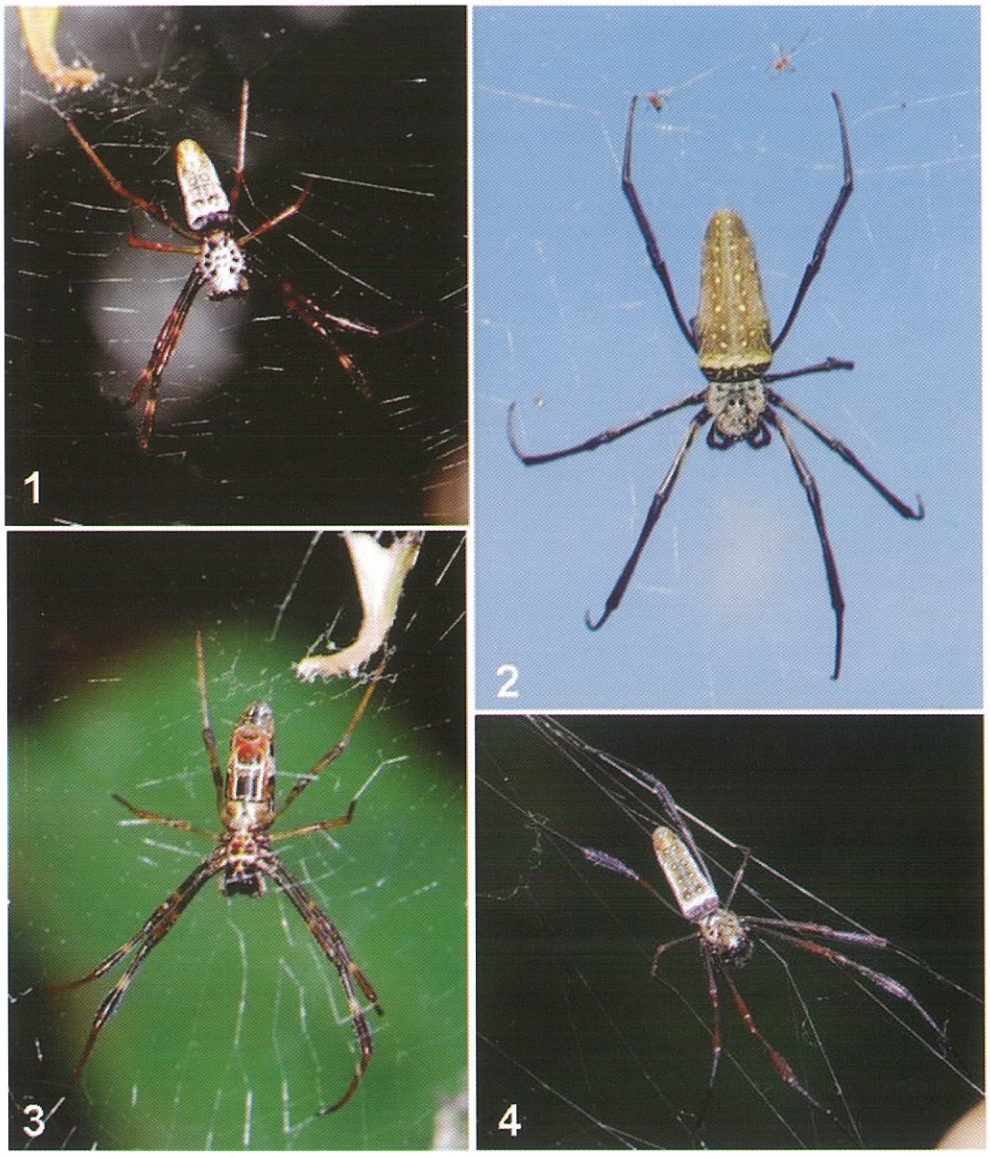

Figure 1. Female *Nephila antipodiana* from Teluk Chempedak, Pahang, Peninsular Malaysia.
Figure 2. Female *N. antipodiana* with black legs and 'typical' colour pattern on the dorsum of abdomen.
Figure 3. Venter of female *Nephila antipodiana* from Teluk Chempedak, Pahang, Peninsular Malaysia.
Figure 4. Female *Nephila antipodiana* with reddish brown legs and dorsal base colour of the abdomen from Singapore.

REFERENCES

1. Platnick N.I. (2009) *The world spider catalog, version 9.5*. American Museum of Natural History, online at http:/research.amnh.org/entomology/spiders/catalog/index.html.
2. Kuntner M. (2006) Phylogenetic systematics of the Gondwanan nephilid spider lineage Clitaetrinae (Araneae, Nephilidae). *Zoologica Scripta* **35**: 19-62.
3. Harvey M.S., Austin A.D. and Adams M. (2007) The systematics and biology of the spider genus *Nephila* (Araneae: Nephilidae) in the Australasian region. *Invertebrate Systematics* **21**: 407-451.
4. Murphy F. and Murphy J. (2000) *An introduction to the spiders of South East Asia*. Malaysian Nature Society, Kuala Lumpur.
5. Barrion A.T. and Litsinger J.A. (1995) *Riceland spiders of South and Southeast Asia*. CAB International, Wallingford, UK.
6. Koh J.K.H. (1989) *A guide to common Singapore spiders*. Singapore Science Centre, Singapore.
7. Song D.X., Zhang J.X. and Li D. (2002) A checklist of spiders from Singapore (Arachnida: Araneae). *The Raffles Bulletin of Zoology* **50**: 359-388.

Journal of Science and Technology in the Tropics (2009) **5**: 23-33

Diversity of bacteria associated with the benthic marine dinoflagellates *Coolia monotis* and *Ostreopsis ovata* from Malaysian waters

Wong Weng Ruh[1*], Asmat Ahmad[2], Mohd Noor Mat Isa[3], Nor Muhammad Mahadi[2,3], Noor Asyikin Marasan[1] and Gires Usup[1]

[1]School of Environmental and Natural Resource Sciences, [2]School of Biosciences and Biotechnology, Faculty of Science and Technology, Universiti Kebangsaan Malaysia,
43600 Bangi, Selangor, Malaysia
[3]Malaysia Genome Institute, UKM-MTDC Smart Technology Centre,
43600 Bangi, Selangor, Malaysia
(*Email: wengruh@Yahoo.com)

Received 20-04-2009; accepted 22-04-2009

Abstract The diversity of bacteria in two clonal cultures of the marine benthic dinoflagellates *Coolia monotis* and *Ostreopsis ovata* were assessed using molecular and culturing methods. Two 16S rDNA libraries were constructed from the directly amplified genomic DNA of bacteria associated with these dinoflagellates. Selective clones from different RFLP group were sequenced and analyzed. A total of 36 phylotypes was obtained from the directly amplified DNA of both cultures, and nine bacterial isolates were cultured from the *C. monotis* culture. A total of 205 sequences was obtained from the 16S rDNA libraries and these could be assigned to the taxa α-proteobacteria (44%), γ-proteobacteria (27%), Cytophaga-Flavobacteria-Bacteroides (27%) and others (2%). The occurrence of common phylotypes between the two dinoflagellate cultures suggested species specification in the bacteria-dinoflagellate association. Only four culturable bacteria isolates were found in the metagenome 16S rDNA sequences of *C. monotis* culture. Culture-independent method is necessary to capture the full diversity of these associated bacteria since a large percentage (44%) of uncultured bacteria sequences were obtained.

Keywords benthic dinoflagellate – bacterial diversity – 16S rRNA sequence analysis –dinoflagellate-culture associated bacteria

INTRODUCTION

Coolia monotis and *Ostreopsis ovata* are epiphytic dinoflagellates living on macroalgae, mostly found in tropical and subtropical seas. These dinoflagellates are usually found together with other epiphytic dinoflagellate taxa such as *Gambierdiscus*, *Prorocentrum* and *Amphidinium* species in ciguatera affected areas [1]. Generally, ciguatera fish poisoning is associated with demersal herbivorous and carnivorous reef fishes and pelagic carnivores such as mackerels and barracudas. *Coolia monotis* has been reported to produce a toxin named cooliatoxin, which induces hypothermia and respiratory failure in mice [2]. When organisms feed on large amounts of these toxic microalgae, shellfish-poisoning events, significant public health problems, and mass mortalities of aquatic organisms can result. Of the 5000 known living phytoplankton species [3], some 300 species can cause water discoloration, although only 80 species produce toxins that can cause human shellfish poisoning [4]. Worldwide, marine algal toxins cause more than 60, 000 poisoning events annually with an associated mortality rate of 1.5% [5]. The economic impact of such blooms can be substantial.

Some studies have suggested that marine algal toxicity is very much related to the associated bacterial assemblages [6-8]. Other studies have shown that bacteria can affect the growth of bloom population

[9-10], cyst formation [11-12] and algicidal activity against dinoflagellate [13-16]. Bacteria may occur inside and/or outside the algae – in the latter case they may be either attached or free-living – and can interact with the alga in widely varying ways [17-19]. The specific mechanism of interaction is still not well understood. An important step towards understanding bacteria-dinoflagellate interactions is to determine whether specific groups of bacteria are consistently involved in these associations. A recent study had demonstrated a persistent and apparently specific association with *Gambierdiscus* of a Bacteroides bacterium which may be involved in ciguatoxin production [20].

In the present study we assess the phylogenetic diversity of associated bacterial assemblages using a metagenomics approach that enables access to both culturable and unculturable bacteria. In addition, cultivable bacteria from the dinoflagellate culture were isolated using conventional bacteriology methods in order to compare the number of culturable and non-culturable bacteria genotypes in the association.

MATERIALS AND METHODS

Algal cultures

The dinoflagellate strains used in this study, *Coolia monotis* (CmSA01) and *Ostreopsis ovata* (OvPR04) were obtained from the Marine Microalgae Culture Collection of Universiti Kebangsaan Malaysia. CmSA01 culture was established from seaweed samples collected from the coral reef of Gaya Island, Kota Kinabalu, Sabah (06°01'02"N and 116°07'06"E) in October 1999 while strain OvPR04 was obtained from Redang Island, Terengganu (5°44'03"N and 102°59'01"E) in July 1997. Clonal cultures were established by single-cell isolation using a very finely-drawn sterile glass tube. Cells were washed three times in sterile filtered seawater before transfer into culture medium. Cultures were routinely grown in sterile ES-DK medium [21] at 26°C under a 14:10 hours light:dark cycle.

Scanning electron microscopy (SEM)

Dinoflagellate cultures were harvested by filtering through a 0.2 µm nitrocellulose membrane filter (Whatman, England) and transferred into a tube. Distilled water was added to the tube containing the membrane with cells, vortexed and centrifuged to obtain cell pellets. Cells were fixed with glutaraldehyde and washed three times with phosphate buffer saline pH 7.4 (140 mM NaCl; 3 mM KCl; 10 mM Na_2HPO_4; 2 mM KH_2PO_4). For dehydration, the cells were first transferred to a polycarbonate membrane (Whatman, England) and dehydration was carried out with a series of acetone as follows: 35%, 50%, 75%, 95% and three changes of 100% at 10 minutes each. The samples were critical point dried (CPD), mounted and sputter coated with gold and viewed on a SEM model XL30 (Philips, Japan).

Metagenome extraction of associated bacterial flora

Cultures were harvested at early stationary phase by filtering through a 0.2 µm nitrocellulose membrane filter (Whatman, England). For bacterial genomic extraction, the membrane filter was first suspended in 6 mL of STE buffer (500 mM NaCl, 10mM Tris-HCl pH 8.0, 0.1M EDTA pH 8.0). The suspension was then added with 300 µL of 10% SDS and 30 µL of proteinase K (20 mg/mL) and incubated at 37°C for 1 h 30 min. This was followed by 10% CTAB extraction and chloroform:isoamyl alcohol (C:I) extraction. After centrifugation, the aqueous layer was used for phenol extraction. Equal volume of phenol: chloroform:isoamyl alcohol (P:C:I) was added. Genomic DNA in the aqueous layer was precipitated with 0.6 volume of isopropanol. The genomic DNA precipitate was collected by centrifugation and washed twice with 70% ethanol. The pellet was then air-dried and resuspended in 30 µL of TE Buffer, pH 8.0.

16S rDNA clone libraries

Approximately 200 ng of genomic DNA was amplified using bacterial 16S rRNA gene-specific primer set 63F and 1389R [22]. The PCR was performed under the following conditions: 2 min initial denaturation at 95°C followed by 24 cycles of denaturation (30 s at 95°C), annealing (1 min at 53°C), and extension (2 min at 72°C) and a final extension at 72°C for 10 min. Purified PCR product from CmSA01 culture was ligated into a pJET (Fermentas) vector and transformed into competent JM 107 *Escherichia coli* while pGEM-T Easy (Promega) vector and competent JM 109 *Escherichia coli* were used for PCR product from OvPR04 culture. A total of 960 clones were selected from each library and purified using Millipore mini-prep kit and analyzed by restriction fragment length polymorphism (RFLP) using the

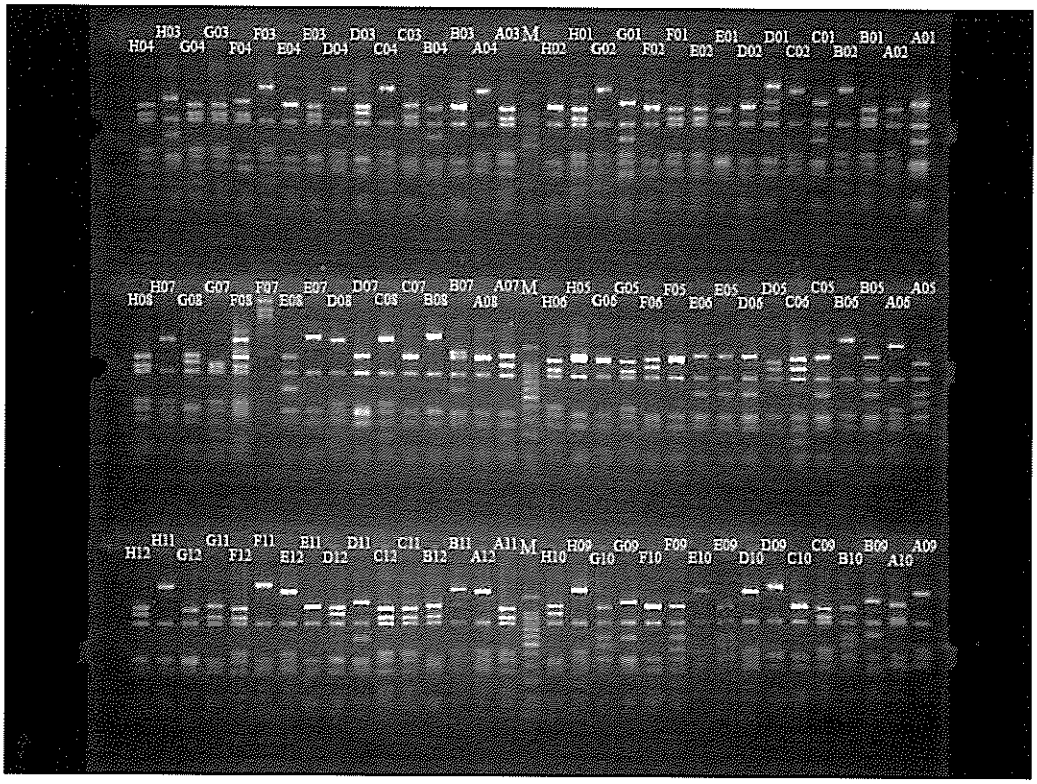

Figure 1. Example of electrophoresis profile for one plate of 16S rRNA gene library for RFLP analysis. M: 100 bp marker. Alphanumerical label indicate the clone number in a 96-well plate.

restriction enzyme *Sau*3AI. The restriction fragments were electrophoresed on 2% agarose gels and sorted according to their RFLP patterns (Fig. 1).

Sequencing and sequence analysis

A representative clone of each RFLP type within a 96-well plate was sequenced using 3 primers which included T7 (forward), SP6 (reverse) and 334F (close gap) [23]. The sequences were assembled in the Staden Package [24] and consensus sequences were compared with other 16S rRNA genes in GenBank using NCBI BLAST [25]. Consensus sequences were also analyzed using the Check-Chimera program on the Ribosomal Database Project (RDP) website [26]. For phylogenetic analysis, each full sequence was aligned with closely related sequences identified from the BLAST search and representative in-group and out-group taxa using ClustalX version 1.8 [27]. Maximum likelihood (ML) analysis was performed using PAUP* version 4b10 [28] and a ML tree was constructed from the estimated rates of transition/ transversion and γ-shape parameters calculated using the general time reversible model [29]. Branching support for the inferred tree was established from resampling of 1000 data sets based on Bayesian analysis [30].

Bacteria isolation and culture, DNA extraction and 16S rDNA amplification

Bacteria were isolated only from the culture of CmSA01. A 1 mL volume of early stationary phase CmSA01 culture was serially diluted in sterile sea water and spread onto marine agar 2216 (Difco, USA). The plates were incubated in the dark at 30°C for up to eight days. Bacterial colonies with distinctly different morphologies were picked and serially passaged on marine agar until the purity of the isolate was assured. The characterization of colony morphologies was according to Cappucino and Sherman [31].

For DNA extraction of each isolate, a colony of bacteria was suspended in 100 µL of TE buffer, pH 8.0. The suspension was then centrifuged to obtain a cell pellet which was then resuspended in 600 µL of TE buffer, pH 8.0. The consecutive DNA extraction steps were done as in the metagenome extraction method above but with downscale volume of 30 µL 10% SDS and 3 µL of proteinase K (20 mg/mL) were used. The genomic DNA was then used for 16S rDNA

amplication using primer set 63F and 1389R [22]. The PCR was performed under the following conditions: 2 min initial denaturation at 95°C followed by 24 cycles of denaturation (30 s at 95°C), annealing (1 min at 53°C), and extension (2 min at 72°C) and a final extension at 72°C for 10 min. Purified PCR products were sequenced and the sequences were compared with other 16S rRNA genes in GenBank using NCBI BLAST.

Nucleotide sequence Genbank accession numbers
Sequences obtained in this study have been deposited in Genbank with Accession No. FJ644574 to FJ644618.

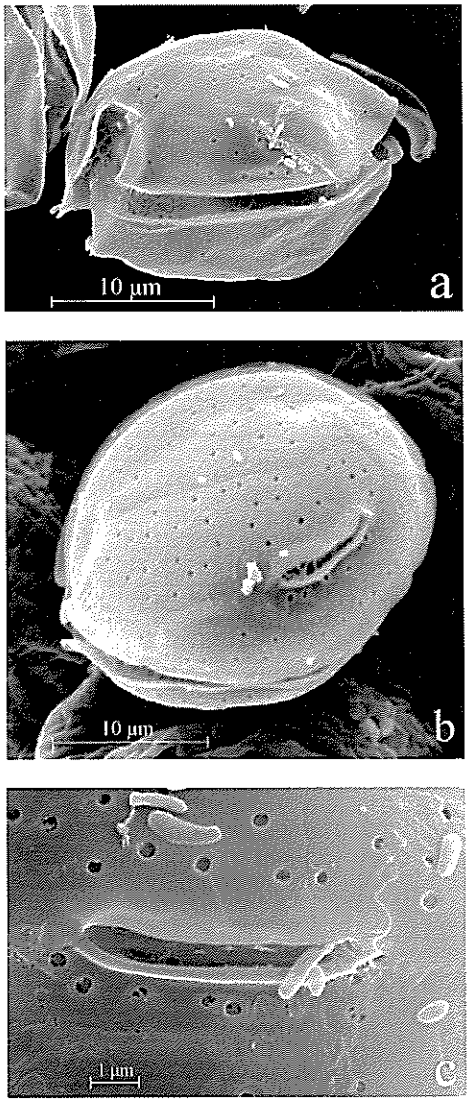

Figure 2. SEM micrograph of (a) *Coolia monotis* culture (CmSA01), (b) *Ostreopsis ovata* culture (OvPR04), and (c) close-up image of bacteria attached to the surface of CmSA01.

RESULTS

Scanning electron microscopy proved the existence of bacteria in the *O. ovata* and *C. monotis* cultures (Fig. 2). Light microscopy observations showed that some of the bacteria were attached to the surface of the host dinoflagellate and some were free-living. The bacteria were of different sizes and most were rod-shaped.

A total of 111 sequences from CmSA01 and 94 sequences from OvPR04 cultures were obtained ranging from 875 bp to 1370 bp in length. Results of the Blastn analysis are shown in Table 1. There were 19 distinct phylotypes from CmSA01 culture and 17 distinct phylotypes from OvPR04 culture. Fifteen out of these 36 phylotypes matched with sequences of uncultured bacteria and nine of them have no phylogenetic group assigned. From both cultures, only four of the sequences produced matches to species level, namely *Gilvibacter sediminis* which was present in both cultures, *Flexibacter aggregans* and *Bacillus methanolicus* from the CmSA01 culture, and *Marinobacter hydrocarbonoclasticus* from the OvPR04 culture.

Phylogenetic relationships of each operational taxonomic unit (OTU) from both cultures are shown in Figure 3. The OTUs with no phylogenetic group assigned could be clustered into specific clades by phylogenetic analysis. In general, the bacteria flora grouped into three main phyla, the subclasses α-proteobacteria, γ-proteobacteria and Cytophaga-Flavobacteria-Bacteroides (CFB) group. The sequences from the CmSA01 culture were dominated by α-proteobacteria (52.2%), followed by CFB (31.5%), γ-proteobacteria (14.4%) and Gram-positive bacteria (1.8%). For the OvPR04 culture, there was equal dominance of γ-proteobacteria (39.4%) and α-proteobacteria (35.4%), followed by CFB (23.3%) and Planctomyces (2.1%).

Nine cultivable isolates were obtained from CmSA01 culture. Partial 16S rRNA gene sequences obtained ranged from 862 bp to 1247 bp. Results of the most similar homologues and observation of colony morphologies are shown in Table 2. Six of the isolates were affiliated with α-proteobacteria, two belonged to the CFB group and one was a γ-proteobacteria. Out of the nine isolates, only one matched to species level, namely *Flexibacter aggregans*. This sequence was also found in the metagenomic sequences. Other sequences

Table 1. Classification of 16S rDNA sequences obtained from the CmSA01 and OvPR04 cultures.

Sequence code and source	Length of sequence (bp)	Phylogenetic group	Closest match in Genbank	Accession no.	Similarity (%)	Abundance among sequences (%)
Coolia monotis (CmSA01)						
MgKD01d001G03	1354	CFB	*Flavobacterium* sp.	AJ391201	96	0.9
MgKD01d001H02	1207	CFB	Uncultured Bacteroidetes bacterium	DQ644019	95	0.9
MgKD01d001H03	1179	Alpha	*Roseobacter* sp. CSQ-2	EF512125	98	8.1
MgKD01d002C04	1355	Unknown	Uncultured bacterium	EF125404	93	1.8
MgKD01d002C12	1240	Alpha	Marine snow associated bacterium	AF030778	97	5.4
MgKD01d002F06	1319	CFB	Uncultured CFB group bacterium	AF445721	90	0.9
MgKD01d002H04	1367	CFB	Uncultured Bacteroidetes bacterium	DQ070811	88	1.8
MgKD01d003B01	1353	Gamma	Uncultured gamma proteobacterium	AB015537	93	4.5
MgKD01d005A03	1347	CFB	*Gilvibacter sediminis*	AB255368	99	18.9
MgKD01d005C06	1277	Alpha	*Roseobacter* sp. B11	DQ659411	99	4.5
MgKD01d005D04	1189	Alpha	Uncultured alpha proteobacterium	DQ446172	97	1.8
MgKD01d007C03	1361	Unknown	Uncultured bacterium	EF574709	99	1.8
MgKD01d007C04	1339	CFB	*Flexibacter aggregans*	AB288294	99	8.1
MgKD01d008E11	1204	Alpha	Alpha proteobacterium MBIC3865	AB015896	99	5.4
MgKD01d008F02	1306	Gram-positive	*Bacillus methanolicus*	AB112729	95	1.8
MgKD01d009G02	1184	Alpha	Alpha proteobacterium GMD21C01	AY162105	98	2.7
MgKD01d011A01	1352	Unknown	Uncultured bacterium	EF574804	99	6.3
MgKD01d011G02	1277	Alpha	Mucus bacterium	AY654757	98	21.6
MgKD01d011H04	1283	Alpha	Uncultured Rhodobacter group bacterium	AF513932	97	2.7
Ostreopsis ovata (OvPR04)						
MgKD02d001F04	1293	Unknown	Bacterium	AY258094	96	2.1
MgKD02d002C12	1363	Unknown	Uncultured bacterium	EF125404	93	4.3
MgKD02d002G02	1296	Unknown	Unidentified bacterium	AY344411	98	4.3
MgKD02d002G08	1331	Unknown	Uncultured bacterium	DQ300579	97	1.1
MgKD02d003A01	1129	Alpha	*Roseobacter* sp.	AY332661	98	2.1
MgKD02d003A05	1174	Unknown	Uncultured bacterium	EF573869	99	2.1
MgKD02d004G02	1282	Alpha	Uncultured alpha proteobacterium	DQ446084	97	4.3
MgKD02d005A01	1321	Alpha	Alpha proteobacterium	DQ985050	98	2.1
MgKD02d005D06	1370	Gamma	*Marinobacter hydrocarbonoclasticus*	DQ768638	99	1.1
MgKD02d005G01	1366	Gamma	Gamma proteobacterium	AY207503	95	8.5
MgKD02d005H01	1278	Alpha	*Roseobacter* sp.	EF512125	97	1.1
MgKD02d006F09	1362	CFB	Uncultured Bacteroidetes bacterium	AY948034	88	2.1
MgKD02d007A07	1296	Unknown	Uncultured bacterium	DQ334624	97	16.0
MgKD02d007B06	1367	CFB	*Gilvibacter sediminis*	AB255368	98	19.1
MgKD02d007E01	1358	CFB	*Flexibacter* sp.	AB058905	96	2.1
MgKD02d007E07	1338	Planctomyces	Planctomycete	AY162118	99	2.1
MgKD02d007G05	1367	Gamma	Gamma proteobacterium	AY207503	96	25.5

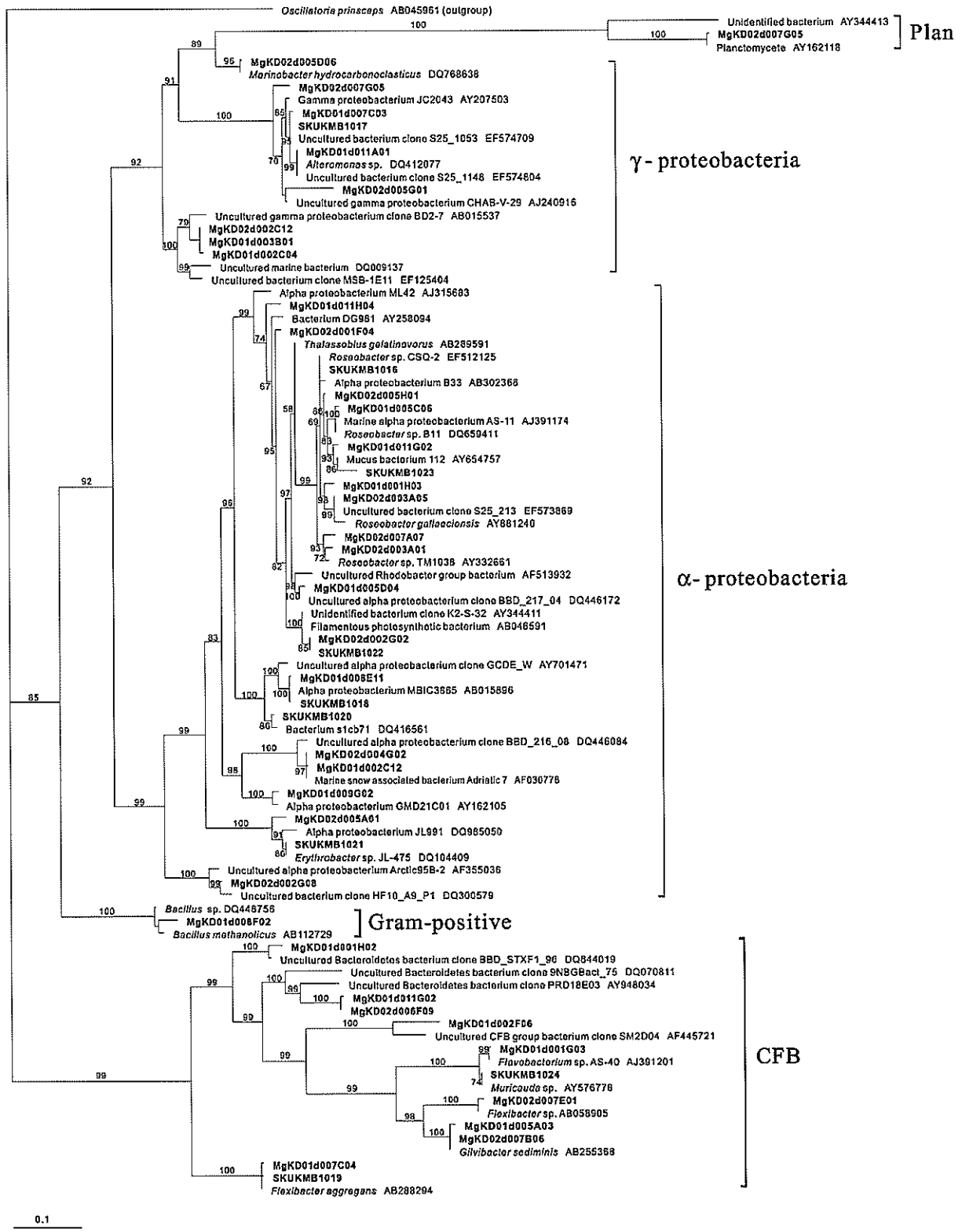

Figure 3. Maximum likelihood analysis phylogram based on 16S rRNA sequences obtained in this study (bold) and related sequences. Sequences from the culturable isolates from CmSA01 culture are indicated by SKUKMB; sequences associated with direct extraction from CmSA01 culture are indicated by MgKD01d; and sequences that were associated with direct extraction from OvPR04 culture are indicated by MgKD02d. Shown are the groups of Gram-positive bacteria, Planctomyces (Plan), Cytophaga-Flavobacterium-Bacteroides (CFB), alpha and gamma subclasses of Proteobacteria. Posterior probability values from Bayesian analysis greater than 50% are shown adjacent to nodes.

Table 2. Phylogenetic affiliation of culturable bacteria isolated from *C. monotis* (CmSA01).

Isolate	Colony morphology (size, color, shape, side, elevation)	Length of sequence (bp)	Phylogenetic group	Closest match in Genbank	Accession no.	Similarity (%)
SKUK MB1016	Moderate, opaque cream, circular, serrate, convex	1182	Alpha	*Roseobacter* sp. CSQ-2	EF512125	99
SKUK MB1017	Large, translucent white, circular, entire, raised	1247	Unknown	Uncultured bacterium clone S25_1053	EF574709	99
SKUK MB1018	Small, opaque pink, circular, entire, umbonate	1202	Alpha	Alpha proteobacterium MBIC3865	AB015896	99
SKUK MB1019	Small, opaque yellow, circular, undulate, umbonate	1174	CFB	*Flexibacter aggregans*	AB288294	99
SKUK MB1020	Small, translucent white, circular, entire, convex	920	Unknown	Bacterium s1cb71	DQ416561	99
SKUK MB1021	Small, opaque orange, circular, entire, convex	862	Alpha	*Erythrobacter* sp.	DQ104409	99
SKUK MB1022	Pinpoint, translucent white, circular, entire, convex	910	Unknown	Filamentous photosynthetic bacterium	AB046591	98
SKUK MB1023	Moderate, translucent light yellow, circular, convex	948	Alpha	Alpha proteobacterium B33	AB302368	97
SKUK MB1024	Small, translucent yellow, irregular, undulate, raised	907	CFB	*Muricauda* sp.	AY576776	99

found in both cultured and metagenomic samples were isolate SKUKMB1016 and clone sequence MgKD01d001H03 that matched with *Roseobacter* sp. CSQ-2, isolate SKUKMB1017 and clone sequence MgKD01d007C03 that matched with an uncultured bacterium clone, and isolate SKUKMB1018 and clone sequence MgKD01d008E11 that matched with an alpha proteobacterium.

DISCUSSION

Culture-independent molecular techniques allow the importance of the numerous non-cultivable bacteria present in various ecosystems to be evaluated. The use of molecular and conventional culturing methods in the present study has enabled us to capture the genetic diversity of bacteria associated with two benthic marine dinoflagellates. Sequencing of the 16S rDNA clones revealed 19 distinct phylotypes from the CmSA01 culture and 17 distinct phylotypes from the OvPR04 culture. However, it was not certain whether those numbers equate to actual phenotypic diversity. As comparison, Green *et al.* [32] obtained 61 distinct cultured bacteria from seven strains of *Gymnodinium catenatum* while Ashton *et al.* [33] obtained only seven DGGE bands from an *Ostreopsis lenticularis* strain.

To a certain extent the number of bacteria species in these cultures will also depend on the techniques used during the initial isolation of the dinoflagellate cells into culture. Since sterile and aseptic techniques are typically employed in subsequent subculturing, the diversity of the associated bacteria will also be influenced by the diversity of bacteria in the ambient seawater from where the dinoflagellate originated. One unexpected result was that from the CmSA01 culture, only four out of nine culturable bacteria isolate were discovered in the metagenome 16S rDNA sequences. It is a fact that most PCR-based methods would be biased towards numerically dominant genotypes in a sample. This suggested that at least half of the culturable isolates were present at low densities in the culture at the time of harvesting. Thus in order to capture the full diversity of such bacteria assemblages, a combination of metagenomics and conventional culturing methods is necessary. Blastn

Journal of Science and Technology in the Tropics (2009) **5**: 3

Editorial

We have only ONE planet Earth and we have all realized that we have to take good care of it for NOW and for future generations. I have often questioned the wanton discharge of pollutants into the air and waterway by the manufacturing factories and was told that dilution was the solution. It has been gargantuan efforts by civil society to bring home the message that clean air and clean drinking water are crucial to the well-being of the human race and other living organisms.

Scientists and technologists have the opportunities to develop green processing technologies and green production of energy including solar energy. Malaysia has pioneered with renewal palm biodiesel. The initiative to produce Roundtable Sustainable Palm Oil (RSPO) has been lauded by the world. There are more innovative solutions such as trapping all methane gases from palm oil mills resulting in zero carbon palm oil, producing palm oil and non-oil food product with minimum discharge of aqueous effluents, etc. We can look forward to innovations in our mode of living. Should our clothing be made of materials which create comfortable environment for our skin under the humid tropical atmosphere without excessive air-conditioning? Should we have commercially available solar powered air-conditioners which are working in harmony with the natural sunlight?

The present Government has initiated a new Ministry of Energy, Green Technology and Water. This will spur Malaysian technologists to intensify efforts to production of green energy and researchers to develop green processes where opportunities exist to convert toxic effluents into useful and harmless wastes such as fertilizers. The possibilities are tremendous and are only limited by our imagination and creativity.

I am sure that with our aim for sustainability, we could introduce innovations for good sustainable standard of living in the Tropical Region of the World.

Academician Professor Emeritus
Tan Sri Datuk Dr Augustine S. H. Ong
Co-Chairman, Editorial Board

analysis showed that most of the sequences from this study had no match at species level. In addition, there were a number of sequences with less than 97% SSU rDNA similarity to published sequences. Nine operational taxonomic units (OTUs) from CmSA01 culture and 6 OTUs from OvPR04 culture matched with sequences of uncultured bacteria. These results showed that there were novel bacteria species in these cultures and some may be unculturable.

One sequence from our cultures matched with a published sequence of *Marinobacter hydrocarbonoclasticus* with 99% similarity and another matched the sequence of *Flexibacter aggregans* with 99% similarity. These two bacteria species were also isolated from different strains of the dinoflagellate *Gymnodinium catenatum* [32]. *Marinobacter hydrocarbonoclasticus* belongs to the Alteromonadaceae and is capable of utilizing aliphatic hydrocarbons as a carbon source. The carbon source for these associated bacteria is probably mainly organic carbon exudates of the dinoflagellate. Some of the bacteria could also probably break down the cellulose cell wall of dead dinoflagellates. We have noticed significantly higher bacteria density in older cultures and many of the bacteria cells congregate around pieces of discarded cell wall.

Phylogenetic analysis of the 16S rDNA sequences showed strong bootstrap support for the branching order of both the Proteobacteria and Bacteroidetes. Based on the ML tree, four phylotypes from each dinoflagellate culture were probably common. These were MgKD01d002H04 and MgKD02d006F09 that grouped with an uncultured Bacteroidetes bacterium; MgKD02d007B06 and MgKD01d005A03 that grouped with *Gilvibacter sediminis*; MgKD02d002C12, MgKD01d003B01 and MgKD01d002C04 that grouped with an uncultured γ-proteobacterium; and MgKD02d004G02 and MgKD01d002C12 that grouped with a marine snow associated bacterium. Co-occurrence of similar bacteria sequences in cultures of these two dinoflagellate strains suggested that dinoflagellate-associated bacteria could be quite specific since the two dinoflagellates originated from different geographical regions. Examples of bacterial functionality, and possibly an example of algal selection of specific bacteria are bacteria adapted to the utilization of algal extracellular products [34]. These groups of bacteria may be of specific importance to the growth and physiology of dinoflagellate cells [35].

Sequences highly similar to that of *Gilvibacter sediminis* were found in both cultures. These sequences were also relatively high in abundance among the sequenced clones. *Gilvibacter sediminis* belongs to the Bacteroidetes group, a novel member of the family Flavobacteriaceae which was originally isolated from marine-sediment samples collected from the coast of Okinawa Island, Japan [36]. Thus one probable habitat of this bacterium is the surface of benthic dinoflagellates. We also obtained some sequences which were closely related to a bacterium associated with marine snow [37]. Our phylogenetic analysis showed that this bacterium belongs to the Alphaproteobacteria group. Marine snow is enriched in nutrients, trace metals, microbial biomass and production compared to the surrounding water [38]. The dinoflagellate phycosphere may provide a similar environment to the associated bacteria.

Sequences similar to *Roseobacter* sp. occurred in both CmSA01 and OvPR04 cultures. *Roseobacter* clade is often found associated with various dinoflagellates, for example *Alexandrium* spp. [18], *Pfiesteria* spp. [39] and *Prorocentrum* spp. [40]. This bacterium is predominantly responsible for the degradation of dimethylsulfoniopropionate (DMSP). DMSP is the major source of organic sulphur in the world's oceans and is degraded by marine bacteria to dimethylsulphide (DMS). These bacteria thus play very important roles in the global sulphur cycle [41]. Other than that, the *Roseobacter* clade-affiliated group bacteria were shown to cause algal bloom decline and believed that the widespread of this group of bacteria may exert significant control over phytoplankton biomass and community structure in the oceans [16].

MgKD01d011A01 sequence matched with an uncultured bacterium which is phylogenetically closely related to *Alteromonas* spp. *Alteromonas*, a member of γ-proteobacteria was always reported as a bacterium associated with the stimulation of dinoflagellate growth. Sakami *et al.* [9] demonstrated that several bacteria, one of which was identified as *Alteromonas* sp., isolated from the cell surface of the ciguatera-producing dinoflagellate *Gambierdiscus toxicus*, stimulated growth of this dinoflagellate. Other than that, *Alteromonas* sp. was observed to be a fundamental part of the bacterial community responsible for growth enhancement of *Alexandrium fundyense* [10]. However, Alteromonads have seemingly ambiguous roles, as it was reported inhibiting another Alexandrium strain of cyst

formation [12].

Two unexpected phylotypes were found from the cultures. From the culture of OvPR04, sequence MgKD02d007E07 matched with the sequence of Planctomycete with 99% identity. So far, we have not found any report of association of this bacterium with any phytoplankton. The second unique phylotype (MgKD01d008F02) matched with the sequence of *Bacillus methanolicus*, a gram-positive bacterium. Gram-positive bacteria are rarely found associated with dinoflagellates although some were reported associated with *Noctiluca scintillans* [42]. Out of the common bacteria taxa usually found associated with microalgae, we suggest that these cultures are potential sources for description of novel bacteria taxa, some of which may be specifically associated with dinoflagellates.

Bacteria present in these dinoflagellate cultures were most probably carried over during isolation of the cells for culture. No subsequent contamination was expected since in all subsequent subculturing sterile medium and techniques were used. Thus the bacteria flora in the cultures to some extent reflects the bacteria flora of seawater from the original isolation locality. However, there is increasing evidence that there are specific bacteria taxa associated with phytoplankton (e.g. [32, 43]). Such specificity would imply some sort of bacteria-dinoflagellate recognition mechanism and also probable mutual benefit for both. Whole genome sequencing of the bacteria community followed by analysis of gene presence and absence could indicate the manner of bacteria contribution to and dependence on the dinoflagellate. This approach would be particularly interesting in the case of toxic dinoflagellates because the role of bacteria in toxigenesis continues to be a subject of speculation.

This study has shown that direct amplification of SSU rRNA gene of associated bacteria from the dinoflagellate cultures is more effective than culturing approach. It is because we were able to extract a large portion of uncultured bacteria according to the matches with Genbank database. Nonetheless, the process of isolating and culturing bacteria continues to be a prerequisite for examining bacterial physiology, and although genomics and metagenomics will to a certain extent minimize the reliance on pure cultures, close partnering of genomics and pure culture studies will likely be the most valuable route to elucidating the functional significance of bacteria associated with harmful algae. Overall, our findings are very much similar to other studies on associated bacterial flora with dinoflagellates where the bacteria were affiliated to the three main groups which include α-proteobacteria, γ-proteobacteria and CFB. On top of that, we believe this study points to a number of bacterial groups that are key to the growth and physiology of dinoflagellates and that their activity may reflect the natural blooms. We would like to suggest that further work to be carried out which involves direct DNA extraction in-situ from the environment, to compare the natural and culture collections in order to give us a more comprehensive overview.

Acknowledgement – This work was supported by a grant from the Ministry of Science, Technology and Innovation, Malaysia under IRPA 09-02-02-008-BTK/ER-36.

REFERENCES

1. Morton S.L., Norris D.R. and Bomber J.W. (1992) Effect of temperature, salinity and light intensity on the growth and seasonality of toxic dinoflagellates associated with ciguatera. *J. Exp. Mar. Biol. Ecol.* **157**: 79-90.
2. Holmes M.J., Lewis R.J., Jones A. and Hoy, A.W. (1995) Cooliatoxin, the first toxin from Coolia monotis (Dinophyceae). *Nat. Toxins* **3**(5): 355-362.
3. Sournia A., Chretiennot-Dinet M.J. and Ricard M. (1991) Marine phytoplankton: how many species in the world ocean? *J. Plankton Res.* **13**: 1093-1099.
4. Hallegraeff G.M. (2003) Harmful algal blooms: a global overview. *In* Hallegraeff G.M., Anderson D.M., Cembella A.D. (eds.). *Manual on harmful marine microalgae*, vol 11, 2nd edn. pp 25–49. IOC-UNESCO, Paris.
5. Gill S., Murphy M., Clausen J., Richard D., Quilliam M., MacKinnon S., LaBlanc P., Mueller R. and Pulido O. (2003) Neural injury biomarkers of novel shellfish toxins, spirolides: a pilot study using immunochemical and transcriptional analysis. *Neurotoxicology* **24**: 593-604.
6. Kim C.H., Sako Y. and Ishida Y. (1993) Variation of toxin production and composition in axenic cultures of *Alexandrium catenella* and *Alexandrium tamarense*. *Nippon Suisan Gakk.* **59**: 633-639.

7. Dantzer W.R. and Levin R.E. (1997) Bacterial influence on the production of paralytic shellfish toxins by dinoflagellated algae. *J. Appl. Microbiol.* **83**: 464-469.
8. Uribe P. and Espejo R.T. (2003) Effect of associated bacteria on the growth and toxicity of *Alexandrium catenella*. *Appl. Environ. Microbiol.* **69**(1): 659-662.
9. Sakami T., Nakahara H., Chinain M. and Ishida Y. (1999) Effects of epiphytic bacteria on the growth of the toxic dinoflagellate Gambierdiscus toxicus (Dinophyceae). *J. Exp. Mar. Biol. Ecol.* **233**: 231-246.
10. Ferrier M., Martin J.L. and Rooney-Varga J.N. (2002) Stimulation of Alexandrium fundyense growth by bacterial assemblages from the Bay of Fundy. *J. Appl. Microbiol.* **92**: 706-716.
11. Adachi M., Kanno T., Matsubara T., Nishijima T., Itakura S. and Yamaguchi M. (1999) Promotion of cyst formation in the toxic dinoflagellate *Alexandrium* (Dinophyceae) by natural bacterial assemblages from Hiroshima Bay, Japan. *Mar. Ecol. Prog. Ser.* **191**: 175-185.
12. Adachi M., Matsubara T., Okamoto R., Nishijima T., Itakura S. and Yamaguchi M. (2002) Inhibition of cyst formation in the toxic dinoflagellate Alexandrium (Dinophyceae) by bacteria from Hiroshima Bay, Japan. *Aquat. Microb. Ecol.* **26**: 223-233.
13. Lovejoy C., Bowman J.P and Hallegraeff G.M. (1998) Algicidal effects of a novel marine *Pseudoalteromonas* isolate (class *Proteobacteria*, Gamma division) on harmful algal bloom species of the genera *Chattonella*, *Gymnodinium*, and *Heterosigma*. *Appl. Environ. Microbiol.* **64**(8): 2806-2813.
14. Mayali X. and Doucette G.J. (2002) Microbial community interactions and population dynamics of an algicidal bacterium active against Karenia brevis (Dinophyceae). *Harmful Algae* 1: 277-293.
15. Kim M.J., Jeong S.Y. and Lee S.J. (2008) Isolation, identification, and algicidal activity of marine bacteria against Cochlodinium polykrikoides. *J. Appl. Phycol.* **20**: 1069-1078.
16. Mayali X., Franks P.J.S and Azam F. (2008) Cultivation and ecosystem role of a marine *Roseobacter* clade-affiliated cluster bacterium. *Appl. Environ. Microbiol.* **74**: 2595-2603.
17. Doucette G.J. (1995) Interactions between bacteria and harmful algae: a review. *Nat. Toxins* **3**: 65-74.
18. Gallacher S., Flynn K.J., Franco J.M., Brueggemann E.E. and Hines H.B. (1997) Evidence for production of paralytic shellfish toxins by bacteria associated with Alexandrium spp. (Dinophyta) in culture. *Appl. Environ. Microbiol.* **63**: 239-245.
19. Cordova J.L., Jamett A., Fauré M.T., Villaroel O. and Cardenas L. (2001) An in vitro assay to detect paralytic shellfish poison. *J. Shellfish Res.* **20**: 55-61.
20. Pérez-Guzmán L., Pérez-Matos A.E., Rosado W., Tosteson T.R. and Govind N.S. (2008) Bacteria associated with toxic clonal cultures of the dinoflagellate *Ostreopsis lenticularis*. *Mar. Biotechnol.* **10**: 492-496.
21. Kokinos J.P. and Anderson D.M. (1995) Morphological development of resting cysts in cultures of the marine dinoflagellate *Lingulodinium polyedrum* (=*L. machaerophorum*). *Palynology* **19**: 143-166.
22. Hongoh Y., Yuzawa H., Ohkuma M. and Kudo T. (2003) Evaluation of primers and PCR conditions for the analysis of 16S rRNA genes from a natural environment. *FEMS Microbiology Letters* **221**: 299-304.
23. Baker G.C., Smith J.J. and Cowan D.A. (2003) Review and re-analysis of domain-specific 16S primers. *J. Microbiol. Methods* **55**: 541-555.
24. Staden R. (1996) The Staden Sequence Analysis Package. *Molecular Biotechnology* **5**: 233-241.
25. Altschul S.F., Gish W., Miller W., Myers E.W. and Lipman D.J. (1990) Basic local alignment search tool. *J. Mol. Biol.* **215**: 403-410.
26. Maidak B.L., Cole J.L., Lilburn T.G., Parker C.T.J., Saxman P.R., Farris R.J., Garrity G.M., Olsen G.J, Schmidt T.M. and Tiedje J.M. (2001) The RDP-II (Ribosomal Database Project). *Nucl. Acids Res.* **29**: 173-174.
27. Thompson J. D., Gibson T.J., Plewniak F., Jeanmougin F. and Higgins D.G. (1997) The ClustalX windows interface: flexible strategies for multiple sequence alignment aided by quality analysis tools. *Nucleic Acids Res.* **24**: 4876-4882.
28. Swofford D.L. (2000) *PAUP*: Phylogenetic analysis using parsimony (*and other methods). Version 4b10.* Sinauer Associates, Sunderland, Massachusetts.
29. Tavaré S. (1986) Some probabilistic and statistical problems in the analysis of DNA sequences. *In* Miura R.M. (eds.). *Some mathematical questions in biology - DNA sequence analysis* pp. 57-86. Amer. Math. Soc., Providence, RI.
30. Ronquist F. and Huelsenbeck J.P. (2003) MRBAYES 3: Bayesian phylogenetic inference under mixed models. *Bioinformatics* **19**: 1572-1574.

31. Cappucino J.G. and Sherman N. (2001) *Microbiology: A laboratory manual.* Pearson Education, Inc., San Francisco.
32. Green D. H., Llewellyn L.E., Negri A.P., Blackburn S.I. and Bolch C.J.S. (2004) Phylogenetic and functional diversity of the cultivable bacterial community associated with the paralytic shellfish poisoning dinoflagellate *Gymnodinium catenatum*. *FEMS Microbiol. Ecol.* **47**: 345-357.
33. Ashton M., Rosado W., Govind N.S. and Tosteson T.R. (2003) Culturable and nonculturable bacterial symbionts in the toxic benthic dinoflagellate *Ostreopsis lenticularis*. *Toxicon* **42**: 419-424.
34. Miller T.R. and Belas R. (2004) Dimethylsulfoniopropionate metabolism by *Pfiesteria*-associated *Roseobacter* spp. *Appl. Environ. Microbiol.* **70**(6): 3383-3391.
35. Tosteson T.R., Ballantine D.L., Tosteson C.G., Hensley V. and Bardales A.T. (1989) Associated bacterial flora, growth, and toxicity of cultured benthic dinoflagellates *Ostreopsis lenticularis* and *Gambierdiscus toxicus*. *Appl. Environ. Microbiol.* **55**(1): 137-141.
36. Khan S.T., Nakagawa Y. and Harayama S. (2007) *Sediminibacter furfurosus* gen. nov., sp. nov. and *Gilvibacter sediminis* gen. nov., sp. nov., novel members of the family Flavobacteriaceae. *Int. J. Syst. Evol. Microbiol.* **57**(2): 265-269.
37. Rath J., Wu K.Y., Herndl G.J. and DeLong E.F. (1998) High phylogenetic diversity in a marine-snow-associated bacterial assemblage. *Aquat. Microb. Ecol.* **14**: 261-269.
38. Alldredge A. and Silver M. (1988) Characteristics, dynamics and significance of marine snow. *Prog. Oceanogr.* **20**: 41-82.
39. Alavi M., Miller T., Erlandson K., Schneider R. and Belas R. (2001) Bacterial community associated with Pfiesteria-like dinoflagellate cultures. *Environ. Microbiol.* **3**: 380-396.
40. Lafay B., Ruimy R., de Traubenberg C.R., Breittmayer V., Gauthier M.J. and Christen R. (1995) Roseobacter algicola sp. nov., a new marine bacterium isolated from the phycosphere of the toxin-producing dinoflagellate Prorocentrum lima. Int. *J. Syst. Bacteriol.* **45**: 290-296.
41. Yoch D.C. (2002) Dimethylsulfoniopropionate: its sources, role in the marine food web, and biological degradation to dimethylsulfide. *Appl. Environ. Microbiol.* **68**: 5804-5815.
42. Seibold A., Wichels A. and Schutt C. (2001) Diversity of endocytic bacteria in the dinofagellate *Noctiluca scintillans*. *Aquat. Microb. Ecol.* **25**: 229-235.
43. Sapp M., Schwaderer A.S., Wiltshire K.H., Hoppe H.G, Gerdts G. and Wichels A. (2007) Species-specific bacterial communities in the phycosphere of microalgae? *Microbial Ecology* **53**(4): 683-699.

Journal of Science and Technology in the Tropics (2009) **5**: 35-37

Calotes emma alticristatus (Reptilia, Squamata: Agamidae) in Kelantan, Peninsular Malaysia

Yong Hoi Sen[1], Rosli Hashim[1], Siti Zaleha Mat Diah[1], Daicus Belabut[1], Mohd Sofian Azirun[1] and Lim Boo Liat[2]
[1]Institute of Biological Sciences, University of Malaya, 50603 Kuala Lumpur, Malaysia
[2]12 Jalan Koop Cuepacs 3E, Taman Cuepacs, 43200 Cheras, Selangor, Malaysia
(Email: yong@um.edu.my)

Received 24-04-2009; accepted 30-04-2009

Abstract In Peninsular Malaysia the agamid lizard *Calotes emma* Gray 1845 is known to be represented by the subspecies *Calotes emma emma* Gray 1845. Recently several specimens were encountered in Jeram Linang, Machang, Kelantan Darul Naim. These belong to a different subspecies, *Calotes emma alticristatus* Schmidt 1925. This subspecies occurs in Thailand and South China. It constitutes a new record for the lizard fauna of Peninsular Malaysia.

Keywords forest crested lizard – *Calotes emma alticristatus* – Agamidae – Peninisular Malaysia – new record

INTRODUCTION

Calotes lizards are members of the subfamily Draconinae of the family Agamidae. They are represented by some 25 species, occurring in India (Assam), Myanmar, Thailand, Laos, Cambodia, Vietnam, South China (Guangdong, Yunnan) and Peninsular Malaysia. The genus *Calotes* Cuvier 1817 does not occur in Sabah and Sarawak as well as other parts of Borneo – the taxon *Calotes kinabaluensis* de Grijs 1937 from Sabah is now referred to as *Hypsicalotes kinabaluensis* [1]. Current taxonomic treatment records two species (*Calotes versicolor* and *Calotes emma*) to be present in Peninsular Malaysia [2].

Calotes versicolor (Daudin 1802) (Common Garden Lizard, Changeable Lizard) is found in all states of Peninsular Malaysia [2] and was introduced into Singapore relatively recently [3]. Prior to the present finding, *Calotes emma* Gray 1845 (Forest Crested Lizard) is represented in Peninsular Malaysia by the subspecies *Calotes emma emma* Gray 1845 which inhabits peninsular Thailand south to Perak and Pulau Rumpia [2]. We report here the occurrence of *Calotes emma alticristatus* Schmidt 1925 in Jeram Linang, Kelantan Darul Naim, Peninsular Malaysia.

MATERIALS AND METHODS

During a recent field trip to Pantai Melawi, Bachok, Kelantan Darul Naim for biodiversity study, a side visit was made to Jeram Linang (Lenang) Forest Recreation Park, along Pasir Puteh/Machang road on 13 April 2009. The recreation forest is located in Compartments 66 and 67 of the Ulu Sat Forest Reserve, with an area of 306 hectares bordering the State of Terengganu. It is about 65 km from Kota Bharu, 10 km from Pasir Puteh and 15 km from Machang.

Upon arrival one of us (YHS) first sighted a *Calotes* lizard low on a tree trunk near to the parking area. Later several specimens were sighted. Two specimens were photographed and collected. They were identified with existing literature (e.g. [4, 5]). These specimens are deposited at the Institute of Biological Sciences, University of Malaya.

RESULTS AND DISCUSSION

The two *Calotes* lizards belonged to the subspecies *Calotes emma alticristatus* (Figs. 1-3). They had an oblique curved skin fold in front of the shoulder, a spine above the eye and two spines above the

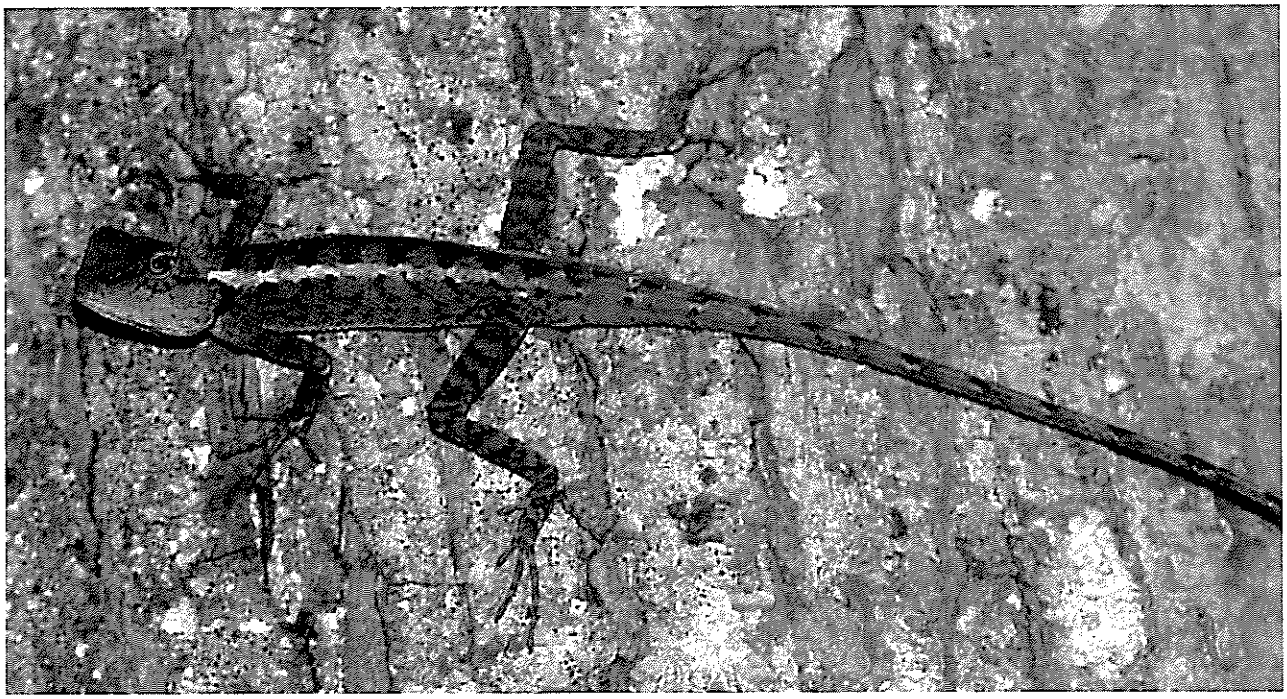

Figure 1. Female *Calotes emma alticristatus* on a tree trunk in Jeram Linang, Kelantan. (photo: H.S. Yong)

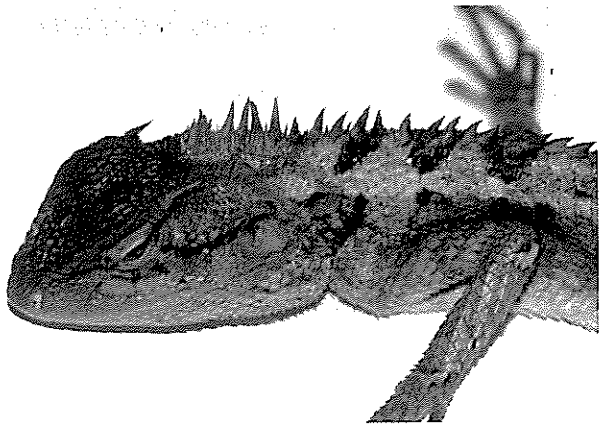

Figures 2. Anterior region of female *Calotes emma alticristatus* showing the characteristic spines and body with whitish longitudinal band and dark transverse markings. (photo: H.S. Yong)

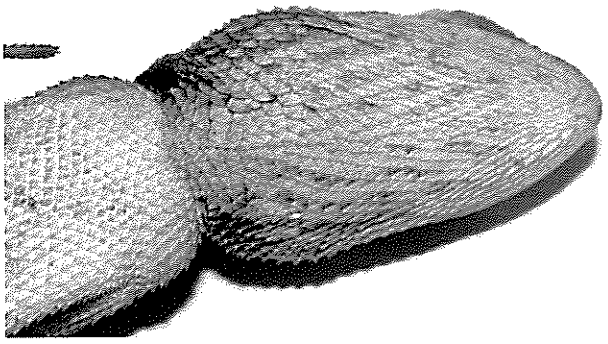

Figure 3. Ventral view of anterior region (head crimson in colour) of female *Calotes emma alticristatus*. (photo: H.S. Yong)

tympanum. The spines above the eye were much smaller than those of *Calotes emma emma*. Both were female. One specimen measured 84 mm in body (snout-vent) length and 316 mm in total length. The other specimen measured 80 mm in body length and 293 mm in total length. Both had a relatively long tail – 0.73 in tail/total length ratio; and a tail length/snout-vent length ratio of 2.76 for the larger specimen and 2.66 for the smaller specimen.

Both specimens when sighted at Jeram Linang had reddish orange head and body with a distinct white longitudinal band at the flank and irregular dark transverse markings on the back. The reddish head coloration appeared to be natural rather than due to stress as stated by Cox *et al.* [5]; the ventral part was crimson in colour.

As in other *Calotes* lizards [6], the present specimens had large dorsal and flank scales which are regular in size, pointed, strongly keeled and arranged in series with the keels pointing backwards and upwards. The tympanum is distinct.

Calotes emma is "a jungle-loving form, and

as such, liable to escape detection. Its powers of colour change are slight, consisting chiefly in an accentuation of the darker markings on annoyance or irritation." [4]. Our encounter with *Calotes emma alticristatus* at Jeram Linang indicated that, like the Common Gliding Lizard *Draco sumatranus* Schlegel 1844 which was also sighted there, the lizard could be easily observed. It did not appear uncommon and therefore noteworthy that it had not been recorded before in Peninsular Malaysia except a picture posted in the web and attributed to *Calotes emma alticristatus* taken in Penang by Milivoje Krvavac in 2007 but without other information [7].

The type locality for *Calotes emma alticristatus* is Yunnan-fu, Yunnan, China [8]. This subspecies occurs typically in South China to peninsular Thailand [5]. It does not occur west of Thailand [9]. The taxon there has been named *Calotes chincollium* Vindum 2003 which does not possess large postorbital spine [9].

It is evident from the literature that the geographical distribution (and taxonomy) of *Calotes emma* as well as the two subspecies needs to be carefully investigated. Specifically, are the two subspecies sympatric? For example, in Peninsular Malaysia is *Calotes emma emma* confined to the western part of the country (Perlis, Kedah and Perak) and *Calotes emma alticristatus* confined to the eastern part (Kelantan in the present report)? And how far south has it extended its range?

Acknowledgement – This study is supported by University of Malaya PJP Research Grant FS295/2008A.

REFERENCES

1. Manthey U. and Denzer W. (2000) Description of a new genus, *Hypsicalotes* gen. nov. (Sauria: Agamidae) from Mt. Kinabalu, North Borneo, with remarks on the genetic identity of *Gonocephalus schultzewestrumi* Urban, 1999. *Hamadryad* **25**: 13-20.
2. Denzer W. and Manthey U. (1991) A nominal list of the lizards inhabiting Peninsular Malaysia and Singapore. *Raffles Bulletin of Zoology* **39**: 309-322.
3. Lim K.K.P. and Chou L.M. (1990) The herpetofauna of Singapore. *In* Chou L.M. and Ng P.K.L. (eds) *Essays in Zoology* pp 49-59. Department of Zoology, National University of Singapore, Singapore.
4. Boulenger G.A. (1903) Report on the batrachians and reptiles. *Fasciculi Malayensis*: 131-176.
5. Cox M.J., van Dijk P.P., Nabhitabhata J. and Thirakhupt K. (1998) *A photographic guide to snakes and other reptiles of Peninsular Malaysia, Singapore and Thailand.* New Holland Publishers (UK) Ltd.
6. Boulenger G.A. (1912) *A vertebrate fauna of the Malay Peninsula from the Isthmus of Kra to Singapore including the adjacent islands. Reptilia and Batrachia.* Government of the Federal Malay States, Kuala Lumpur.
7. Ekspedicija "Malaja '07". www.ib.ns.ac.yu.
8. Schmidt K.P. (1925) New Chinese amphibians and reptiles. *American Museum Novitates* (175): 1-3.
9. Vindum J.V., Win H., Thin T., Lwin K.S., Shein A.K. and Tun H. (2003) A new *Calotes* (Squamata: Agamidae) from the Indo-Burman range of western Myanmar (Burma). *Proceedings of the California Academy of Sciences* **54**: 1-16.

Journal of Science and Technology in the Tropics (2009) **5**: 39-43

Operating parameters for extreme ultraviolet radiation generation based on the United Nations University/International Centre for Theoretical Physics (UNU/ICTP) plasma focus device

P. Tangjitsomboon[1], D. Ngamrungroj[1], C. S. Wong[2] and R. Mongkolnavin[1*]
[1]Department of Physics, Faculty of Science, Chulalongkorn University,
Bangkok 10330, Thailand
(*E-mail: rmongkolnavin@gmail.com)
[2]Plasma Research Laboratory, Physics Department, Faculty of Science, University of Malaya,
50603 Kuala Lumpur, Malaysia

Received 4-2-2009; accepted 27-3-2009

Abstract Extreme ultravilolet (EUV) radiation sources are currently drawing much interests, as they are being developed to comply with the demands of the production of the next generation semiconductor chips. The wavelength of interest for next generation lithography is around 13.5 nm. In this work, the United Nations University/International Centre for Theoretical Physics (UNU/ICTP) plasma focus device which is known to be a powerful source of radiation is considered as the possible source. A plasma computational model is used to determine the suitable parameters for EUV radiation production. For the determination of EUV production, the physical parameters such as the configuration of the electrodes are fixed while the input energy and operating pressure using xenon gas are varied. From the calculation, the discharges with input energy range of 184 J to 454 J and using xenon gas at pressure of 1 mbar is found to be able to yield radiation covering the 13.5 nm EUV region with total power in the range of 6×10^{10} W to 1.6×10^{11} W. This shows and confirms the possibility of developing a plasma focus as a powerful EUV radiation source for future semiconductor industry.

Keywords extreme ultraviolet radiation – semiconductor – plasma focus – lithography

INTRODUCTION

Recently, extreme ultraviolet (EUV) radiation at a wavelength of 13.5 nm has attracted much interests as there are demands for the production of the next generation semiconductor chips [1]. Many plasma based EUV radiation sources such as the laser produced plasma and pulsed discharge sources such as the capillary discharge, vacuum spark and plasma focus are being considered by researchers worldwide [2]. These radiation sources, especially the pulsed discharge sources, could be the sources for Next Generation Lithography (NGL) because of their lower cost and simplicity compared to laser produced plasma and synchrotron sources. Various plasmas such as argon, xenon and tin have been investigated for generating EUV radiation around 13.5 nm [2-5]. The demands for high power EUV radiation lead to the requirement for optimization of these plasma discharge devices.

In this paper, we report a possibility of using the plasma focus as a EUV radiation source by simulating the plasma generation process using a computation model [6]. It is well known that the plasma focus device [7] is capable of producing dense transient high temperature plasmas since the 1960s. It is an inexpensive and compact source of intense X-rays [8-9], neutrons [10], and beams of ions [11] and electrons [12]. It also has potential applications as a high-brightness source for lithography and soft X-ray microscopy [8]. The X-ray energy produced in a plasma focus discharge can be as much as ~10% of the stored capacitor energy [13]. It is known that these X-rays emitted from the plasma focus may consist of Bremsstrahlung, recombination, and line radiation [14]. The detailed characteristics of the radiation emission from a plasma focus device may depend, in a rather complicated way, on the design and operating parameters of the plasma focus device such as the stored capacitor energy, the plasma

discharge current, the physical configuration, as well as the materials of the electrodes and insulator, the gas pressure and its composition. A simulation based on the 5 phase dynamics of a plasma focus is used to calculate the radiation power that covers the EUV wavelength region by varying the physical parameter of the plasma focus as well as its initial stored energy and the operating pressure. The calculation of the radiation power produced during the radiation phase would give a good indication of possible emission power as well as optimized values of plasma focus parameters when operating as EUV radiation source.

COMPUTATIONAL MODEL

For a plasma at electron temperature T_e, the peak of the continuum of its radiation emission spectrum is expected to be at a wavelength of $\lambda_0 = 620/T_e$, where T_e is in eV and λ_0 is in nm [14]. The line radiation emitted from the plasma depends on the ionic species present, as predicted by the Corona Equilibrium (CE) Model, which is again determined by the electron temperature of the plasma. The species of xenon that may be of interest are Xe^{10+} and Xe^{25+}, as these two species have line radiations around the wavelength of interest [15]. Considering both the continuum and line emissions, a xenon plasma with electron temperature ≅40 eV is expected to emit prominantly the 13.5 nm EUV radiation.

By using the computation model developed by Lee [6] which simulates the dynamics of five phases of the plasma focus, the plasma temperature can be determined. In this simulation, the five phases are axial phase, radial inward shock phase, radial reflected shock phase, radiation phase and expanded column axial phase. During the radiation phase we assume that the pinched plasma column has reached equilibrium at maximum electron temperature. The computational model has been verified with experiments on the 3 kJ UNU/ICTP plasma focus device and is found to be in good agreement [6].

According to the CE model, the population of ions with charge z+1 and z can be related by:

$$N_{z+1}/N_z = 1.27\times10^8 \times \zeta T_e^{3/4} \exp(-\chi_z/T_e)/\chi_z^{11/4}$$

where N_{z+1} and N_z are the number densities of ions in z+1 and z ionized sate respectively, ζ is the number of electron in the outer shell and χ_z is the ionization potential of z^{th} ion in eV.

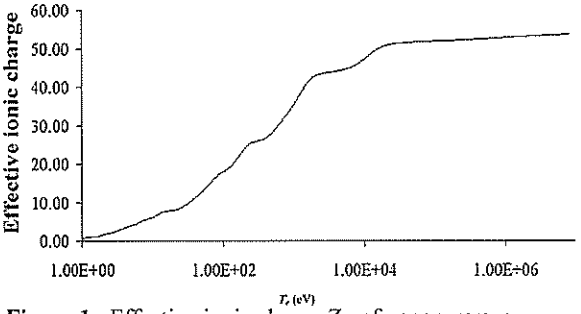

Figure 1. Effective ionic charge Z_{eff} of xenon versus electron temperature T_e based on the CE Model.

The effective ionic charge, Z_{eff} is calculated by $Z_{eff} = N_e/N_i = \sum_{z=0} z \cdot N_z \Big/ \sum_{z=0} N_z$, where the fractional density α_z is defined by $\alpha_z = N_z/N_i$, N_e is the electron number density while N_i is the ion number density. From the above equations the relationship between Z_{eff} and T_e can be plotted as shown in Figure 1.

We consider the radiation emission during the radiation phase, where the power of radiation generated by the plasma is given by [13]:

$$\frac{dQ_{rad}}{dt} = \int_{V_p} (P_b + P_l + P_r)dV,$$

where P_b is the power density of Bremsstrahlung given by $1.69\times10^{-38} N_e T_e^{1/2} \sum_z N_z Z^2$,

P_l is the power density of line radiation given by $3.95\times10^{-35} N_e N_i Z_n^4 / T_e$, and P_r is the power density of recombination given by $5.5\times10^{-37} N_e T_e^{-1/2} \sum_z N_z Z^4$.

The plasma temperature during this phase can be determined by equating the magnetic pressure and the plasma pressure that is given by:

$$T_e = \mu f_c^2 I^2 / (8\pi^2 e(1+Z_{eff}) N_i r_p^2),$$

which depends on the radial position of the piston during the radiation phase r_p and the discharge current I. In this expression, μ is the permuability of free space and f_c is the fraction of current that is flowing in the current sheet. For plasma with electron temperature suitable for EUV emission, the electron density N_e is given by:

$$N_e \approx 6.5\times10^{16}(z+1)^6 T_e^{1/2} \exp[0.1(Z+1)^2/T_e],$$

and N_i is assumed to be N_e/Z_{eff}.

Based on this computational model which takes into account the movement of the plasma and the electrical discharge of the plasma focus as well as the radiation process, we can investigate the relationship between the plasma temperature and the power of the radiation. As mentioned earlier, the radiation power P_b, P_r and P_l mentioned earlier consist of radiations of all possible wavelengths. We will consider only plasma focus discharges where the electron temperature at the radiation phase is ≅40 eV where radiations with wavelength in the 13-14 nm range is dominant.

The radiation power from the UNU/ICTP plasma focus device is computed for discharge voltage in the range of 1–10 kV, and the length of the anode in the range of 1-5 cm when operating at pressures between 0.5 mbar and 2.5 mbar. With reference to Figure 2, the cathode radius is fixed at b = 3.2 cm and that of the anode is a = 0.95 cm. The discharge voltage is varied in a 0.5 kV step while the length of the anode by 0.5 cm step for a compilation of resulting radiation power at different operating pressures.

The calculation of the radiation power is carried out for discharges with electron temperature of around 40 eV at the radiation phase. In this work, xenon gas is chosen as the operating gas since in previous work this gas is widely used as a source of EUV radiation by pulsed plasma discharge device. The plasma focus device characteristic constants used in the computational are 0.08 for the mass factor (MASSF) which is the fraction of mass swept down the plasma focus tube in the axial direction, 0.7 for the fraction of the current flowing in the current sheath (CURRF) and 0.16 for the radial mass swept up factor (MASSFR). These factors are obtained by fitting the typical experimental current waveform of a UNU/ICTP plasma focus device that has an inductance L_0 = 110 nH, resistance r_0 = 0.012 Ω and the capacitance C_0 = 30 μF [6].

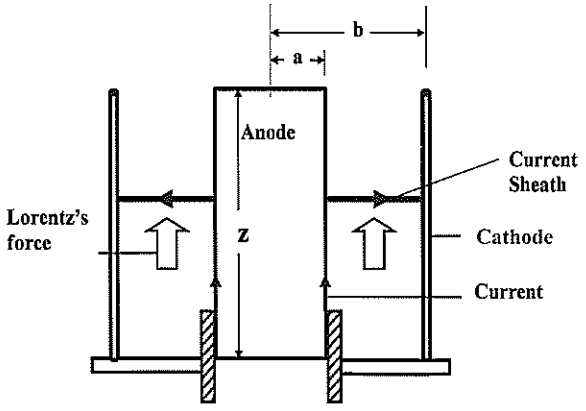

Figure 2. Schematic of the geometry of a plasma focus device.

RESULTS AND DISCUSSION

Figure 3 shows the surface plots of radiation power for discharges at various operating voltages, and the length of the anode. In this case the range of input electrical energy is 135 J to 1,215 J which correspond to discharge voltage of 3 kV and 9 kV respectively. It can be seen that there is a specific relationship between the input energy and the length of the anode. More input energy is required if the anode is lengthened which, in general, is in a ratio of 4 cm to 3 kV. Also by using higher operating gas pressure, the plots show that higher total radiation power can be obtained even though the velocity of the current sheath is observed to decrease as predicted by the model computation . At the same length of anode when operating pressure is increased, the input energy must also be increased in order to obtain the targeted plasma temperature. The increase in operating voltage required can be estimated to be 1 kV for every 0.5 mbar increase in operating pressure. A pressure of more than 1.5 mbar in combination with input energy of 375 J and anode length of 2 cm is required to yield a radiation power of more than 25×10^{10} W.

By looking closely at the required plasma temperature of around 40 eV that is possible to produce EUV radiation, combinations of parameters of V, z as well as the operating pressure that allow UNU/ICTP plasma focus to give maximum radiation power, where a majority is expected to be contributed by the line radiation, are shown in Figure 4. The size of the bubble represents the radiation power obtained for each combination of parameters. It can be seen that 1 mbar operating pressure gives the highest radiation power, which can be as much as 10.4×10^{10} W, when having longer anode of 4 cm and operating with stored input energy of 375 J. Other operating pressures are also possible to produce plasma with the required temperature but with less resulting radiation power. By selecting the length of the anode to be 2 cm, it can be seen from the result that this length can accommodate different operating pressures with their corresponding discharge voltages to yield reasonable radiation power of approximately 7.7×10^{10} W.

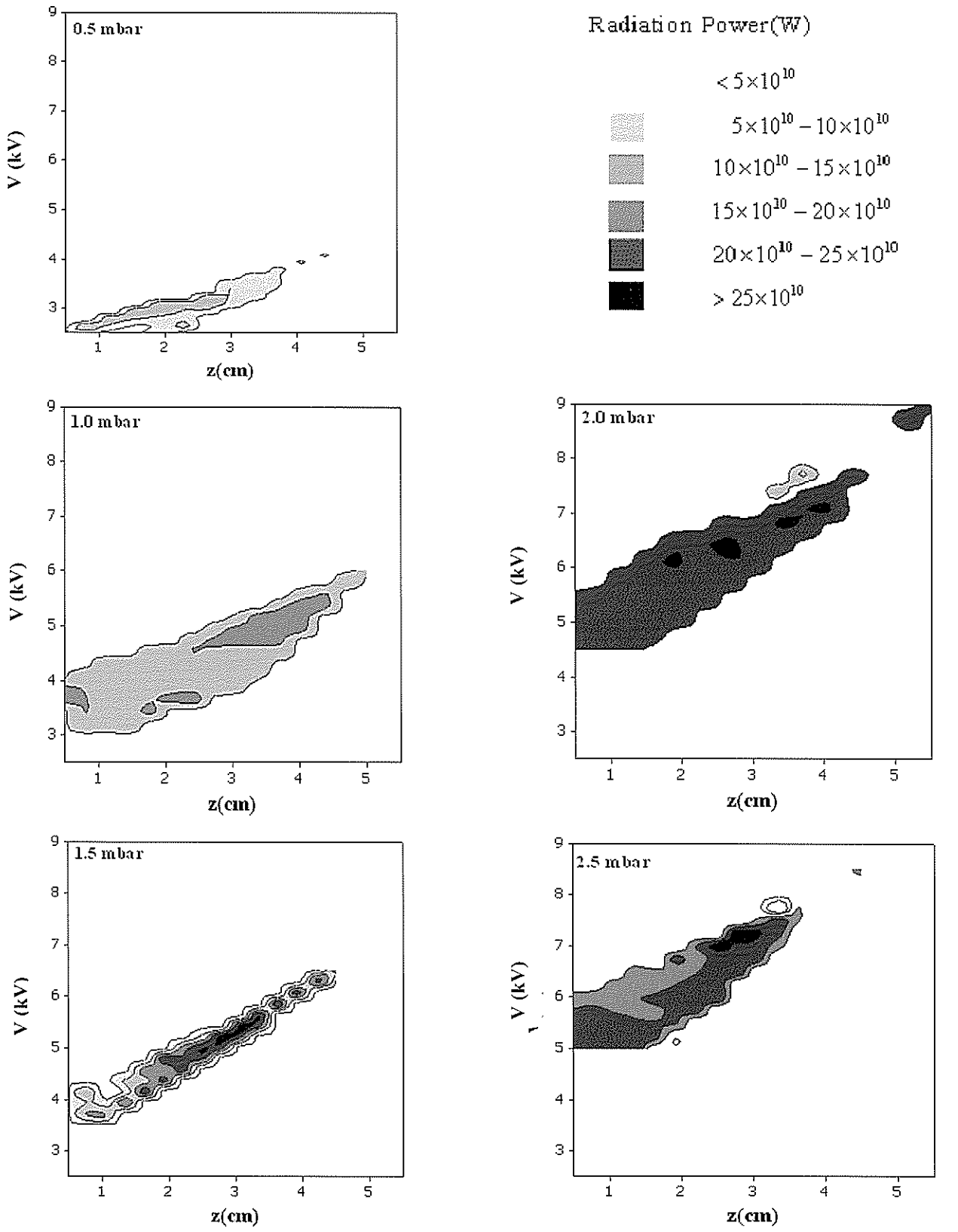

Figure 3. Surface plots showing total radiation power for different operating voltages, V, and lengths of anode, z, under different operating pressures.

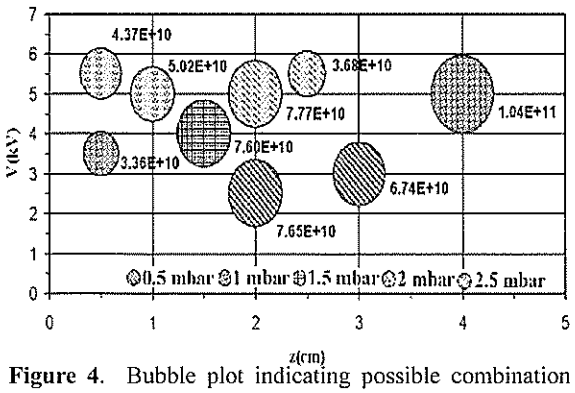

Figure 4. Bubble plot indicating possible combination of voltages, V, and length of the anode, z, at different operating pressures in producing radiation power that correspond to plasma temperature of 40 eV.

CONCLUSION

It has been demonstrated from the theoretical point of view that a UNU/ICTP plasma focus device can produce EUV radiation by its radiation mechanism with suitable operating parameters. From the calculation, it was found that with input energy range of 184 J to 454 J, operation with xenon gas at pressure of 1 mbar can yield 13.5 nm EUV radiation with total power in the range of 6×10^{10} W to 1.6×10^{11} W. The optimum operating voltage is found to be 5 kV with the anode length of 4 cm for producing maximum radiation power of 10.4×10^{10} W associated with the required plasma temperature of 40 eV. This shows and confirms the possibility of developing a plasma focus as a powerful EUV radiation source for NGL as well as showing the possibility of physical scaling of the plasma focus in the future. Further work that may be carried out is to experimentally verify this result and varying other parameters for future compact EUV generating plasma focus device.

Acknowledgements – The authors would like to extend great appreciation to Asian African Association for Plasma Training (AAAPT) for its support to initiate plasma focus research in this laboratory.

REFERENCES

1. Banine V., et al. (2004) Plasma source for EUV lithography exposure tools. *J. Phys. D: Applied* **37**: 3207-3212.
2. Chew S.H. and Wong C.S. (2006) X-ray and EUV emission characteristics of a vacuum spark *J. Sci. Technol. in the Tropics* **2**: 125 - 129.
3. Bowering N., et al. (2004) Extreme ultraviolet emission spectra of highly ionized xenon and their comparison with model calculations. *J. Appl. Phys.* **95**: 16-23.
4. Sasaki A., et al. (2004) Simulation of the EUV Spectrum of Xe and Sn Plasmas. *IEEE J. Quantum Electronics* **10**: 1307-1314.
5. Kieft E.R., et al. (2005) Comparison of experimental and simulated extreme ultraviolet spectra of xenon and tin discharges. *Phys. Rev. E*: **71**: 1539-3755.
6. Lee S. (2005) Plasma Focus (Radiative) Computation Model ICTP. *Italy Open Access Archive*,Trieste.
7. Mather J.W. (1964) *Phys. Fluid Suppl* **7**: 28.
8. Rawat R.S., et al. (2004) Effect of insulator sleeve length on soft x-ray emission from a neon-filled plasma focus device. *Plasma Sources Sci. Technol* **13**: 569-575.
9. Herold H., et al. (2002) Measurement of Argon Ion Beam and X-ray Energies in Plasma Focus Discharge. *Physica Scripta* **65**: 350-355.
10. Yap S.L., Wong C. S., Choi P., Dumitrescu C. and Moo S. P. (2005) Observation of two phases of neutron emission in a low energy plasma focus. *Jpn. J. Appl. Phys* **44**: 8125-8132.
11. Wong C.S. and Yap S.L. (2005) Generation of deuteron beam from the plasma focus. *Solid State Phenomena* **107**: 151-155.
12. Choi P., Deeney C., Herold H. and Wong C.S. (1990) Characterization of self-generated intense electron beams in a plasma focus. *Laser and Particle Beams* **8**: 469-476.
13. Liu M. (1996) *Soft X-rays from compact plasma focus*. PhD Thesis, Nanyang Technological University.
14. Wong. C.S. (2002) Plasma radiation sources. *J. Fiz. Mal.* **23**: 4-10.
15. http://physics.nist.gov/PhysRefData/ASD/lines_form.html.

Journal of Science and Technology in the Tropics (2009) **5**: 45-51

Global oscillations in networks of integrate-and-fire neurons

S. C. Chan, Danny W. K. Ng and S. Y. Goh
Faculty of Engineering and Science, University Tunku Abdul Rahman,
Jalan Genting Kelang, 53300, Setapak, Kuala Lumpur, Malaysia
(Email: chansc@mail.utar.edu.my)

Received 15-12-2008; accepted 08-04-09

Abstract. We analyzed the dynamics of a sparsely connected network consisting of inhibitory integrate-and-fire (IF) neurons using a numerical simulation based on the standard Euler algorithm. The frequency of the global oscillations obtained from this simulation is in good agreement with a parallel computation based on the exact analytical solution of the basic equations of the IF model, confirming the accuracy of the numerical simulations. We were also able to generate simulation results that are in good agreement with a special case reported in an earlier publication. We further investigated the effect of other parameters of the IF model on the frequency of the global oscillations. The results show that the global oscillations are significantly affected by the form of the leakage term, the network size, the connection probability, the external noise, the synaptic delay and the synaptic weight.

Keywords oscillation – inhibitory – integrate-and-fire – neurons – network

INTRODUCTION

Electrical recordings of brain activity show the presence of oscillation in different brain structures, with frequencies ranging from 0.5 Hz (δ rhythm) to 40-80 Hz (γ rhythm), and even up to 200 Hz [1]. In vivo [2] and in vitro [3] experiments and theoretical studies [4-10] showed that recurrent inhibition plays an important role in the synchronization of neural firing. Brunel et al. [11] using a simple integrate-and-fire (IF) neuron model [12] showed that recurrent inhibition allows a sparsely connected network to generate a distinct and robust type of global oscillation possessing a fast rhythm.

The IF neuron model is often used to study the behaviour and properties of large, interacting neuronal networks instead of more detailed neuronal models (such as Hodgkin-Huxley model) [13]. The IF neuron model has been used widely in many studies of phase-locking, clustering [4, 6, 7] and synchronization [13] phenomena observed in biological neural network. This model serves as the basis for exploration on the mechanisms of basic brain functions such as associative memory [14, 15] and pattern recognition [16].

The present paper investigates the effect of the various parameters of the IF neuron model on the global oscillations of a network of sparsely connected neurons.

MATERIAL AND METHODS

Description of the network

We analyzed the dynamics of a network which is composed of N identical inhibitory IF neurons. Each neuron received C randomly inhibitory connections from other neurons in the network and excitatory external inputs of rate $C_{ext}\nu_{ext}$ from neurons outside the network.

In the network, each neuron i is described by its membrane potential, $V_i(t)$ at time t_i. When the pre-synaptic neuron j emits a spike at time t, the potential of the postsynaptic neuron is increased or decreased by postsynaptic potential (PSP) amplitude J_{ij} at time t + D. For simplicity, we took a single transmission delay, D and PSP amplitudes to be the same at each synapse. For excitatory external synapses, $J_{ij} = J_{ext}$ where $J_{ext} > 0$ and $J_{ij} = -J$ for inhibitory synapses. When $V_i(t)$ crosses the prescribed threshold, neuron i emits a spike and the firing is followed by the

instantaneous resetting of the membrane potential to resting potential, V_r.

Excitatory external input

In this study, we assumed each neuron within the network received an excitation signal from external network. The total effect of the external network is denoted as an external Poisson input. External spikes are statistically independent and can be well approximated by a Poisson distribution with mean firing rate $C_{ext}\nu_{ext}$. The average part, μ_{ext} and fluctuating part, σ_{ext} of the external synaptic input are explicitly given by equations (1a) and (1b) [11] where τ is membrane time constant.

$$\mu_{ext} = c_{ext} J_{ext} \upsilon_{ext} \tau \qquad (1a)$$

$$\sigma_{ext} = J_{ext} \sqrt{c_{ext} \upsilon_{ext} \tau} \qquad (1b)$$

Integrate-and-fire neurons model

The differential equation that governs the dynamics of the membrane potential for neuron i (i =1, 2, 3... N) at time tt can be written as follow:

$$cV_i(t) = -L(V_i, t) + I_i(t) \qquad (2)$$

where $I_i(t)$ is the total synaptic currents arriving at the soma and $L(V_i, t)$ is the generic leakage term.

The general leakage term can be modeled as $L(V_i, t) = \dfrac{(V_i - V_r)}{R}$ [17]. The membrane potential $V_i(t)$ at the soma obeys the equation.

The time evolution of depolarization $V_i(t)$ of neuron i, is as shown in equation (3).

$$\tau \frac{dV_i(t)}{dt} = -(V_i(t) - V_r) + RI_i(t) \qquad (3)$$

The above equation takes into account the resting potential of the simulated neuron. The simplest form of representation of input current [13] is chosen for this solution where

$$I_i(t) = \sum_j w_j \sum_k q\delta(t - t_j^k - D) \qquad (4)$$

Having the total charge that is injected in a postsynaptic neuron, $q=CJ_{ij}$ and efficacy $w_{ij}=1$ the equation $RI_i(t)$ will become

$$RI(t) = \tau \sum_j J_j \sum_k \delta(t - t_j^k - D) \qquad (5)$$

where t_j^k is the emission time of k-th spike at neuron j.

Here we will attempt to reproduce the results using two different methods of solving equation (3).

Numerical and analytical solution

We solved equation (3) numerically to obtain a numerical solution defining the membrane potential. The forward Euler difference scheme [18, 19] turns equation (3) into the following discrete form,

$$V_i(t + \Delta t) - V_i(t) = \frac{\Delta t}{\tau}[-V_i(t) + RI(t)] \qquad (6)$$

We approximated Dirac-delta function with a unit square of width Δt, equation (5) becomes

$$RI(t) = \frac{\tau}{\Delta t} \sum_j J_j \sum \delta(t - t_j^k - D) \qquad (7)$$

With the fixed time step Δt, the changes in the membrane potential is approximated by

$$V_i(t + \Delta t) = V_i(t) + \sum_j J_j \sum_k \delta(t - t_j^k - D) - \frac{\Delta t}{\tau}(V_i(t) - V_r) \qquad (8)$$

To determine the accuracy of the numerical equation, equation (3) was then solved analytically using Laplace transform to get the exact solution. The Laplace transform of the membrane potential $V_i(t)$ is denoted by

$$W_i(t) = L[V_i(t)] = \int_0^\infty e^{-st} V_i(t) dt \qquad (9)$$

The Laplace transform of equation (3) equates to

$$sW_i(s) - V_i(0) = -\frac{1}{\tau}\left[W_i(s) - \frac{V_r}{s}\right] + \sum_j J_{ij} \sum_k e^{-(t_j^k + D)s} \qquad (10)$$

The membrane potential below the firing threshold is described by

$$V_i(t) = L^{-1}[W_i(s)]$$
$$= (V_i(0) - V_r)e^{-\frac{t}{\tau}} + V_r +$$
$$\sum_j J_j \sum_k u(t - t_j^k - D) e^{-\left(\frac{t - t_j^k - D}{\tau}\right)} \qquad (11)$$

where u(t) is the unit-step function defined by

$$u(t) = \begin{cases} 1 & t \geq 0 \\ 0 & t < 0 \end{cases} \text{ and}$$

The membrane potential $V_i(t)$ evolves continuously until it reaches a threshold V_{th}.

It is noted that Brunel *et al.* [11] used a simplified leakage term $L(V_i,t)=\frac{V_i}{R}$ in his equations. For the purposes of comparison with their results, the use of the simplified leakage term $L(V_i,t)=\frac{V_i}{R}$ will yield corresponding relationships to replace equations (8) and (11).

The corresponding formula for the changes in the membrane potential using the Forward Euler difference scheme is as follows:

$$V_i(t+\Delta t)=V_i(t)+\sum_j J_j \sum_k \delta(t-t_j^k-D)-\frac{\Delta t}{\tau}(V_i(t)) \quad (12)$$

And the corresponding formula for the exact solution method is

$$V_i(t)=V_i(0)e^{-\frac{t}{\tau}}+\sum_j J_j \sum_k u(t-t_j^k-D)e^{-(\frac{t-t_j^k-D}{\tau})} \quad (13)$$

RESULTS AND DISCUSSION

Comparison of numerical simulation results with those obtained from the exact solution

The simulations were carried out using parameters similar to those used by Brunel *et al.* [11] which are 5000 inhibitory neurons with 1000 connections, $\tau = 20$ ms, $D = 2$ ms, $J_{ij} = 0.1$ mV, $\sigma_{ext} = 1$ mV, $\mu_{ext} = 25$ mV.

The numerical simulation results are shown in figure 1 and the results based on the exact solution are shown in figure 2. They are in good agreement confirming the accuracy of the numerical simulations.

Simulation using the simplified leakage term produced result shown in figures 3 and 4. Figure 3 shows the numerical simulation results and figure 4 shows the results based on the exact solution method. It may be observed that the frequency of global oscillations obtained from both methods is in close agreement with the results by Brunel *et al.* [11].

It may be noted that the frequency of global

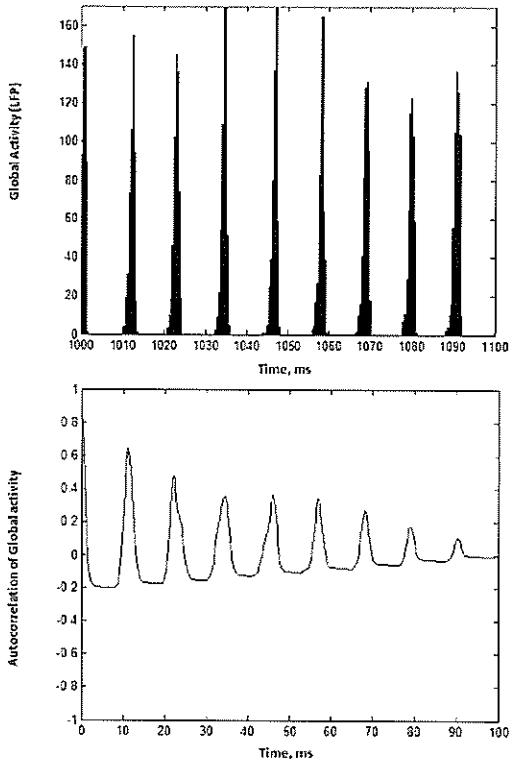

Figure 1. Global activity (top) and autocorrelation of global activity (bottom) for more general leakage term during 100 ms interval using Standard Euler Algorithm.

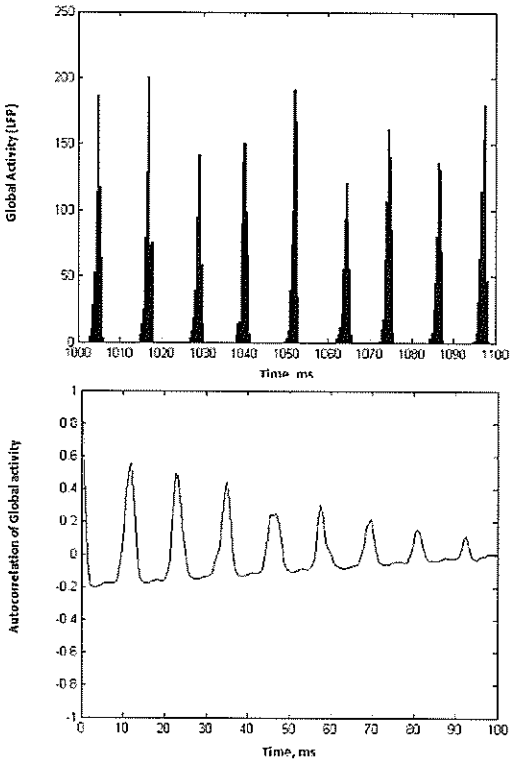

Figure 2. Global activity (top) and autocorrelation of global activity (bottom) for More General Leakage Term during 100ms interval using Exact Analytical Solution.

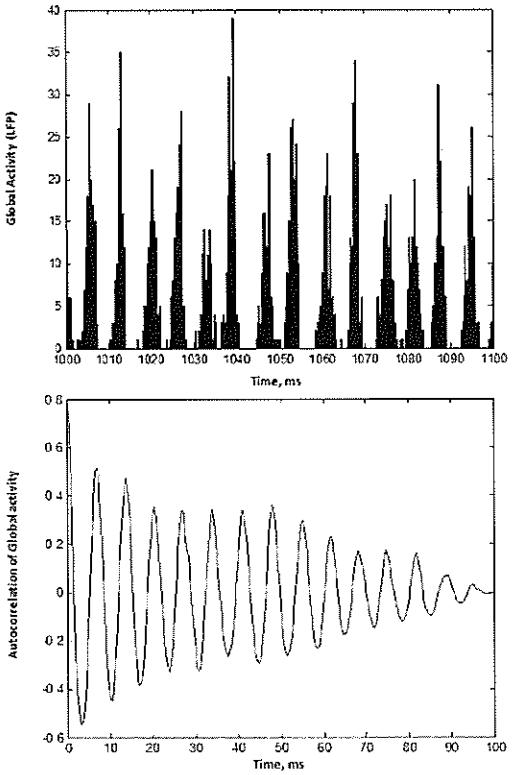

Figure 3. Global activity (top) and autocorrelation of global activity (bottom) for Simplified Leakage Term during 100ms interval using Standard Euler Algorithm

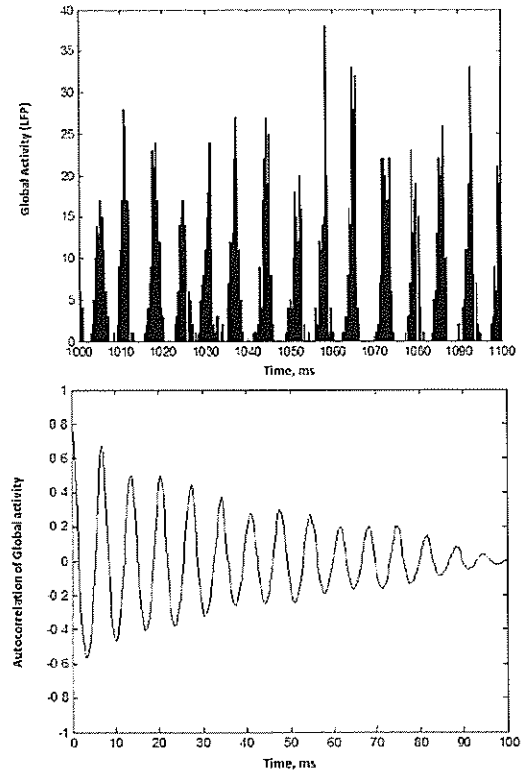

Figure 4. Global activity (top) and autocorrelation of global activity (bottom) for Simplified Leakage Term during 100ms interval using Exact Analytical Solution.

oscillations is 140 Hz if the simplified leakage term is used as compared to 90Hz if the more general leakage term is used.

Investigation of the effect of other network parameters

Numerical simulations using the more general form of the leakage term are used to investigate the effect of other network parameters – the network size (N), the connection probability (ε), the external noise (σ_{ext}), the synaptic delay (D) and the synaptic weight (w_{ij}) of the IF model on the global oscillations.

Network size The size of the neuronal network (N) was increased while other parameters of the network were kept constant. The other parameters of the network were ε = 0.2, τ = 20 ms, D = 2 ms, J_{ij} = 0.1 mV, and μ_{ext} = 25 mV. Figure 5 shows the variation of the global oscillation frequency with size of the neuronal network for three noise levels of 1 mV, 4 mV and 8 mV. The frequency of global oscillations decreases sharply as the number of neurons N in the network increases for N less than 50,000. For N greater than 100,000, the frequency of global oscillations did not change significantly. It may be observed that the frequency of global oscillations increased with external noise from 1 mV to 8 mV.

External noise For this simulation, N was chosen to be 130,000 neurons to eliminate the effect of network size on the frequency of global oscillations. The effect of different external noise levels to the network was investigated. The following parameters were kept constant: N = 130,000 neurons, τ = 20 ms, ε = 0.2, D = 2 ms, J_{ij} = 0.1 mV, and μ_{ext} = 25 mV. Figure 6 shows that the frequency of global oscillation increases with external noise until 8 mV after which it remains relatively constant.

Connection probability Different connection probability for the network was simulated. A network of 130,000 neurons was chosen to eliminate the effect of N on the global oscillations. For each curve, with the exception of connection probability, the other parameters remained the same:

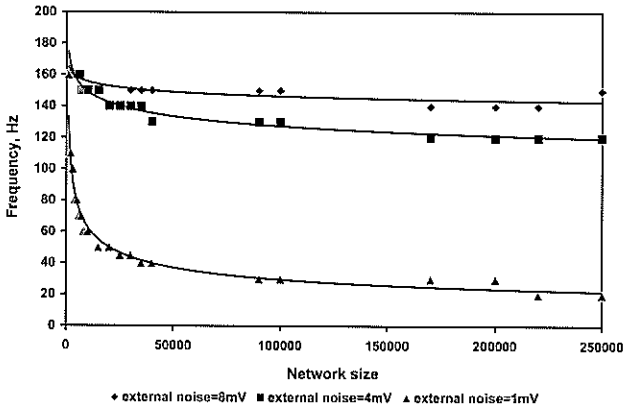

Figure 5. Frequency of global oscillation for different network size.

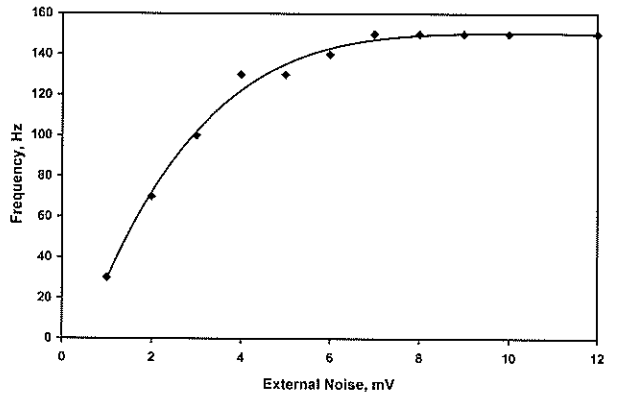

Figure 6. Frequency of global oscillation for different external noise.

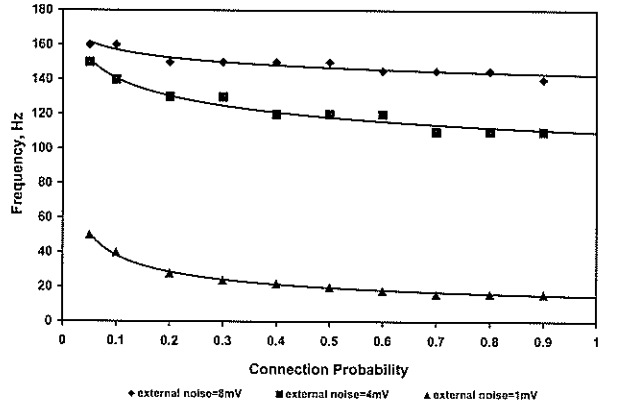

Figure 7. Frequency of global oscillation for different connection probability.

τ = 20 ms, D = 2 ms, J_{ij} = 0.1 mV, and μ_{ext} = 25 mV. Three curves were generated for external noise, σ_{ext} = 1 mV, σ_{ext} = 4 mV and σ_{ext} = 8 mV. Figure 7 shows that the frequency of oscillation

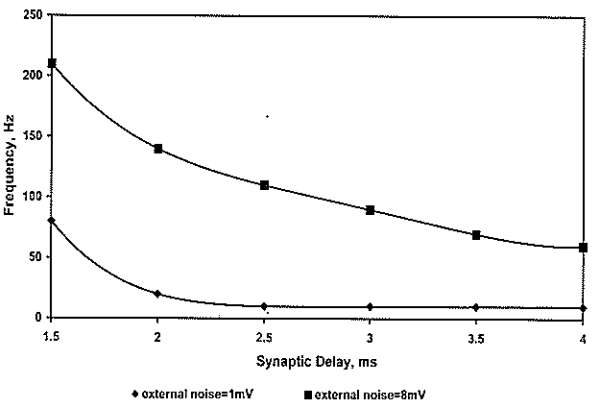

Figure 8. Frequency of global oscillation for different synaptic delay.

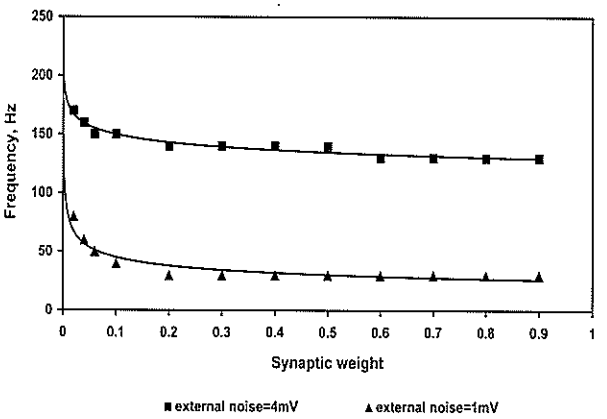

Figure 9. Frequency of global oscillation for different synaptic weight.

decreases slightly when the network varies from sparsely to highly connected.

Synaptic delay The next parameter that we varied was the synaptic delay of the network. A network size of 130,000 with connection ratio of 0.2 was used. Other parameters of the network were τ = 20 ms, J_{ij} = 0.1 mV and μ_{ext} = 25 mV. External noise level of σ_{ext} = 1 mV and σ_{ext} = 8 mV were used for the simulation. Figure 8 shows the results of the simulation. At low synaptic delays, the frequency of the oscillation is very high. With higher delay times, the frequency of global oscillation decreases.

Synaptic weight The synaptic weights in between the neurons were varied in the section. Synaptic

Journal of Science and Technology in the Tropics (2009) **5**: 5-9

Fish faeces as a potential food source for cultivating the water flea, *Moina macrocopa*

Jiun Yan Loh[1], Chee Wun How[1], Yii Siang Hii[2], Gideon Khoo[1]* and Han Kiat Alan Ong[1]

[1]Faculty of Engineering and Science, Universiti Tunku Abdul Rahman, Setapak 53300, Kuala Lumpur, Malaysia

[2]Department of Fishery Science and Aquaculture, Faculty of Agro-technology and Food Science, Universiti Malaysia Terengganu, 21030 Kuala Terengganu, Malaysia

*(Email: gideonkhoo@utar.edu.my)

Received 20-01-2009; accepted 05-02-2009

ABSTRACT The reproductive performance and survival of the freshwater cladoceran, *Moina macrocopa*, fed with faeces of *Oreochromis niloticus*, *Chlorella* powder and *Spirulina* powder were investigated for a period of 12 days. *M. macrocopa* neonates were treated with the diets at 3.5 g/L throughout the experiment. Complete mortality of *M. macrocopa* fed with *Chlorella* was noted on day 10 while the peak population was reached on day 9. For *M. macrocopa* fed with *Spirulina*, 100% mortality occurred on day 8 and it took 7 days for the population to reach its peak. Survival of *M. macrocopa* fed with fish faeces was the highest among the diets (12 days), but it also took the longest time to reach the population peak. Treatment with fish faeces also produced the highest number of neonates. These findings indicate that fish faeces is a potential medium for livefeed culture.

Keywords *Moina macrocopa* – fish faeces – neonates – *Spirulina* – *Chlorella*

INTRODUCTION

Sustainable development in agriculture is a contemporary global issue. Environment-friendly strategies such as generation of renewable energy from waste materials and recycling of effluent water from human activities have been promoted to improve the quality of life. One area that has shown great potential for commercial and industrial application is the conversion of liquid and solid wastes of animal and plant origins into a recyclable resource that can be further utilized by society.

Liquid and solid wastes from commercial farms and households contain high amounts of nutrients, e.g., nitrogen- and phosphorus-based compounds. Excess uneaten fish feed and fish faeces are the main contributors of nitrogenous wastes (ammonia, nitrites and nitrates) in effluent water discharged from intensive aquaculture farms [1]. In a study by Fivlstad *et al.* [2], it was shown that approximately 10-20% of total nitrogen in fish feed was lost through fish faeces. In the natural environment, these compounds provide the essential nutrients for phytoplankton and rooted aquatic macrophytes [1]. However, continuous discharge of wastewater into rivers, streams, lakes and other water bodies increases their organic load, which subsequently results in pollution. In order to better manage these natural resources without increasing the costs of wastewater treatment, organic wastes should be recycled rather than eliminated in an unproductive manner [3].

Several classes of zooplanktonic organisms, e.g., rotifers, brine shrimp, copepods and cladocerans (or water fleas) occupy an important position in the aquatic food web of tropical countries. Major sources of these organisms are collections from natural waters or cultures under controlled conditions, where they survive on organic matter and bacteria [4]. In many South-East Asian countries including Malaysia, domestic wastewater and sewage are commonly

weights of the network were varied from 0.02 to 0.9. Parameters of the network were N = 130,000, ε = 0.2, τ = 20 ms, J_{ij} = 0.1 mV and μ_{ext} = 25 mV. External noise level of σ_{ext} = 1 mV and 8mV were used for the simulation. The oscillation frequency remained relatively constant for most the synaptic weights. At lower synaptic weight, the stability of the oscillation was affected producing a noise like oscillation. Figure 9 shows the result for the simulation.

CONCLUSION

The dynamics of a sparsely connected network consisting of inhibitory integrate-and-fire (IF) neurons were investigated using a numerical simulation method based on the standard Euler algorithm. The frequency of the global oscillations obtained from this simulation is in good agreement with a parallel computation based on the exact analytical solution of the basic equations of the IF model, confirming the accuracy of the numerical simulations. The results are also in good agreement with published results.

We further investigated the effect of a more general form of the leakage term as well as other parameters of the IF model on the frequency of the network global oscillations. The network global oscillations are significantly affected by the form of the leakage term, the network size, the connection probability, the external noise, the synaptic delay and the synaptic weight.

REFERENCES

1. Gray C.M. (1994) Synchronous oscillations in neuronal systems: mechanisms and functions. *J. Comp. Neurosci.* **1**: 11-38.
2. MacLeod K. and Laurent G. (1996) Distinct mechanisms for synchronization and temporal patterning of odor-encoding neural assemblies. *Science* **274**: 976-979.
3. Whittington M.A., Traub R.D. and Jeffery J.G.R. (1995) Synchronized oscillations in interneuron networks driven by metabotropic glutamate receptor activation. *Nature* **373**: 612.
4. Van Vreeswijk C., Abott, L.F., and Ermentrout G.B. (1994) When inhibition not excitation synchronizes neural firing. *J. Comp. Neurosci.* **1**: 313-321.
5. Wang X-J. and Buzsáki G. (1996) Gamma iscillation by synaptic inhibitaion in a hippocamal interneuronal networn model. *J. Neurosci.* **16**: 6402.
6. Hansel D., Mato G. and Meunier C. (1993) Phase reduction and neural modeling. In Functional Analysis of the brain based on multiple-site recordings, *Concepts in Neuroscience* **4**: 192-210.
7. Abott L.F. and Van Vreeswijk C. (1993) Asynchronous states in networks of pulse-coupled oscillators. *Phys, Rev. E.* **48**: 1483-1490.
8. Hansel D., Mato G. and Meunier C. (1995). Synchrony in excitatory neural networks. *Neural Comp.* **7**: 307-337.
9. Gerstner W., van Hemman J.L., and Cowan L. (1996) What matters in neuronal locking. *Neural Comp.* **8**: 1653-1676.
10. Gerstner W., and Kistler W. (2002) *Spiking neuron models: Single neurons, populations, plasticity*. Cambridge University Press, Cambridge.
11. Brunel N. and Hakim V. (1999) Fast global oscillations in networks of integrate-and -fire neurons with low firing rates. *Neural Comp.* **11**: 1621-1671.
12. Knight B.W. (1972) Dynamics of encoding a population of neurons. *J. Gen. Physiol.* **59**: 734-766.
13. Mirollo R.E. and Strodatz S.H. (1990) Synchorization of pulse-coupled biological oscillators. *Siam J. Appl. Math.* **50**: 1645-1662.
14. Lee G. and Farhat N.H. (2001) The bifurcation neuron network 2: an analog associative memory. *Neural Networks* **15**: 69-84.
15. Lee G. and Farhat N.H. (2001) The bifurcation neuron network 1. *Neural Networks* **14**: 109-125.
16. Ruf B. and Schmitt M. (1998) Self-organization of spiking neurons using action potential timing. *IEEE Trans. Neural Networks* **9**: 575-578.
17. Abbott L.F. and Dayan P. (2001) *Theoretical neuroscience: computational and mathematical modeling of neural systems*. MIT Press, Cambridge, Mass.
18. Lee G. and Farhat N.H. (2001) The double queue method: a numerical method for integrate-and-fire neuron networks. *Neural networks* **14**: 921-932.
19. Hansel D., Mato G., Meunier C. and Neltner L. (1998) Numerical simulations of

integrate-and-fire neural networks. *Neural Comp.* **10**: 467-483.
20. Press W.H., Flannery B.P., Teukolsky S.A. and Vetterling W.T. (1992) *Numerical recipes: The act of scientific computing.* Cambridge University Press, Cambridge.

Journal of Science and Technology in the Tropics (2009) 5: 45-51

Journal of Science and Technology in the Tropics (2009) **5**: 53-57

Fatty acids from the cocoa butter deodorizer distillate

Samuel Yap Kian Chee[1], H. Sarini[1], A. Aminah[2] and S. Sabariah[1]
[1]Malaysian Cocoa Board, Lot 3, Jalan P/9B, Seksyen 13, 43650 Bandar Baru Bangi, Selangor, Malaysia
[2]Faculty Science & Technology, Universiti Kebangsaan Malaysia, Bangi, Selangor, Malaysia
(E-mail: Samuel@koko.gov.my)

Accepted 8-5-2009

Abstract Cocoa butter deodorizer distillate from one of the local cocoa grinders was selected and analyzed qualitatively and quantitatively by gas chromatography and gas chromatography mass spectrometer (GCMS). Crude cocoa butter deodorizer distillate contains about 80% of fatty acids. To eliminate compounds other than fatty acids, sample of the crude cocoa butter deodorizer distillate was treated with sodium hydroxide, dissolved in distilled water, and filtered. Fatty acids were precipitated by adding hydrochloric acid and vacuum dried. Analysis by gas chromatography showed that palmitic acid was the major compounds followed by oleic acid, stearic acid and linoleic acid.

Keywords cocoa butter deodorizer distillate – purification of fatty acids

INTRODUCTION

Cocoa butter is a pale yellow-to-yellow, transparent liquid at 37°C and above and solid at room temperature. It is obtained from well winnowed cocoa nib (cotyledons) of the cocoa tree, *Theobroma cacao*, after fermentation and roasting by hydraulic or expeller pressing [1].

Pure press butter needs no cleaning at all (besides filtration) but is frequently deodorized for use in milk chocolate in order to obtain the desired mild flavour [2]. In cocoa industry, deodorization of cocoa butter is done using superheated steam under vacuum. It entails the steam stripping of volatile substances from the butter. The process can take between 30 minutes and 3 hours depending on the degree of deodorization required. Cocoa butter is pumped into the deodorizer and heated to about 105°C. A vacuum is drawn and steam is admitted through the bottom of the deodorizer and distributed through the cocoa butter via a sparging system. The volatiles are carried over to a condenser where they are removed. Analysis showed that cocoa butter deodorizer distillate had total organic matter (TOM) more than 98%, saponification value (SAP) as 283.2 mg of sodium hydroxide, and contained unsaponifiable matter of 1%. Ash content was determined as 0.02%, moisture content was 1.17%, and pH of the sample was 4.85. The sample waste had 96.16 % m/m as oleic acid [3]. The objective of this paper is to report the fatty acids composition in the cocoa butter deodorizer distillate quantitatively and qualitatively and the method to extract fatty acids from the cocoa butter deodorizer distillate.

MATERIALS AND METHODS

Cocoa butter deodorizer distillate was collected from one of the local grinders in Malaysia. The sample, which is dark in colour and solid at room temperature, was melted in an oven at 55°C and homogenized. Standard mixture fatty acids methyl ester of C4–C24 was from Sigma. The quantitative of the standards used is listed in Table 1. Other chemicals used were from analytical grade reagents.

Sample preparation for analysis with gas chromatography

Fifty milliliters of the sample (crude cocoa butter deodorizer distillate or purified cocoa butter deodorizer distillate) was drawn, added with 150 mL methanol and 2 mL 37% concentrated sulphuric acid, and refluxed for 30 minutes. It was then washed twice with distilled water when cooled in a separating funnel. The organic layer, namely FAME, was collected, dried by anhydrous sodium sulphate and filtered. Ten milliliters filtered FAME was drawn and diluted with 90 mL of n-hexane.

Table 1. Quantitative of FAME standard mixture used.

PkNo	Time	Conc	Name
1	6.616	4.0000	C 4
2	8.389	4.0000	C 6
3	10.790	4.0000	C 8
4	13.209	4.0000	C 10
5	14.317	2.0000	C 11
6	15.441	4.0000	C 12
7	16.630	2.0000	C 13
8	17.969	4.0000	C 14
9	18.590	2.0000	C 14:1
10	19.477	2.0000	C 15
11	20.213	2.0000	C 15:1
12	21.234	6.0000	C 16
13	21.834	2.0000	C 16:1
14	23.149	2.0000	C 17
15	23.846	2.0000	C17:1
16	25.329	4.0000	C 18
17	25.662	2.0000	C 18:1n9t
18	25.911	4.0000	C 18:1n9c
19	26.413	2.0000	C 18:2n6t
20	27.030	2.0000	C 18:2n6c
21	27.719	2.0000	C 18:3n6G
22	28.482	2.0000	C 18:3n3A
23	29.971	4.0000	C 20:0
24	30.595	2.0000	C 20:1n9
25	31.844	2.0000	C 20:2
26	32.368	2.0000	C 20:3n6
27	32.568	2.0000	C 20:4n6
28	33.027	2.0000	C 20:3n3
29	33.397	2.0000	C 21:0
30	34.607	2.0000	C 20:5n3
31	34.853	4.0000	C 22
32	35.509	2.0000	C 22:1n9
33	36.800	2.0000	C 22:2
34	37.271	2.0000	C 23:0
35	39.821	4.0000	C 24:0
36	40.237	2.0000	C 22:6n3
37	40.555	2.0000	C 24:1n9
		100.0001	

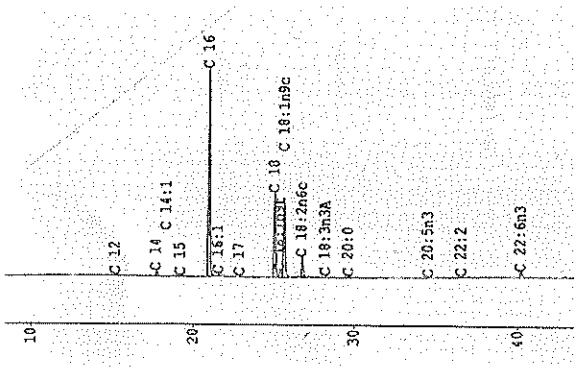

Figure 1. GCFID Chromatogram of crude cocoa butter deodorizer distillate.

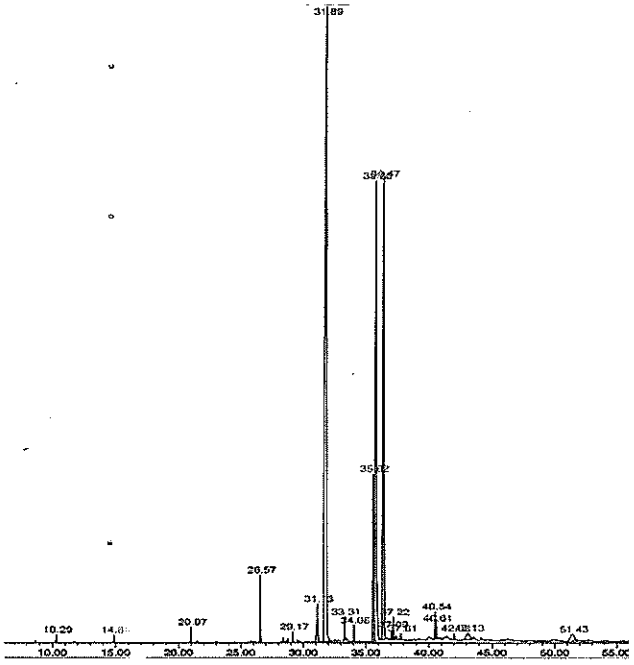

Figure 2. Total Ion Chromatogram (TIC) of crude cocoa butter deodorizer distillate.

Table 2. Fatty acids composition in cocoa butter and purified cocoa butter deodorizer distillate.

Fatty acid		Percent (%) In cocoa butter (Source: [5,6,7])	Percent (%) In purified cocoa butter deodorizer distillate
Lauric	C 12:0	<0.01	0.23
Myristic	C 14:0	<0.09	0.96
Palmitic	C 16:0	22.6-30.4	38.92
Palmitoleic	C 16:1	0.1-0.5	0.89
Stearic	C 18:0	30.2-36.0	24.70
Oleic	C 18:1	29.2-36.4	27.21
Linoleic	C 18:2	1.3-4.0	4.96
Linolenic	C 18:3	<0.5	0.40
Aracidic	C 20:0	<1.2	0.49

Analysis with gas chromatography mass spectrometer (GCMS)

One micro-liter of sample in hexane was injected split-less into gas chromatography model HP6890 series fitted with DB5 MS (5% Phenyl Methyl crosslink siloxane, 30.0 m x 250 μm x 0.25 μm) column. The program of the oven temperature was set at 60°C and increased to 230°C at 4°C/min and held at 230°C for 17.50 min. Determination of the compounds in the samples was based on the Wiley275.L spectrum library with the aids of computer software.

Analysis with gas chromatography with flame ionization detector (GC-FID)

One micro-liter of standard mixture fatty acids methyl ester of C4–C24 was injected split-less into gas chromatography model Shimadzu GC-17A with FID and C-R6A Chromatopac integration instrument fitted with DB23 cis/trans (50% cyanopropyl/ 50% methyl polysiloxane) column. Mobile phase was helium gas with the flow rate of 1.8mL/min at 3.2 psi. Injection port temperature was set at 250°C and detector temperature was set at 260°C. The program of the oven temperature was set at 90°C and increased to 130°C at 20°C/min followed by 4°C/min until temperature reached 200°C. Finally, the temperature of the oven was increased from 200°C to 220°C at 1.2°C/min.

Under the same conditions, 1.0 μL of FAME sample in hexane was injected into gas chromatography. Determination of compounds qualitatively and quantitatively in the sample was based on the retention time and corrective reaction factor (CRF) respectively with the chromatogram produced from the standard mixture fatty acids methyl ester of C4–C24 with the aids of computer software.

Purification of cocoa butter deodorizer distillate

Based on the SAP value of 283.2 mg of sodium hydroxide, a 2.0 N sodium hydroxide in ethanol was prepared and refluxed with the crude cocoa butter deodorizer distillate for 30 minutes. The excess of ethanol was distilled out and the soap produced was vacuum dried and dissolved in distilled water at 40°C. Without micelles formation, 1.0 N hydrochloric acid was added to precipitate the fatty acids. The precipitated fatty acids were filtered and vacuum dried. Effectiveness of the purification method was evaluated qualitatively and quantitatively by gas chromatography.

RESULTS AND DISCUSSION

Chromatogram (Fig. 1) reviewed that 16 compounds were detected when the crude cocoa butter deodorizer distillate was subjected to GC-FID analysis. Identification of compounds in GC-FID was based on the retention time with regards to the standard. Therefore, compounds identified by the computer software may not necessary be correct because impurities such as hydrocarbon that are dissolved in FAME (fatty acids methyl ester) have a similar retention time with the particular fatty acid which will be identified as such by the software. Confirmation of the compounds is therefore needed either by instrumentation such as GCMS and theory. Cocoa butter is a natural vegetable fat and it should not contain *trans*-fats [4]. Literature reviewed that prime press cocoa butter contains no C14:1, C20:5n3, C22:2 and C22:6n3 (Table 2) and therefore, should not be present in cocoa butter deodorizer distillate. When the crude cocoa butter deodorizer distillate was subjected to GCMS analysis, 20 compounds were detected by GCMS (Fig. 2). However, out of the 20 compounds detected, only 16 were successfully identified with the matching quality by mass spectra more than 95% with the majority of the possible compounds identified being fatty acids in the form of fatty acid methyl ester (Table 3). Small amount of hydrocarbon such as cyclotetradecane and cholesterol as suggested by MS and four unidentified compounds in GCMS chromatogram together with some questionable peaks identified in the GC-FID chromatogram suggested that there were some hydrocarbon compounds other than fatty acids present in the sample of crude cocoa butter deodorizer distillate.

Saponification process converts all the free fatty acids, triglyceride, diglyceride, and monoglyceride that may be present in the cocoa butter deodorizer distillate into soap, leaving the unsaponifiable matter such as hydrocarbons, theobromine and tocopherolacetate. Dissolving the soap in distilled water and filtration were able to remove much of the insoluble materials from the soap solution. Fatty acids can be precipitated from the soap solution by adding mineral acids such as hydrochloric acid. The average yield from three replicates of the fatty acids from these processes was 80%, showing that about 20% of the crude cocoa butter deodorizer distillate was not fatty acids.

When this purified cocoa butter deodorizer distillate

Table 3. Composition of the crude cocoa butter deodorizer distillate by tentative MS identification.

Retention time (min)	Peak area (%)	Compound
20.98	0.34	Dodecanoic acid, methyl ester
26.58	1.48	Methyl tetradecanoate
29.17	0.24	Pentadecanoic acid, methyl ester
31.13	1.41	9-hexadecenoic acid, methyl ester
31.89	43.83	Hexadecanoic acid, methyl ester
33.30	0.50	Hexadecanoic acid, ethyl ester
34.05	0.38	Heptadecanoic acid, methyl ester
35.62	5.86	9,12- octadecadienoic acid, methyl ester
35.86	21.52	9- octadecenoic acid, methyl ester
36.47	20.00	Octadecanoic acid, methyl ester
37.08	0.21	Ethyl linoleate
37.23	0.48	9- octadecenoic acid, ethyl ester
37.81	0.15	Octadecanoic acid, ethyl ester
40.61	0.35	Eicosanoic acid, methyl ester
43.13	0.89	cyclotetradecane
51.44	1.13	Cholesterol

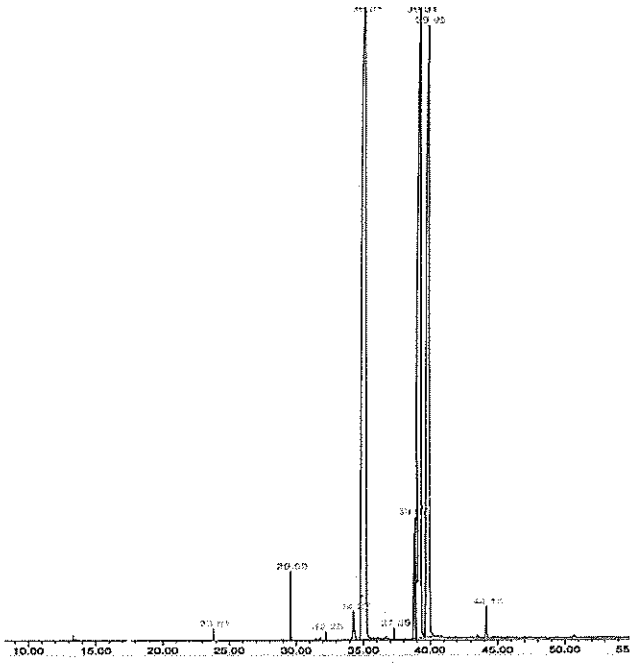

Figure 3. Total Ion Chromatogram (TIC) of purified cocoa butter deodorizer distillate.

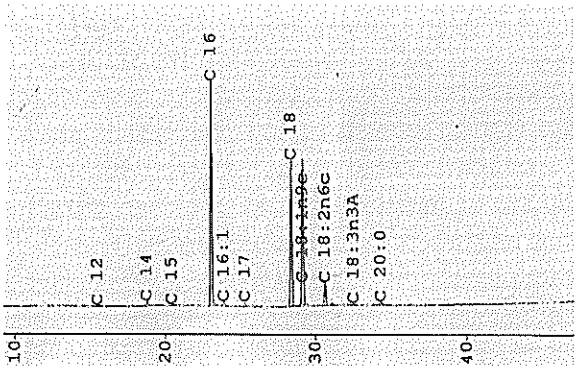

Figure 4. GCFID chromatogram of purified cocoa butter deodorizer distillate.

was analysed by GCMS, nine out of 10 compounds detected (Fig. 3) were successfully identified as fatty acids in the form of methyl ester with the matching quality by mass spectra more than 95%. They are dodecanoic acid, tetradecanoic acid, 9-hexadecenoic acid, hexadecanoic acid, heptadecanoic acid, 9,12- octadecadienoic acid, 9-octadecenoic acid, octadecanoic acid and eicosanoic acid. The only peak at 32.25 minute was identified as pentadecanoic acid with only 87% of matching quality. No unidentified peak was observed generally and cyclotetradecane and cholesterol were eliminated.

From the chromatogram of GC-FID for purified cocoa butter deodorizer distillate, 11 compounds were detected and identified as C12 (0.23%), C14 (0.96%), C15 (0.21%), C16:0 (38.92), C16:1 (0.89%), C17 (1.02%), C18 (24.70%), C18:1n9c (27.21%), C18:2n6c (4.96%), C18:3n3A (0.40%) and C20:0 (0.49%) (Fig. 4). Most of the compounds detected and identified were in agreement with the GCMS findings and with the literature (Table 1). Small amount of C15 and C17, which are with odd number carbon that should not exist in vegetable oils [5], may be due to the contribution from the fats of microorganisms, which was left over from the fermentation process. In fats of microorganisms, odd-numbered chain lengths can contribute up to 15% of all fatty acids. Existence of margaric acid or C17 fatty acid may be also due to a mixture residue of C16 and C18 that was not separated successfully [5].

In conclusion, crude cocoa butter deodorizer distillate contains about 80% of fatty acids. Among these fatty acids, palmitic acid was the major

compound followed by stearic acid and oleic acid. Other major fatty acids detected were linoleic acid and myristic acid.

Acknowledgements – Research project is supported by eScience Funds of Ministry of Science, Technology and Innovation of Malaysia.

REFERENCES

1. Minifie B.W. (1982) *Chocolate, Cocoa and Confectionery: Science And Technology* Second Edition. AVI Publishing Company, Inc., Westport.
2. Anon (1999) *The De Zaan Cocoa Products Manual.* ADM Cocoa B.V., Netherlands.
3. Yap K.C.S., Sarini H., Aminah A. and Sabariah S. (2008) Analysis of the cocoa butter deodorizer distillate. *Malaysian Cocoa Journal* **4:** 73-75.
4. Soleha I. (1993) *Kimia Makanan* Edisi Kedua. Dewan Bahasa Dan Pustaka, Kuala Lumpur.
5. Bockisch M. (1998) *Fats and Oils Handbook.* AOCS Press, Illinois.
6. Asimah H. (2007) Physical stability and color changes of Malaysian cocoa butter. *Malaysian Cocoa Journal* **3:** 20-25.
7. Fisal A., Rosinah R. and Suzannah S. (2007) The effects of cocoa butter equivalent addition to the cocoa butter melting and crystallization profiles. *Malaysian Cocoa Journal* **3:** 58-64.

Journal of Science and Technology in the Tropics (2009) **5**: 59-65

Ion-conductive poly (methyl methacrylate) gel polymer electrolytes for lithium batteries

S. Ramesh, G. P. Ang and W. C. Wong
Faculty of Engineering & Science, Universiti Tunku Abdul Rahman, Setapak,
53300 Kuala Lumpur, Malaysia
(Email: ramesh@utar.edu.my)

Accepted 14-5-2009

Abstract Thin films of poly (methyl methacrylate) (PMMA) blend with lithium sulphate salt (Li_2SO_4) were prepared by solution casting method. The conductivity and dielectric measurements were carried out on the films. The highest room temperature ionic conductivity of 4.50×10^{-10} Scm^{-1} was achieved for the composition 95 wt% PMMA:5 wt% Li_2SO_4. The presence of salt improved the ionic conductivity. The variation of ionic conductivity for different concentrations of Li_2SO_4 salt was reported. The dielectric data were analyzed using dielectric permittivity (ε') and dielectric modulus (M') of the samples. The complexation of salt with PMMA was confirmed by structural and thermal studies. FTIR analysis showed some shift in peaks between the polymer complex with different concentrations of lithium salt. Differential scanning calorimetry (DSC) studies suggested that the Li_2SO_4 salt affected the glass transition temperature (T_g) and melting point (T_m) of the polymer electrolytes. The thermogravimetric (TGA) studies showed that the thermal stability of the polymer electrolytes decreased with the addition of Li_2SO_4 salt.

Keywords poly(methyl methacrylate) – lithium sulphate – ionic conductivity – dielectric – FTIR

INTRODUCTION

Ionically conducting polymers were first discovered about 20 years ago and were subsequently used as electrolytes in solid-state batteries. The development of polymeric systems with high ionic conductivity is one of the main objectives in polymer research. This is due to their potential application as an electrolyte in solid state batteries [1-4].

Among the polymer electrolytes that are currently experimented, PMMA based electrolyte has a special significance in view of its well known chemistry and cheaper method of processing them as laminates [5, 6]. Currently PMMA is extensively studied due to its ability to solvate inorganic salts to form a polymer-salt complex [7].

The main aim of the present work was to develop a polymer electrolyte with PMMA as the host polymer and Li_2SO_4 as salt. Addition of the salt which has low lattice energy such as Li_2SO_4, was effective for improvement of the ionic conductivity. The solubility increases with an increase in conductivity. This is because the conductivity is directly proportional to the free ion in the polymer complex system. Free ions increased when the solubility of salt is high. FTIR spectroscopy was used to study the interaction between the polymer and salt. DSC and TGA were used to study the thermal stability of the polymer complex prepared. In this paper, we present the data on the effect of the salt to the ionic conductivity of the polymer complex.

EXPERIMENTAL

PMMA and Li_2SO_4 were obtained from Fluka, while tetrahydrofuran (THF) AR grade was obtained from J. T. Baker. PMMA and Li_2SO_4 were dissolved in THF and stirred for 48 hours. The mixture was then casted into glass dishes and left to dry by evaporation in a desiccator at room temperature. This procedure yields mechanically stable and free standing films. The thickness of the films was measured by micrometer screw gauge. Conductivity measurement was performed by impedance spectroscopy using a HIOKI Model 3532-50 bridge interfaced to a computer for data acquisition over a frequency range

employed to cultivate cladocerans such as *Moina macrocopa*, *Moina micrura* and *Daphnia* sp. for the aquaculture industry [5]. Untreated wastewater, which has a high organic load [6], has been a traditional medium for raising high densities of freshwater cladocerans, rotifers and copepods [7, 8].

A recent study [9] demonstrated that human urine, cow urine, cow dung, poultry droppings and vermin-compost could be utilized for zooplankton cultivation. Human urine was found to be a highly effective liquid nutrient source for mass production of cladocerans, which are commonly used as livefeed for larval and post-larval rearing of fish and shellfish [10]. Cladocerans have been found to be rich in essential nutrients, are easily ingested and digested by larvae, fulfil the larval dietary requirements and improve water quality by minimizing the need for artificial feeding [11-13].

The practice of fertilizing ponds with manures and organic wastes may introduce harmful micro-organisms, antibiotics and hormones, which may directly or indirectly affect the cultured animals as well as consumers [14, 15]. However, aquaculture foods generally have a good safety record since the environment of each production cycle can be relatively controlled. It has been the task of the aquaculture industry to hygienically produce livefeed organisms to ensure the safety of fish and crustacean larvae that possess low immunity, produce pathogen- and chemical-free stocks, and prevent disease outbreaks [11-13]. Recent efforts at bioconversion of wastes have also led to products that are comparatively safer for the environment.

In this study, faeces from drug-free Nile tilapia, *Oreochromis niloticus*, were harvested from a recirculating aquaculture system (RAS) and tested as a food source for the freshwater cladoceran, *Moina macrocopa*. The reproductive performance and survivorship of this zooplankton were then assessed. Two commercially available algal powders, *Chlorella* and *Spirulina*, were employed as reference diets.

MATERIALS AND METHODS

Water fleas, *Moina macrocopa* (Fig. 1), were obtained from Cheras Aquarium in Kuala Lumpur, Malaysia and cultured at the Faculty of Engineering & Science, Universiti Tunku Abdul Rahman. Mass cultivation was carried out in transparent tanks with natural green water under natural light illumination at a temperature of 25 ± 2°C, pH 7 ± 1 and a dissolved oxygen level of 3-6 mg/L [16]. The green water comprised a mixture of *Chlorella*, *Scenedesmus* and *Coelastrum* species.

Only healthy adult *M. macrocopa* females with brood pouches were selected to produce neonates (offspring) in this study. These females were transferred into Petri dishes containing de-chlorinated tap water and fed with baker's yeast during the breeding period. Neonates of less than 24 hours old were collected for the experiments.

Each treatment was prepared at a concentration of 3.5 g/L based on the total ammonia-nitrogen (~3.5 mg/L), NO_3-N (~1.0×10^{-3} mg/L) and NO_2-N (~4.0×10^{-5} mg/L) levels detected in the rearing water of our Nile tilapia (*Oreochromis niloticus*) recirculating aquaculture system (RAS). Total ammonia-nitrogen (TAN), NO_3-N and NO_2-N levels were monitored with a DR/890 datalogging colorimeter (Hach Co., USA) following the standard procedures of APHA [16].

The Nile tilapias were fed once a day with Cargill™ formulated feed based on 2-3% body weight. Fish faeces, collected from the rearing tanks and blot-dried with filter paper, were blended for 5 minutes at the desired concentration of 3.5 g/L in de-chlorinated tap water. Two types of algal powder, *Chlorella* (Yakult Microbiological Central Institute, Japan) and *Spirulina* (YanLing Natural Hygiene Sdn. Bhd., Malaysia), were prepared as described for the fish faeces and used as reference diets. De-chlorinated tap water was used as control in this study.

M. macrocopa neonates were transferred into Petri dishes at a density of one neonate per 20 mL treatment diet. The treatments were renewed every two days. Survival and reproduction (fecundity) of *M. macrocopa* were monitored daily. The length of time to the first reproduction and total number of neonates produced by each parthenogenetic female were recorded in order to evaluate its fecundity. Neonates were counted daily and discarded [17]. To calculate cumulative birth, the total number of neonates produced by each female was summed up. All experiments were run in triplicate for up to 12 days or until the *M. macrocopa* died. Life table parameters were tabulated to calculate net reproduction rate (R_o) and generation time (T) [18] as shown below:

$$\text{Net reproduction rate } (R_o) = \sum_{0}^{\infty} l_\chi m_\chi$$

from 50 Hz to 1 MHz. FTIR studies were carried out with FTIR Spectrometer Spectrum RX1 (Perkin Elmer) in the wave region between 4000 and 400 cm^{-1}, resolution 4 cm^{-1}. DSC was performed with a DSC 823^e instrument. The samples were heated to 350 °C at a rate of 20 °Cmin^{-1}. TGA analysis was performed with a TGA/SDTA 851^e. The samples were heated to 350 °C at a rate of 10 °Cmin^{-1}.

RESULTS AND DISCUSSION

Conductivity studies

The conductivity values for PMMA-Li_2SO_4 were in the range of 10^{-10} to 10^{-12} S cm^{-1} for various composition ratios of PMMA and Li_2SO_4. The conductivity exhibited an increasing trend when Li_2SO_4 content was added. Ionic conduction in polymer is caused by the diffusion of ions through their free volumes [8-11]. Polymer dissolves in salt to form mixtures which support ionic conductivity.

Figure 1 shows the variation of ionic conductivity at different Li_2SO_4 content in PMMA: Li_2SO_4 films. By calculating the bulk resistance (R_b) values from the impedance plots, it was found that the PMMA: Li_2SO_4 (95:5) complex gave the highest conductivity value, 4.50×10^{-10} Scm^{-1}. This was due to the ionic mobility of Li_2SO_4 within the polymer electrolytes. However, this ionic conductivity is still low to be used in batteries.

According to Chowdari *et al.* [12], it is possible that the two competing factors, segmental mobility which affects the mobility of charge carriers and the mobile charge carrier concentration which depends on the nature of inorganic salt and its interaction with polymer chain, are optimized for the composition of 95 wt% PMMA:5 wt% Li_2SO_4, resulting in highest conductivity. Salts having low lattice energy are generally expected to promote greater dissociation of the salt, thereby providing more ions. The presence of mobile ions like Li^{++} also increases the amorphous structure of the polymer by imparting disorderness and creating free volume in between polymer chains. Therefore, the ion migration can take place easily.

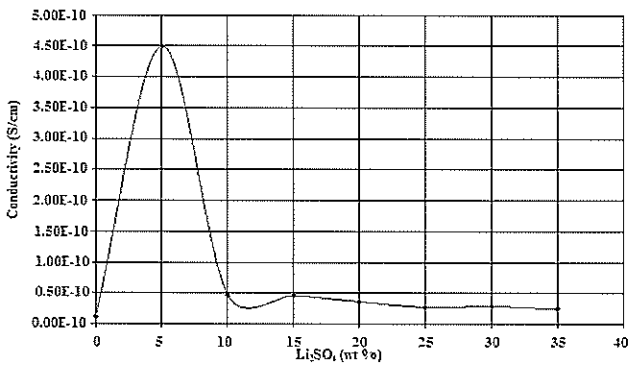

Figure 1. Variation of conductivity as a function of weight percentage of Li_2SO_4 in PMMA:Li_2SO_4 polymer electrolytes.

The conductivity decreased markedly from 4.50×10^{-10} to 4.70×10^{-11} Scm^{-1}, as the composition of salt was increased from 5 wt.% to 10 wt.%. As the salt concentration increases, the number of carrier ions of the complex increases and this leads to stronger ion-ion interactions and, thereby, possibly impedes the polymer backbone's segmental motion which ultimately causes a lowering of conductivity.

When the Li_2SO_4 salt was further added from 15 wt% to 35 wt% the ionic conductivity value decreased. This is due to the further addition of salt will have greater tendency towards the formation of neutral ion pairs [13]. Thus, this reduces the number density of mobile ions and subsequently reduces the ionic conductivity. When higher concentration of Li_2SO_4 is present, part of the oxygen coordination is necessarily provided by SO_4^{2-} in sulphate composition. Therefore, there will be enough oxygen coordination so that lithium ions are locked up in the deeper potential wells and their contribution to conductivity is reduced.

Dielectric relaxation studies

The investigation of dielectric behaviour is considered as very helpful in understanding the behaviour of polymer. Dielectric constant is the measurement of charge carrier density being stored. Figure 2 shows the frequency dependence of the real (ε') and imaginary (ε") parts of dielectric constant. Both the real (ε') and imaginary (ε") parts of the dielectric constant for the 95 wt% PMMA:5 wt% Li_2SO_4 rise sharply toward low frequencies due to the electrode polarization effects [14]. At high frequencies, the periodic reversal of the electric field occurs so fast that there is no excess ion diffusion in the direction of the field. The polarization due to the charge accumulation decrease, leads to the observed decrease in the value of ε' and ε" [15]. A further analysis of the dielectric behaviour would be more successfully achieved by using the formulation of dielectric modulus, which suppresses the effects of the electrode polarization.

Variations of real (M') and imaginary (M") parts

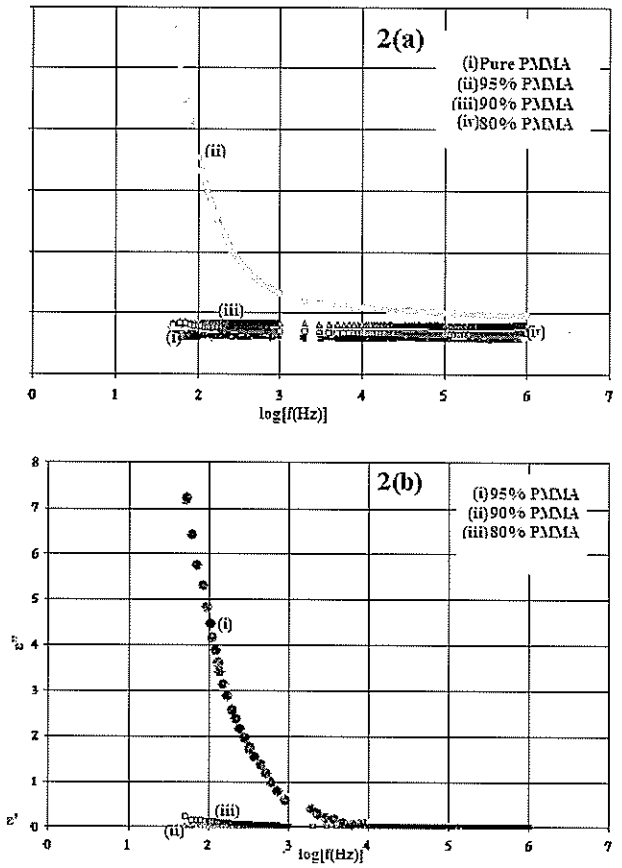

Figure 2. Variation of (a) real (ε') part and (b) imaginary (ε") part of dielectric constant, with frequency for various composition ratios of PMMA : Li_2SO_4 polymer electrolytes.

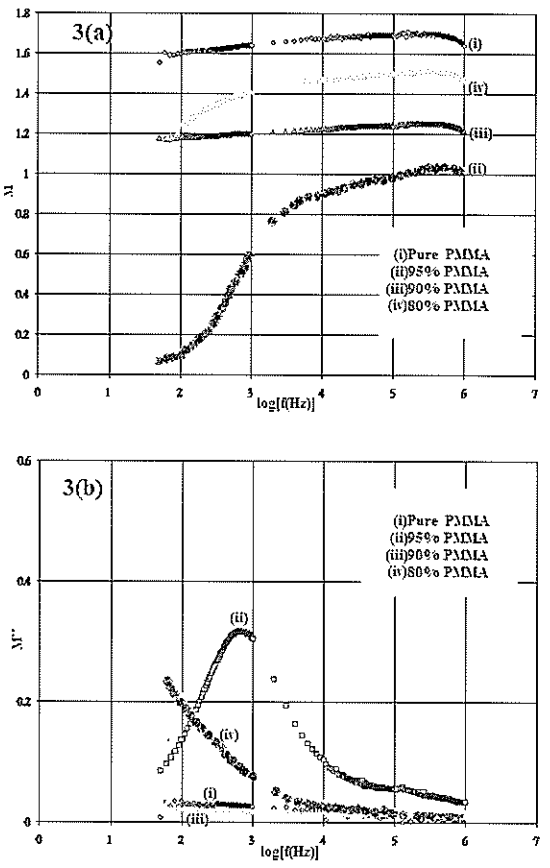

Figure 3. Variation of (a) real (M') part and (b) maginary (M") part of modulus, with frequency for PMMA : Li_2SO_4 polymer electrolytes.

of dielectric modulus are shown in Figure 3 for the same polymer electrolytes. M' and M" increase towards high frequencies. The presence of the peaks in the modulus formalism at higher frequencies for pure PMMA, 95 wt% PMMA:5 wt% Li_2SO_4, 90 wt% PMMA:10 wt% Li_2SO_4 and 80 wt% PMMA:20 wt% Li_2SO_4 imply that the polymer electrolyte films are ionic conductors. The peaking curve at higher frequencies may be caused by bulk effect. Lower M' value in high conducting polymer electrolyte containing 5 wt% Li_2SO_4 indicates the faster relaxation process in this polymer system.

FTIR analysis

Polymer complexes with ionic salts have been characterized by FTIR spectroscopy [16]. FTIR is a powerful tool to study the local structural change. The FTIR spectra of the starting materials PMMA, Li_2SO_4 and polymer electrolytes with various composition ratios of PMMA:Li_2SO_4 are shown in Figure 4.

The FTIR spectrum for pure PMMA is shown in Figure 4(a). Pure PMMA contains a carbonyl group, yielding a γ(C=O) stretching mode at 1734 cm^{-1}. In PMMA, which is saturated polymeric ester, the C=O symmetrical stretching frequency gives rise to an intense, strong and sharp peak at 1734 cm^{-1}. Pure PMMA also produces a strong band at 1458 cm^{-1}, assigned as O-CH_3 asymmetrical bonding. The peak at 2947 cm^{-1} is assigned to CH_3 stretching in PMMA. Pure PMMA also shows strong absorption band at 1150 cm^{-1}, ascribed to the asymmetrical stretching vibration of the C-O-C bond.

The characteristic peaks of pure Li_2SO_4 salt are shown in Figure 4(b). The inorganic sulphate ion absorbs strongly at 1200-1120 cm^{-1} (out-of-phase SO_4 stretch), three triply degenerate components. The symmetric in-phase SO_4^{2-} stretch is forbidden by symmetric if the environment around the SO_4^{2-} ion is also symmetrical. If oxygen is not in a symmetrically equivalent environment, the in-phase SO_4^{2-} stretch may be seen as a very weak sharp band near 1150 cm^{-1}.

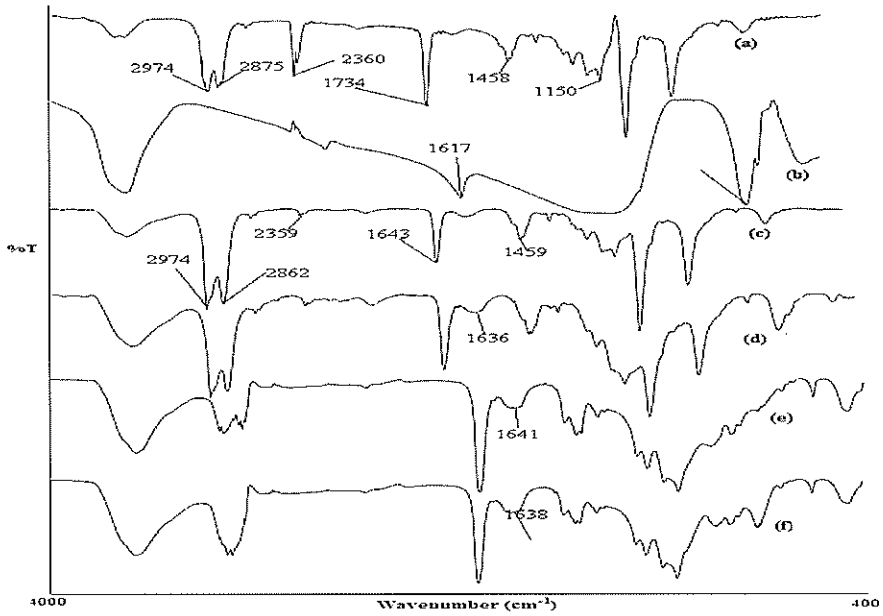

Figure 4. FTIR spectra of PMMA-Li_2SO_4 based polymer electrolytes. (a) pure PMMA; (b) pure Li_2SO_4; (c) 90 wt% PMMA: 10 wt% Li_2SO_4 (d) 80 wt% PMMA: 20 wt% Li_2SO_4 (e) 70 wt% PMMA: 30 wt% Li_2SO_4 (f) 60 wt% PMMA: 40 wt% Li_2SO_4

The FTIR spectra of samples for 90 wt% PMMA:10 wt% Li_2SO_4, 80 wt% PMMA:20 wt% Li_2SO_4, 70 wt% PMMA:30 wt% Li_2SO_4 and 60 wt% PMMA:40 wt% Li_2SO_4 are shown in Figure 4(c-f). The peak of 90 wt% PMMA:10 wt% Li_2SO_4 at 1643 cm^{-1} changed from a weak broad peak to a medium broad peak in 70 wt% PMMA:30 wt%Li_2SO_4 polymer electrolyte. This might be due to the overlapping with the characteristic of Li_2SO_4 sharp peak at 1617 cm^{-1}. The medium sharp peak at 1150 cm^{-1} also shows the change in shape to a broad peak at 1192 cm^{-1} in 60 wt% PMMA:40 wt% Li_2SO_4 polymer electrolyte. This is because the sulphate ions absorb strongly at 1200-1120 cm^{-1} and thus causes the overlapping of the peaks.

The pure PMMA peaks at 2947 cm^{-1}, 2875 cm^{-1}, 2360 cm^{-1} and 1458 cm^{-1} are slightly shifted to 2974 cm^{-1}, 2862 cm^{-1}, 2359 cm^{-1} and 1459 cm^{-1} respectively in the 90 wt% PMMA:10 wt% Li_2SO_4 polymer electrolyte. This is due to the interaction between Li^{++} ions with the carbonyl oxygen. With the addition of Li_2SO_4 salt to PMMA, the C=O stretching band broadened and shifted to lower wave number. This indicates that there is an interaction between the carbonyl group of ester and lithium salts via a coordination bond and hence complexation has occurred. The C=C stretching peak of 90 wt% PMMA:10 wt% Li_2SO_4 at 1643 cm^{-1} is shifted to 1634 cm^{-1} and 1638 cm^{-1} in 80 wt% PMMA:20 wt% Li_2SO_4 and 70 wt% PMMA:30 wt% Li_2SO_4 polymer electrolytes, respectively. This shift in peak is due to addition of Li_2SO_4 to the PMMA causing the overlapping of the peaks between these two compounds.

Thermogravimetric analysis

The TGA curve for pure PMMA and 95 wt% PMMA:5 wt% Li_2SO_4 polymer electrolytes is shown in Figure 5(a). For pure PMMA, the data show a weight loss about 7 % at a temperature below 100 °C. This initial loss results from residual solvent evaporation and the transition of the polymer electrolyte sample. The weight loss below 100 °C is also due to the removal of moisture in the sample. The first weight loss begins at a temperature of above 123 °C. The percentage of the weight loss for pure PMMA is around 7 %. The second weight loss is started at a temperature around 340 °C. This may be due to the crystallization of the polymer electrolyte samples. For the 95 wt% PMMA:5 wt% Li_2SO_4 film, the first weight loss begins at a temperature around 133 °C and the percentage weight loss is around 8 %.

The thermogravimetric curves for 90 wt% PMMA:10 wt% Li_2SO_4 and 80 wt% PMMA:20 wt% Li_2SO_4 polymer electrolytes are shown in Figure 5(b).

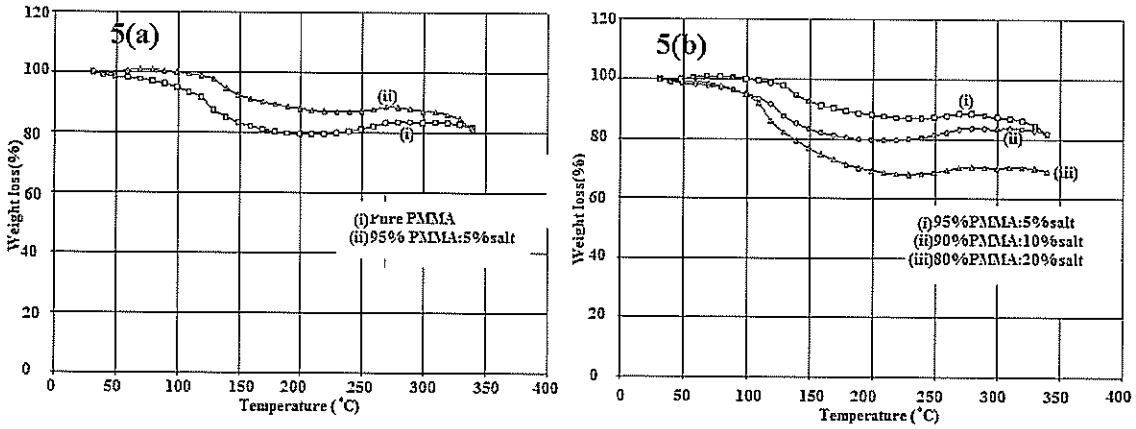

Figure 5. TGA analysis of PMMA-Li_2SO_4 based polymer electrolytes.

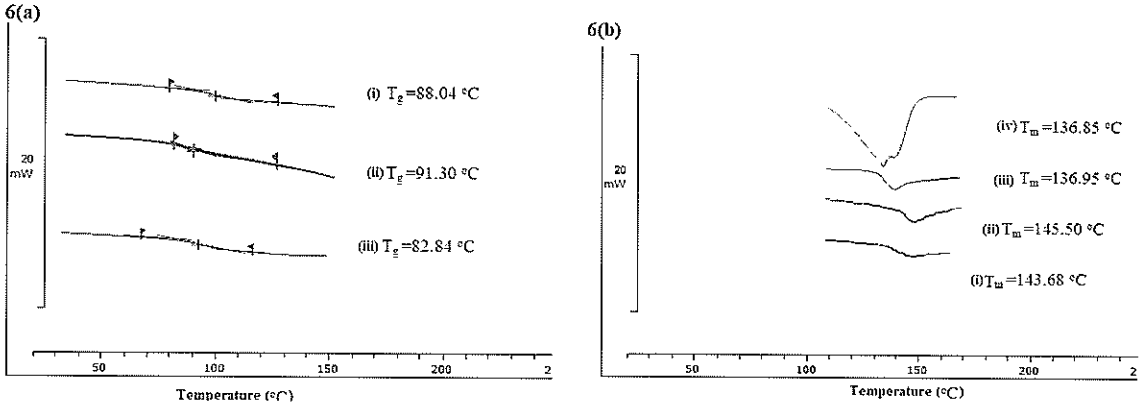

Figure 6. DSC thermogram of (a) T_g regions and (b) T_m regions for various composition ration of PMMA : Li_2SO_4 polymer electrolytes.

The first weight loss for 90 wt% PMMA:10 wt% Li_2SO_4 and 80 wt% PMMA:20 wt% Li_2SO_4 begins at 117 °C and 153 °C, respectively. For the 80 wt% PMMA:20 wt% Li_2SO_4 film, the weight loss below temperature 150 °C is found to be highest within four of the polymer electrolytes, which is around 27 %. By comparing the first weight loss of the four polymer electrolytes, the weight loss for 95 wt% PMMA:5 wt% Li_2SO_4 is the lowest. This shows that polymer complex which contains 95 wt% PMMA and 5 wt% salt has relatively good thermal stability and also shows the highest ionic conductivity.

Differential scanning calorimetry (DSC)

The DSC thermogram of T_g region for polymer electrolytes is shown in Figure 6(a). The glass transition temperature for pure PMMA is around 88°C, as shown in Figure 6a(i). The T_g value for 95 wt%PMMA:5 wt% Li_2SO_4 is around 91°C as shown in Figure 6a(ii) . This shows that the glass transition of the polymer electrolyte is shifted towards higher temperature. The addition of salt in the polymer mixtures causes the presence of cross-linking, which will decrease the free volume and increase the interaction of the parts of compound, thus increasing the T_g value. In other words, the addition of salt will decrease the local chain mobility.

The T_g has a small dependence on the heating or cooling rates in DSC and other methods of thermal characterization. Samples that are slowly heated through the glass transition exhibit a lower T_g than those that are rapidly heated due to the non-equilibrium state of the glass [17].

The DSC thermogram of T_m region for pure PMMA, 95 wt% PMMA:5 wt% Li_2SO_4, 85 wt% PMMA:15 wt% Li_2SO_4 and 70 wt% PMMA:30 wt% Li_2SO_4 polymer electrolyte samples, are shown in Figure 6b(i-iv). Upon heating pure PMMA, the endothermic peak is observed at around 143°C. This peak is due to the melting point of the pure PMMA sample. 95 wt% PMMA:5 wt% Li_2SO_4 sample shows the highest melting temperature, 145.50 °C. This is

because the addition of 5 wt% salt increases the chain flexibility of PMMA:Li_2SO_4 polymer electrolyte. With further addition of Li_2SO_4 salt in polymer mixtures, the melting temperature of the polymer electrolytes dropped to 136 °C for composition 70 wt% PMMA:30 wt% Li_2SO_4. The main reason for this situation is due to the increase in molecular rotation of the polymer electrolyte. The SO_4^{2-} ions increase space between characteristic group in PMMA and lead to a reduction in melting temperature.

Conclusion

The influence of salt in optimizing polymer electrolyte design for PMMA has been proved through ionic conductivity studies. FTIR studies suggest that the amount of salt concentration added into the mixture of PMMA polymer complex will change the environment of certain functional groups upon complex formation. On the other hand, the TGA and DSC studies can further explain the thermal stability of the polymer complexes through measurements of glass transition temperature, melting temperature and the weight loss temperature.

REFERENCES

1. Hooper A. and North J.M. (1983) The fabrication and performance of all solid state polymer-based rechargeable lithium cells. *Solid State Ionics* **9-10:** 1161-1166.
2. MacCallum J.R. and Vincent C.A. (1987/1989) *Polymer Electrolytes Reviews 1 and 2*. Elsevier, London.
3. Acosta J.L. and Morales E. (1996) Structural, morphological and electrical characterization of polymer electrolytes based on PEO/PPO blends. *Solid State Ionics* **85:** 85-90.
4. Kim J.Y. and Kim S.H. (1999) Ionic conduction behavior of network polymer electrolytes based on phosphate and polyether copolymers. *Solid State* Ionics **124:** 91-99.
5. Iijima T., Toyoguchi Y. and Eda N. (1985) Quasi-solid organic electrolytes gelatinized with polymethylmethacrylate and their applications for lithium batteries. *Denki Kagaku* **53:** 619 [in Japanese].
6. Appetecchi G.B., Croce F. and Scrosati B. (1995) Kinetics and stability of the lithium electrode in PMMA-based gel electrolytes. *Electrochimica Acta* **40:** 991-997.
7. Rajendran S., Sivakumar M. and Subadevi R. (2004) Investigations on the effect of various plasticizers in PVA–PMMA solid polymer blend electrolytes. *Material Letters* **58:** 641-649.
8. Valee A., Besner S. and Prud'homme S. (1992) Comparative study of poly (ethylene oxide) electrolytes made with $LiN(CF_3SO_2)_2$, $LiCF_3SO_3$ and $LiClO_4$: Thermal properties and conductivity behaviour. *Electrochimica. Acta* **37:** 1579-1583.
9. Torrel L.M. and Schantz S. (1989) Light Scattering in Polymer Electrolyte *In* MacCallum J. and Vincent C.A. (Eds.) *Polymer Electrolyte Reviews*, vol. 2 pp1-43 Elsevier, New York
10. Jacob M.M.E. and Arof A.K. (1998) Proceedings of the 6th. Asian Conference on Solid State Ionics *In* Chowdari B.V.R., Lal K., I. A. Agnihotry I.A., Khare N., Sekhon S.S., Siwastava P.C. and Chandra S. (Eds.) *Solid State Ionics: Science and Technology* pp 457-463. World Scientific, Singapore.
11. Ramesh S., Rekha L., Radhakrishna S. and Arof A.K. (1998) Electrical conductivity of impurity doped poly vinyl chloride, *In* Chowdari B.V.R., Lal K., Agnihotry I.A., Khare N., Sekhon S.S., Siwastava P.C. and Chandra S. (Eds.) *Solid State Ionics: Science and Technology* pp 201-205. World Scientific. Singapore.
12. Chowdari B.V.R., Huq R. and Farrington G.C. (1992) Thermal and electrical characterization of PEO-based polymer electrolytes containing mixed Co(II) and Li(I). *Solid State Ionics* **57:** 49-58
13. Ostrovshii D., Brodin A., Torell M., Appetecchi G.B. and Scrosati B. (1998) Molecular and ionic interactions in poly (acrylonitrile)- and poly (methylmetacrylate)-based gel electrolytes *Journal of Chemical. Physics* **109:** 7618-7624.
14. Mishra R. and Rao K.J. (1998) Electrical conductivity studies of poly (ethyleneoxide) -poly (vinylalcohol) blends. *Solid State Ionics* **106:** 113-127.
15. Ramesh S. and Arof A.K. (2001) Ionic conductivity studies of plasticized poly(vinyl chloride) polymer electrolytes. *Materials Science and Engineering* **B85:** 11-15.
16. Sreekanth T., Jaipal R.M., Subramanyam S.

and Subba Rao U.V. (1999) Ion conducting polymer electrolyte films based on (PEO+KNO_3) system and its application as an electrochemical cell. *Materials Science and Engineering*. **B 64:** 107-112.

17. Moynihan C.T., Easteal A.J., Wilder J. and Tucker J. (1974) Dependence of the glass transition temperature on heating and cooling rate. *Journal of Chemical. Physics* **78:** 2673-2677.

Journal of Science and Technology in the Tropics (2009) 5: 59-65

Journal of Science and Technology in the Tropics (2009) **5**: 67-71

Preparation and characterization of poly (vinyl chloride) polymer electrolytes complexed with lithium sulphate

S. Ramesh, J. Y. Lim and R. K. Teo
Faculty of Engineering & Science, Universiti Tunku Abdul Rahman, Setapak,
53300 Kuala Lumpur, Malaysia
(Email: ramesh@utar.edu.my)

Accepted 14-05-2009

Abstract Polymer electrolytes with different composition ratio were constructed based on low molecular weight poly (vinyl chloride) (PVC) as the host polymer, lithium sulphate (Li_2SO_4) as the dopant salt and ethylene carbonate (EC) as the plasticizer. Thin films of low molecular weight polyvinyl chloride with lithium sulphate salt and ethylene carbonate were prepared by solution casting method. The ionic conductivity and dielectric measurements were carried out on these films over a wide frequency regime at various compositions of salt and plasticizer. The addition of salt improved the ionic conductivity. The highest ionic conductivity (3.83 x 10^{-9} S cm^{-1}) was obtained for 30% EC in the polymer complex. The dielectric behaviour was analyzed using dielectric modulus of the samples. FTIR studies show some simple overlapping and shift in peaks between low molecular weight PVC with Li_2SO_4 salt and EC in the polymer electrolyte complexes. Thermogravimetric analysis (TGA) shows thermal stability of the different composition of polymer, salt and plasticizer. Polymer electrolytes with higher content of PVC and lower plasticizer amount had a relatively good stability. Thermal stability of the polymer electrolytes decreased with addition of plasticizers. Differential scanning calorimetry (DSC) studies suggest that the plasticized samples had lower values of the glass transition temperature T_g.

Keywords low molecular weight PVC – polymer electrolytes – conductivity – dielectric – FTIR – TGA – DSC

INTRODUCTION

Solid polymer electrolytes (SPE) are currently receiving a great deal of attention because of their proposed large scale use in secondary lithium ions batteries [1]. In the past, most-in-depth efforts have focused on the PEO, PAN, PVC, PMMA, PVdF and blend based SPEs to improve their electrical conductivity [2-6]. In order to improve the conductivity, several approaches have been made to overcome the limitation without sacrificing mechanical integrity, including the use of a flexible, low glass transition temperature (T_g) polymer host and by adding plasticizing agent to those polymers. The addition of a salt has a highly disturbing effect on the arrangement of the polymer chains, ensuring conductivity [7, 8].

There has been a growing demand for high energy density rechargeable lithium batteries for portable electronic products because of their advantages including safety, high energy density, high single cell voltage, geometry and no memory effect. However, the ionic conductivity of polymer electrolytes is generally low, often too low for practical application.

In the present work, conductivity, structural and thermal studies were performed on PVC based solid polymer electrolytes with Li_2SO_4 as salt and EC as plasticizer.

EXPERIMENTAL

Low molecular weight PVC and Li_2SO_4 were obtained from Fluka, ethylene carbonate (EC) from Acros Organics and tetrahydrofuran (THF) AR grade from J. T Baker. Prior to the preparation of polymer electrolytes, Li_2SO_4 was dried at 100 °C for 1 hour in order to eliminate trace amounts of water in the material. The low molecular weight PVC-Li_2SO_4- EC systems were prepared by using solution cast technique with THF as solvent. The

solution thus obtained was cast on a petri dish and allowed to evaporate slowly inside a desiccator. This procedure yields mechanically stable and free standing films. Conductivity measurement was performed by impedance spectroscopy using HIOKI Model 3532-50 bridge interfaced to a computer for data acquisition over frequency range of 50 Hz to 1 MHz. FTIR studies were carried out using FTIR Spectrometer Spectrum RX1 (Perkin Elmer) in the wave region between 4000 cm^{-1} to 400 cm^{-1}, resolution 4 cm^{-1}. Thermogravimetric analysis was carried out using Mettler Toledo TGA/SDTA 851^e module. The sample was heated from 30 to 350 °C with heating rate of 10 °C/min in the nitrogen flow of 20 ml/min. Differential Scanning Calorimetric technique was used to find out the glass transition temperature (T_g) of the polymer electrolyte. DSC analysis was carried out using Mettler Toledo DSC 832^e module. The heat flow rate was 20 °C/min and the nitrogen gas flow rate 50 mL/min. The polymers were heated from 20 °C to 120 °C. After that, the polymers underwent a cooling process to 20 °C.

RESULTS AND DISCUSSION

Conductivity studies

In PVC: Li_2SO_4: EC polymer electrolyte, part of the coordination is from Li^{++} ions which are themselves mobile and contribute to conductivity [9]. Figure 1 represents the variation of conductivity as a function of percentage of EC in the PVC: Li_2SO_4: EC system. The maximum conductivity of the polymer electrolyte was at 30 wt% EC, 3.83×10^{-9} Scm^{-1}. A possible explanation is that most of the EC molecules are involved in shielding the hydrogen and chlorine atoms from interacting while the remaining EC molecules (which are not many in number) are involved in reducing the columbic interaction between the anions and cations of the salt. From another perspective, the 30 wt% EC complex has reached the critical percolation limit. Percolation is a process where formation of percolation paths gives rise to conductivity characteristic of metal salts in the polymer electrolytes. Since the number of EC molecules involved in dissociating the polymer salt is not that many, the number of extra mobile ions is also not many which leads to an insignificant increase in conductivity. Conductivity increases with an increase of percentage of plasticizer in PVC: Li_2SO_4: EC polymer electrolytes. However, this trend tends to decrease after PVC- Li_2SO_4 - 30 wt% EC. The addition of more than 30 wt% EC decreases the electrical conductivity of the polymer. This is attributed to the formation of linkages between the plasticizer itself, causing it to crystallize [10-12].

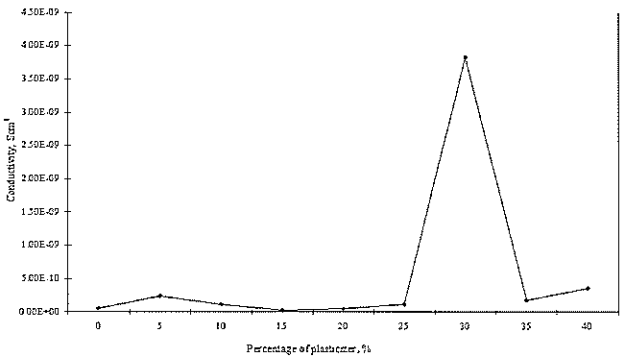

Figure 1. Variation of conductivity as a function of percentage of EC in the PVC-Li_2SO_4: EC system.

Dielectric studies

Figure 2 shows the variation of real part of dielectric modulus (M') as a function of frequency for PVC-Li_2SO_4 complexes with different content of EC.

The M real shows an increase at the high frequency end. The possible presence of peaks in the modulus formalism at higher frequencies for all the polymer system indicates that the polymer electrolyte films are ionic conductors. The peaking curve at higher frequencies may be attributed to the bulk effect. At low frequencies, it is observed that the value of M' is in the vicinity of zero, indicating that the contribution of electrode polarisation is negligible [13, 14].

FTIR studies

Molecular interactions between polymers, salt and plasticizers were analyzed using FTIR spectra. The FTIR spectra of different composition of low

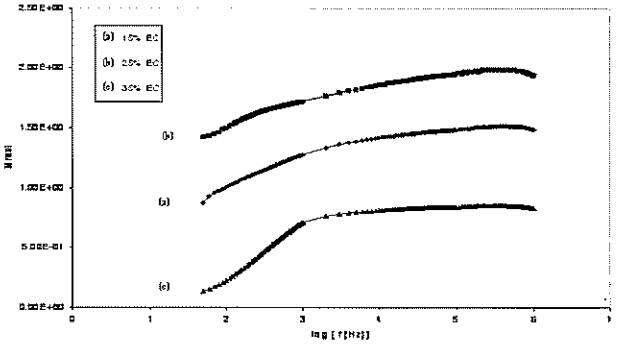

Figure 2. Variation of real part of modulus (M') as a function of frequency for (a) PVC-Li_2SO_4:EC (85:15), (b) PVC-Li_2SO_4: EC (75:25) and (c) PVC-Li_2SO_4:EC (65:35) complexes.

molecular weight PVC, Li_2SO_4, EC and polymer complexes are shown in Figure 3. The vibrational bands and peak assignments of the FTIR spectrum of low molecular weight PVC obtained in this work are as follows: C-H stretching mode observed at 2912 cm^{-1}, CH_2 symmetrical bending vibration at 1426 cm^{-1}, CH_2 deformation at 1331 cm^{-1}, CH rocking at 1254 cm^{-1}, *trans*-CH wagging mode at 958 cm^{-1}, C-Cl stretching mode at 833 cm^{-1} and *cis*-CH wagging at 635 cm^{-1}. On the other hand, for EC, 1773 cm^{-1} assigned to C=O stretching vibration was observed. In addition to this, the bands at 1617 cm^{-1}, 1111 cm^{-1} and 649 cm^{-1} are characteristic frequencies of Li_2SO_4.

The FTIR spectrum of PVC-Li_2SO_4 (80:20) (Fig. 3d) was taken to study the interactions between PVC and Li_2SO_4. Flattening of C-Cl stretching mode of PVC in PVC-Li_2SO_4 (80:20) showing that Li_2SO_4 salt interacts with the chlorine atom of PVC. The CH rocking of pure PVC at 1254 cm^{-1} was shifted to lower frequency of 1241cm^{-1} with increased intensity from 4 % T to 18.2 % T. The characteristic peak of pure Li_2SO_4 at 649 cm^{-1} changed from a sharp peak to a small shoulder peak at higher wave number in the broad band at 616 cm^{-1}. This might be due to overlapping with a moderate peak at 635 cm^{-1} originating from pure PVC.

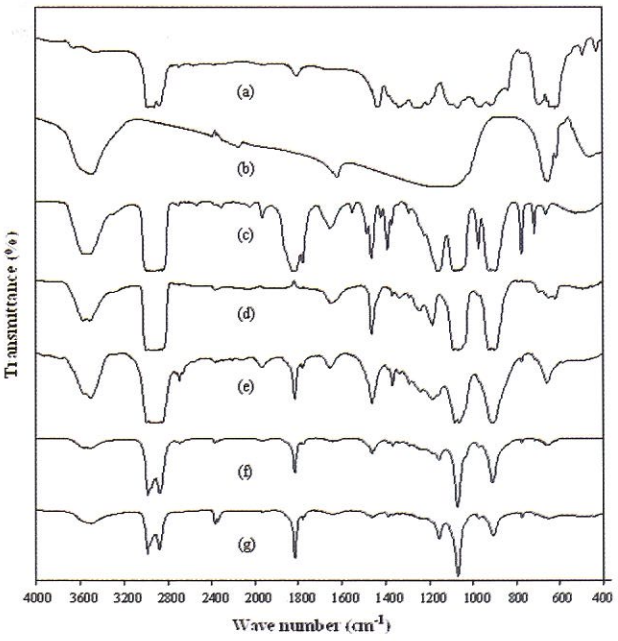

Figure 3. FTIR spectra of (a) pure low molecular weight PVC, (b) pure Li_2SO_4, (c) pure EC, (d) PVC:Li_2SO_4 (80:20), (e) PVC-Li_2SO_4:EC (80:20), (f) PVC-Li_2SO_4:EC (70:30), and (g) PVC-Li_2SO_4:EC (60:40).

In order to investigate the interaction and effect of the plasticizer in PVC-Li_2SO_4-EC samples, the infrared spectra of the samples with different concentrations of EC added were analyzed. Sharp vibrational peak at 1773 cm^{-1} was assigned to C=O stretching vibrations of pure EC, which had been shifted to1774 cm^{-1} in 20 wt% EC complexes. The vibrations of vinylidene group at 1649 cm^{-1} of pure EC were shifted to 1654 cm^{-1}, 1641 cm^{-1} and 1643 cm^{-1} in 20, 30 and 40 wt% EC respectively. On the other hand, the characteristic peak of pure EC at 2965 $cm^{-1}$and 2838 cm^{-1} became sharper as the composition of EC increased in PVC:Li_2SO_4:EC complexes. These shifts in frequency, changes in intensity and disappearance of some peaks on blending electrolyte prove the occurrence of complex formation within the polymer-lithium sulphate salt-plasticizer system.

Thermogravimetric analysis (TGA) studies

In order to ascertain the thermal stability of the polymer electrolytes, the obtained films were subjected to TGA analysis. Figure 4 represents the thermogravometric analysis curve of low molecular weight PVC-Li_2SO_4 complexes with 10 wt% and 30 wt% EC. Two steeps are observed in Figure 4(a). The steep around 100 °C is due to the removal of moisture and the second predominant steep around 270 °C is an indication of the stability of the complexes [15]. The weight loss for first decomposition steep is ~15% and it is due to crystallization and decomposition of the sample. Volatilization of monomers and oligomers adsorbed in the matrix can also be responsible for this initial weight loss [16]. The weight of the polymer electrolyte decreased gradually above 270 °C. This shows that the complex is stable up to about 270 °C.

In Figure 4(b), the weight loss for the first decomposition had increased sharply and reached

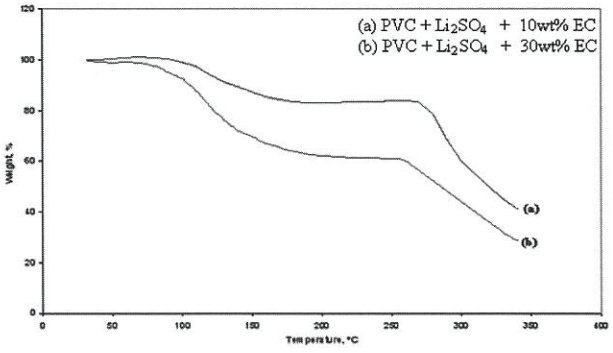

Figure 4. The thermogravimetric analysis of PVC-Li_2SO_4: EC complexes.

$$\text{Generation time } (T) = \sum_{0}^{\infty} I_\chi m_\chi \chi / R_o$$

where, I_χ = the proportion of individuals surviving to age$_\chi$ (survivorship); m_χ = the age specific fecundity (number of neonates produced per surviving female at age$_\chi$) and χ = days.

The initial age of reproduction was referred to as the average age (in days) at which a female started to produce her first batch of offspring. Longevity was referred to as the average total number of days the female survived during the course of study. The reproduction rates of *M. macrocopa* were compared by one-way ANOVA. Statistical significance among the different treatments was accepted at $p < 0.05$.

RESULTS AND DISCUSSION

The average longevity of the cladoceran, *M. macrocopa* (Fig. 1), did not vary significantly (p = 0.226) among the three treatments, which were 7.0 days for *Spirulina*, 7.7 days for *Chlorella* and 8.0 days for fish faeces (Table 1). In de-chlorinated tap water (control), the neonates started to die from day 2 and complete mortality was observed by day 3 (Fig.2).

Table 1. Life table of *Moina macrocopa* fed with different diets at a concentration of 3.5 g/L.

Diet type	Average longevity (days)	Initial age of reproduction (days)	Net reproduction rate (R_o)	Generation time (T)
Control	1.70 ± 0.58	–	–	–
Chlorella	7.70 ± 1.15	4	8.32	4.10
Spirulina	7.00 ± 0.00	5	4.01	4.50
Fish faeces	8.00 ± 2.65	3	17.27	4.03

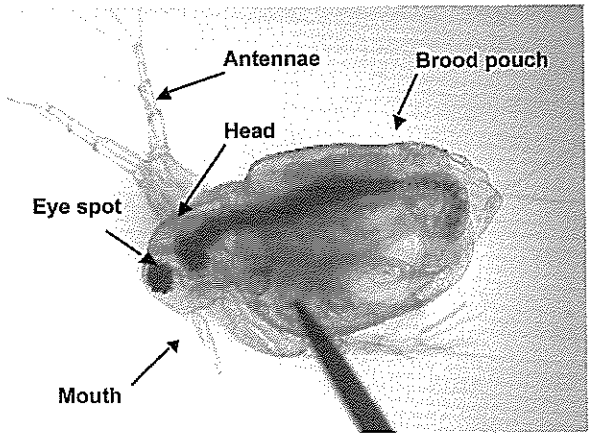

Figure 1. High magnification photomicrograph of an adult water flea, *Moina macrocopa* (1000×).

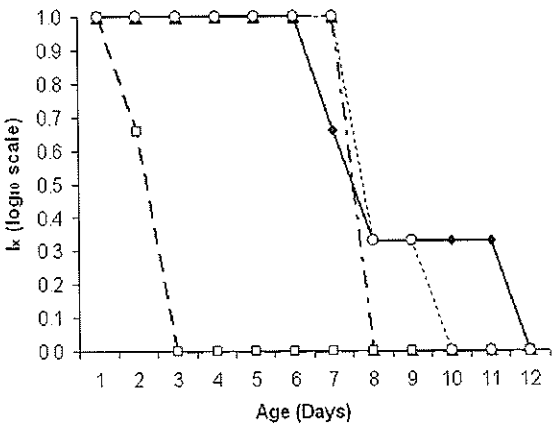

Figure 2. Survivorship of *Moina macrocopa* under different treatments. –□– control; –▲– *Spirulina* sp.; –○– *Chlorella* sp.; –◆– fish faeces.

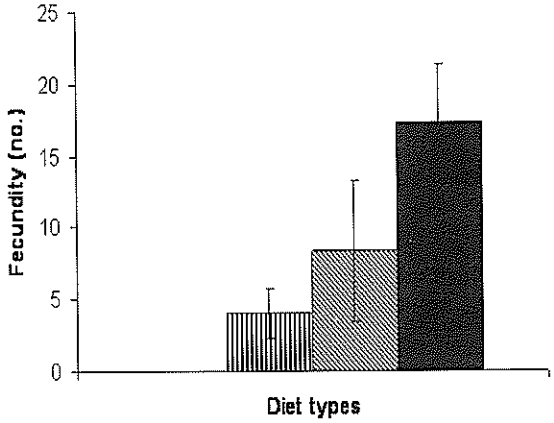

Figure 3. Average fecundity of *Moina macrocopa* under different treatments. No values are shown for the control experiment as the females did not produce any neonates. Error bar = mean ± standard deviation. control; *Spirulina* sp.; *Chlorella* sp.; fish faeces.

Mortality did not occur with any of the treatments during the first 6 days. *M. macrocopa* fed with *Spirulina* and *Chlorella* started to die from day 7, but the latter showed longer survivorship. The survival of *M. macrocopa* treated with 3.5 g/L *Chlorella* powder appeared similar to the findings with live *Chlorella vulgaris* [19]. Some *M. macrocopa* fed with fish faeces began dying from day 6 (Fig. 2). Nonetheless, a stable population was achieved between days 8 to 11, with complete mortality only on day 12.

The average number of neonates produced by the parthenogenetic females was significantly different (p = 0.022) among the three treatments and control experiments. Females fed with fish faeces showed the highest average fecundity followed by those treated

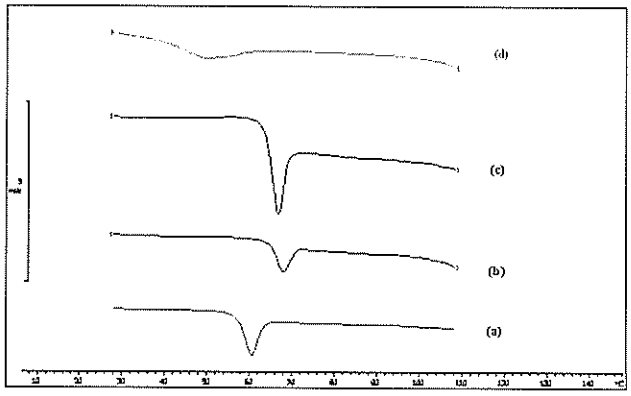

Figure 5. The DSC thermogram of (a) pure low molecular weight PVC, (b) PVC: Li_2SO_4 (80:20),(c) PVC-Li_2SO_4: EC (90:10), and (d) PVC-Li_2SO_4:EC (70:30).

around 30%. It shows that as the percentage of plasticizer increases, the weight loss for the first decomposition of the compound also increases. As the amount of plasticizer added to the polymer electrolyte system increases, the thermal stability decreases. This is because the movement of the ions in the polymer chain becomes easier and free to move as the amount of plasticizer increases. Polymer electrolytes of higher PVC content and lower plasticizer amount are found to have a relatively good stability.

Differential scanning calorimetric (DSC) studies

The DSC thermogram of a pure PVC is shown in Figure 5(a). At the glass transition temperature, T_g, an endothermic reaction is observed, i.e. the specific heat of the sample increases. The T_g for pure PVC is around 59 °C which is near to the literature value from Ramesh *et al.* [15]. The DSC thermogram of lithium sulphate (20 wt. %) and PVC (80 wt %) complex is given in Figure 5(b). The value of T_g is around 67 °C. This shows that the glass transition of PVC-salt complex is shifted towards higher temperatures relative to pure PVC, which is expected because of the lower degree of chain movement caused by chlorine coordination. Since the glass transition involves the freezing of large-scale molecular motions without change in structure or the evolution of the latent heat, it can be concluded that Li_2SO_4 decreases the local chain mobility.

The DSC thermogram for 10 wt % of EC in the plasticized polymer electrolyte is shown in Figure 5(c). The T_g is 65 °C. The 10 wt% of EC in the plasticized sample presents a lower value of T_g than plasticizer-free sample due to a lubricating effect. The plasticizer behaves like a solvent when mixed with a polymer and results in a lowering of the T_g value. The plasticization effect is related to the weakening of the dipole-dipole interaction due to the presence of the plasticizer molecules between the PVC chains [17]. The decrease in T_g helps to soften the polymer backbone and increase its segmental motion. The DSC thermogram for 30 wt % of EC in the plasticized polymer electrolyte is shown in Figure 5(d). The T_g of this composition of complex is 48 °C. The T_g decreases when the percentage of plasticizer added to the polymer electrolyte increases.

Conclusion

The introduction of salts and plasticizers increases the ionic conductivity to values applicable for device fabrication. The study on the dielectric modulus behaviour is very useful for understanding the behaviour of polymers electrolyte complexes. The FTIR studies which had shown some shift in peaks, change in intensity and change in shape proved the effects of polymer blending with salt and plasticizer. The study of TGA and DSC is very useful to identify the thermal stability of the PVC when blended with salt and plasticizers.

REFERENCES

1. Gray F.M. (1991) *Solid Polymer Electrolytes*. VCH publishers Inc. New York.
2. Abraham K.M. and Alamgir M. (1990) Li^+-Conductive solid polymer electrolytes with liquid-like conductivity. *Journal of Electrochemical Society.* **137**: 1657-1658.
3. Alamgir M. and Abragam K.M. (1993) Li Ion Conductive electrolytes based on poly(vinyl chloride). *Journal of Electrochemical Society.* 140: L96-L97.
4. Bohnke O., Frand G., Rezrazi M., Rousslot C. and Truche C. (1993) Fast ion transport in new lithium electrolytes gelled with PMMA. 1. Influence of polymer concentration. *Solid State Ionics* **66:** 97-104.
5. Tsuchida E., Ohno H. and Tsunemi K. (1983) Conduction of lithium ions in polyvinylidene fluoride and its derivatives—I . *Electrochimica. Acta* **28:** 591-595.
6. Rajendran S., Mahendran O. and Mahalingam T.

(2002) Thermal and ionic conductivity studies of plasticized PMMA/PVdF blend polymer electrolytes. *European Polymer Journal* **38:** 49-55.

7. Blonsky P.M., Shriver D.F., Austin P. and Allcock H.R.(1986) Complex formation and ionic conductivity of polyphosphazene solid electrolytes. *Solid State Ionics* **18:** 258-264.
8. Chowdari B.V.R., Huq R. and Farrington G.C. (1992) Thermal and electrical characterization of PEO-based polymer electrolytes containing mixed Co(II) and Li(I). *Solid State Ionics* **57:** 49-58.
9. Mishra R., Baskaran N., Ramakrishnan P. A. and Rao K.J. (1998) Lithium ion conduction in extreme polymer in salt regime. *Solid State Ionics* **112:** 261-273.
10. Golodnitshy D. and Farrington G.C. (1996) Effect of plasticizers on the CPE conductivity and on the Li-CPE interface. *Solid State Ionics* **85:** 231-238.
11. Kim D.W., Park J.K. and Moon S.I. (1998) Electrical properties of the plasticized polymer electrolytes based on acrylonitrile-methyl methacrylate copolymers. *Solid State Ionics* **106:** 329-337.
12. Chung S.H., Heitjans P., Winter R., Bzaucha W., Florjanczyk Z. and Onoda Y. (1998) Enhancement of ionic conductivity by the addition of plasticizers in cationic monoconducting polymer electrolytes. *Solid State Ionics* **112:** 153-159.
13. Mishra R. and Rao K.J. (1998) Electrical conductivity studies of poly(ethyleneoxide)-poly(vinylalcohol) blends. *Solid State Ionics* **106:** 113-127.
14. Venkateswarlu M. and Satyanarayana N. (1998) AC conductivity studies of silver based fast ion conducting glassy materials for solid state batteries. *Materials Science and Engineering B.* **54:** 189-195.
15. Ramesh S. and Arof A.K. (2001) Structural, thermal and electrochemical cell characteristics of poly(vinyl chloride)-based polymer electrolytes. *Journal of Power Sources* **99:** 41-47.
16. Chiodelli G., Ferloni P., Magistris A. and Sanesi M. (1998) Ionic conduction and thermal properties of poly (ethylene oxide)-lithium tetrafluoroborate films. *Solid State Ionics* **28-30:** 1009-1013.
17. Mano V., Felisbersti M.I. and De Paoli M.A. (1997) Influence of $FeCl_3$ on the mechanical, thermal, and dynamic mechanical behavior of PVC. *Macromolecules* **30**: 3026-3030.

Journal of Science and Technology in the Tropics (2009) **5**: 73-78

Experimental investigation of single groove parallel coupled microstrip line bandpass filter with harmonic suppressed

Jayaseelan Marimuthu and Mazlina Esa
Microwave/RF and Antenna Research Group, Department of Radio Communication Engineering, Faculty of Electrical Engineering, 81310 UTM Skudai, Johor Darul Takzim, Malaysia
(jayaseelan.marimuthu@yahoo.com, mazlina@fke.utm.my)

Accepted 15-04-2009

Abstract This paper describes, the experimental performance of a fabricated single grooved Parallel Coupled Microstrip Bandpass Filter (PCMBF) on a low cost laminate board, with improved passband response and first harmonic suppression for various operating bandwidth. The suppression of the first harmonic spurious response is possible through transmission zero frequency realignment method. A single groove of specific dimensions located at the center of the parallel coupled line has been employed for the realignment of the transmission zero and first harmonic frequencies. An implemented single-stage bandpass filter with various coupling gaps, on a low cost laminate board, showed excellent harmonics suppressions with optimized groove. Then, two–stage bandpass filters of different operating bandwidth were designed for optimized groove. It was then implemented on a low cost laminate board and tested. The measured results validate real harmonics suppression performance with controllable single groove parameters.

Keywords bandpass filter – harmonic suppression – transmission zero – J-inverter network – groove

INTRODUCTION

In many microwave systems, parallel coupled microstrip bandpass filters (PCMBF) have been widely used. The parallel coupled microstrip line (PCML) structure has been used as the main coupling component in PCMBF design [1, 2]. However, one of the disadvantages is, the first spurious passband of a PCMBF appears at twice the basic passband frequency and the rejection of the upper stopband is worse than the lower stopband. Consequently, this greatly limits its applications and degrades system performance. This resulted from the inequality of the even and odd mode phase velocities of coupled lines in each stage [3, 4].

For a given PCML design, the odd mode is propagating faster than the even mode, i.e. the phase constant for the odd mode is less than the phase constant of the even mode; $\beta odd < \beta even$. In addition, the electromagnetic energy for the odd mode concentrates around the centre gap, while for the even mode it concentrates around the outer metallic edges [3, 4]. Various techniques have been proposed to equalize the even and odd mode velocities or their electrical line lengths. These leads to the minimization of harmonic response. All the techniques proposed above lead to the restructuring or redesigning of the filter with new physical design parameters [3, 4]. The technique proposed in this paper does not require restructuring or redesigning of PCMBF. It involves simple modification by introducing a single groove or notch at the centre of PCML. The initial studies involving varying number of grooves were reported in [5, 6]. Similar studies involving multiple grooves arranged periodically in structures have been reported [7–10].

The studies on suppression of harmonic response were carried out by transmission zero realignment method using a single groove at the center of PCML [11, 12]. The studies were done using numerical simulation software [13]. It was found that a single groove of specific dimension located at the center of PCML structure is able to realign the transmission zero frequency and its harmonic response frequency. The initial studies involving single groove were reported in [14] for wideband bandpass filter, fabricated on low cost, high loss laminate board. Further investigation involving single groove PCMBF for various operating

bandwidth fabricated on low-loss microwave board RT/duroid have been reported [15] with improved performance.

PCMBF is usually formed by few couplers with various coupling coefficient based on the filter order. A three-stage bandpass filter is traditionally designed with tight couplers (TCg) arranged at the input and output of the filter and the weak couplers (WCg) at the middle section of the filter. The operating bandwidth of PCMBF depends on the coupling coefficient of PCML utilized at the middle section of the filter. In this paper, various operating bandwidth three-stage single groove PCMBF were designed and fabricated on low cost high loss laminate board. This study was done to validate the proposed single groove PCMBF harmonic suppression techniques applicable at various operating bandwidth of PCMBF structure regardless of type of microwave board utilized for fabrication.

FILTER DESIGN

The configuration of a single stage bandpass filter is illustrated in Figure 1(a). The dimensions were computed based on the physical parameters: (a) the feeding line with characteristic impedance $Z_o = 50\Omega$, width $W_f = 3$ mm, length $l_f = 16$ mm; and (b) the parallel coupled microstrip line (PCML) with $Z_{even} = 70.7\Omega$, $Z_{odd} = 36.6\Omega$, $\beta_{even} = 97.1$ m-1, $\beta_{odd} = 87.8$ m-1, width $W = 2$ mm, coupling gap $S = 0.2$ mm, length of couple $l = 16$ mm [13]. The filter was fabricated on laminate FR4 board of dielectric constant $\varepsilon_r = 4.4$, substrate height $h = 1.524$ mm and dielectric loss of 0.025. Figure 1(b) shows the equivalent J-inverter network of single stage bandpass filter of Figure 1(a). The fabricated single stage bandpass filter is shown in Figure 2. The simulated and measured responses are shown in Figure 3. It can be seen that the insertion loss S_{21}, has fundamental response f_o at 2.52 GHz, first harmonic response f_h at 5.18 GHz and transmission zero fz_o at 5.86 GHz.

From the equivalent J-inverter network of two PCMLs shown in Figure 1(b), the middle transmission-line resonator is actually formed by cascading two identical electrical lengths of $\theta/2$, where its overall length become θ. The transmission-line resonator resonates at the frequencies of $\theta = 180°, 360°, 540°$, etc. The first resonance happens at $\theta = 180°$ [$f_o = 2.52$ GHz in Figure 3], and is usually

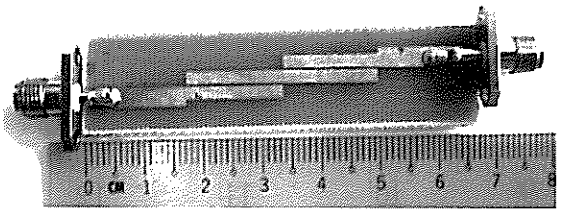

Figure 2. Single-stage PCMBF without groove.

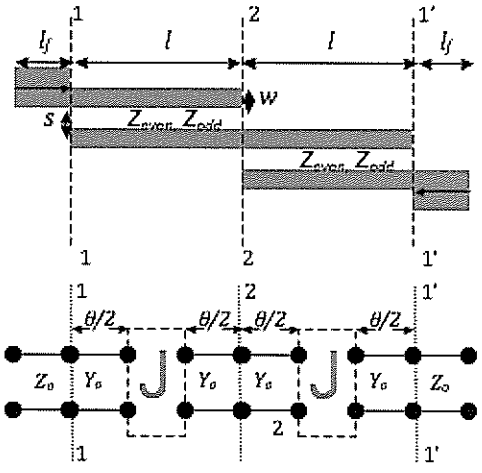

Figure 1. Physical layout (a) and equivalent J-inverter circuit (b) for single-stage PCMBF.

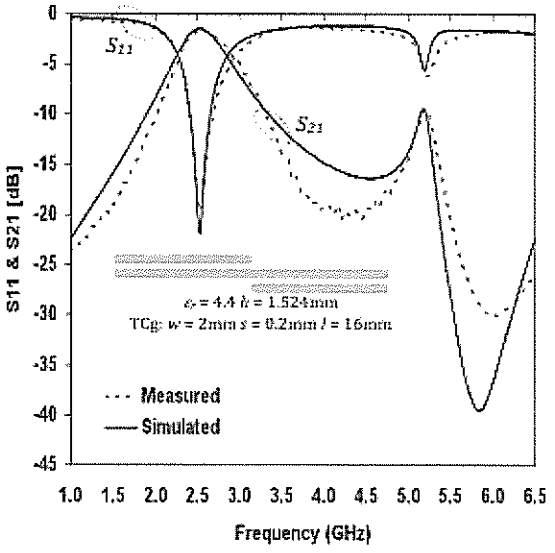

Figure 3. Response of single-stage PCMBF without groove.

utilized to make up the dominant passband in the design of a bandpass filter. The second resonance at θ = 360° [f_h = 5.18 GHz in Figure 3] contributes to the first-harmonic spurious passband.

FILTER DESIGN WITH GROOVE

The presence of harmonic response in the PCMBF is mainly due to the non-equivalent velocity of even and odd modes which are present in the PCML structure. The odd mode which has the current density concentrated at the inner edges of the microstrip conductors propagates faster than the even mode with current density at the outer edges of the microstrip conductors. In order to equalize the even and odd mode phase velocities at second resonance of the middle resonator, a single rectangular groove or notch was introduced at the center of the PCML inner edges of the two microstrip conductors as shown in Figure 4. The effect of the groove on the designed single stage bandpass filter was investigated.

The single stage bandpass filter was designed with single groove located at the centre of the PCML for various sizes of groove. The design was simulated. Figure 5 shows the simulated insertion loss S_{21}, response of a single stage bandpass filter with various groove sizes. It clearly shows clearly that as the groove height H varies with fixed width W, the first harmonic frequency f_h and transmission zero frequency f_{zo} approach each other. At one particular frequency, transmission zero f_{zo} cancels off the harmonic response f_h. The behavior of the first harmonic frequency f_h and transmission zero frequency f_{zo} against various groove sizes is plotted as shown in Figure 6.

In Figure 6, it can been seen that $f_{zo} > f_h$ when $0 < H < 1.1$ mm and $f_{zo} < f_h$ when $H > 1.1$ mm, for $W = 0.8$ mm. It can also be seen that $f_{zo} = f_h = 4.76$ GHz when $H = 1.1$ mm. Hence, it can be inferred that when a groove with dimension $W = 0.8$ mm and $H = 1.1$ mm is embedded at the center PCML, the transmission zero frequency equals to the first harmonic response frequency, thus canceling it.

Figure 7 shows the fabricated single stage bandpass filter with optimized groove dimensions.

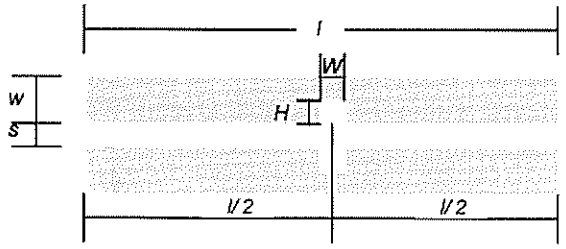

Figure 4. Structure of PCML with groove located at the centre.

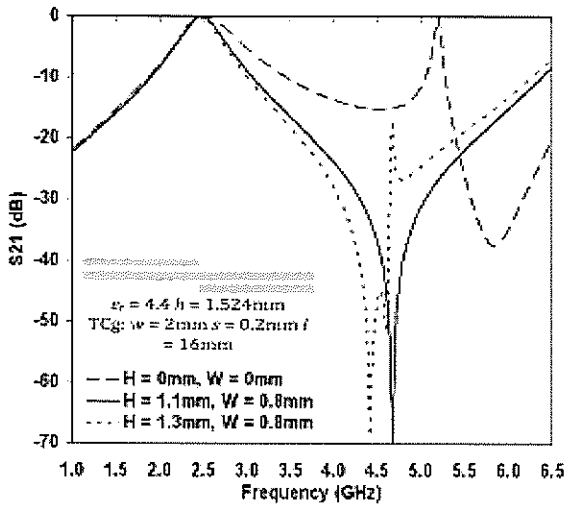

Figure 5. Frequency response of single-stage bandpass filter with single groove of W = 0.8mm and different H for TCg.

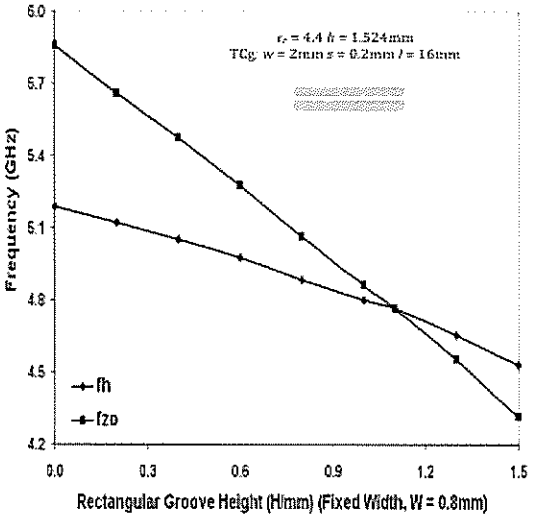

Figure 6. Frequency of transmission zero and harmonic resonance for single groove with W = 0.8 mm and different H for TCg.

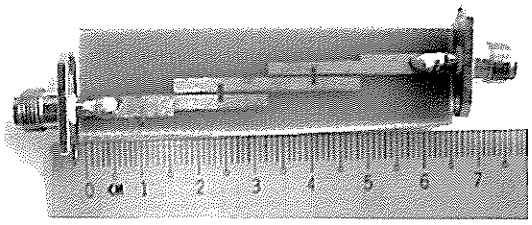

Figure 7. Single-stage PCMBF with optimized groove.

The simulated and measured results are compared as shown in Figure 8. The return and insertion losses response of the single stage bandpass filter with optimized groove dimension H = 1.1 mm and W = 0.8 mm clearly shows the cancellation of the first harmonic response.

From the previous discussion, a PCML with single groove was able to realign transmission zero frequency which cancels the first harmonic frequency of a single stage bandpass filter. Hence harmonic suppression of single stage PCMBF at the first-order spurious passband is possible with only an embedded single groove. The research proceeds to designing multistage bandpass filters with harmonic suppression feature.

Two-stage PCMBF was designed with various combinations of single–stage PCMBF with optimized groove for harmonic suppression at different operating bandwidths. Figure 9 shows two–stage PCMBF made by cascading of two various coupling gap single–stage PCMBF with optimized groove. Filter 1 was designed by using two TCg1 with optimized groove, Filter 2 was designed by using TCg1 and WCg1 with optimized groove and finally Filter 3 was designed by using TCg1 and WCg2 with optimized groove. All three filters simulated and groove at TCg1, WCg1 and WCg2 were further optimized to achieve full harmonics suppression of two–stage PCMBF. The optimized filters were then fabricated on low cost laminate board with dielectric constant ε_r = 4.4, substrate height h = 1.524 mm and dielectric loss of 0.025 as shown in Figure 10, and measured.

The filters were design to operate at 2.45GHz. The selected frequency and bandwidth is suitable for full-duplex Local Area Network (LAN) communication for indoor and outdoor applications. The simulated and measured return and insertion losses responses of the two-stage bandpass filter were compared as shown in Figure 11. It clearly shows that the both results agree well with each other, showing full suppression of harmonic response for various operating bandwidths. A centre frequency of 2.45 GHz can be observed for simulated and measured results for various operating bandwidth. An acceptable return loss of below -3 dB or half power is achieved within the passband. Overall the rejection bands exhibit less than -50 dB low insertion losses

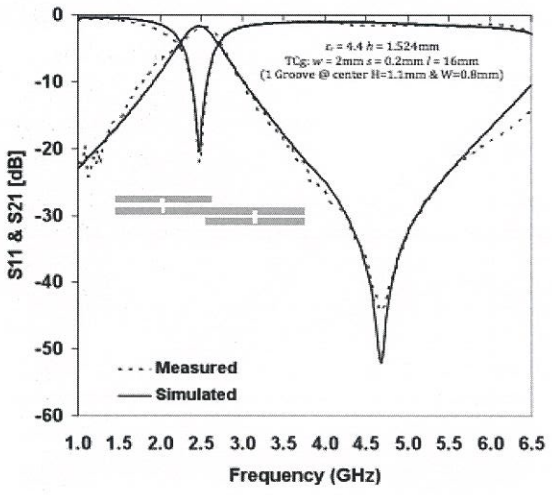

Figure 8. Response of single-stage PCMBF with optimized groove.

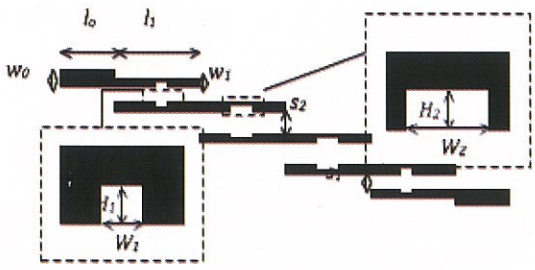

Figure 9. Layout of two–stage PCMBF with single groove at center of PCML structure.

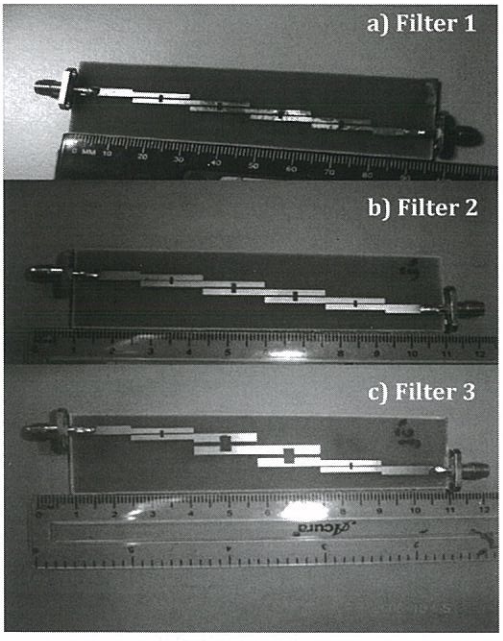

Figure 10. Two-stage PCMBF with optimized groove dimension.

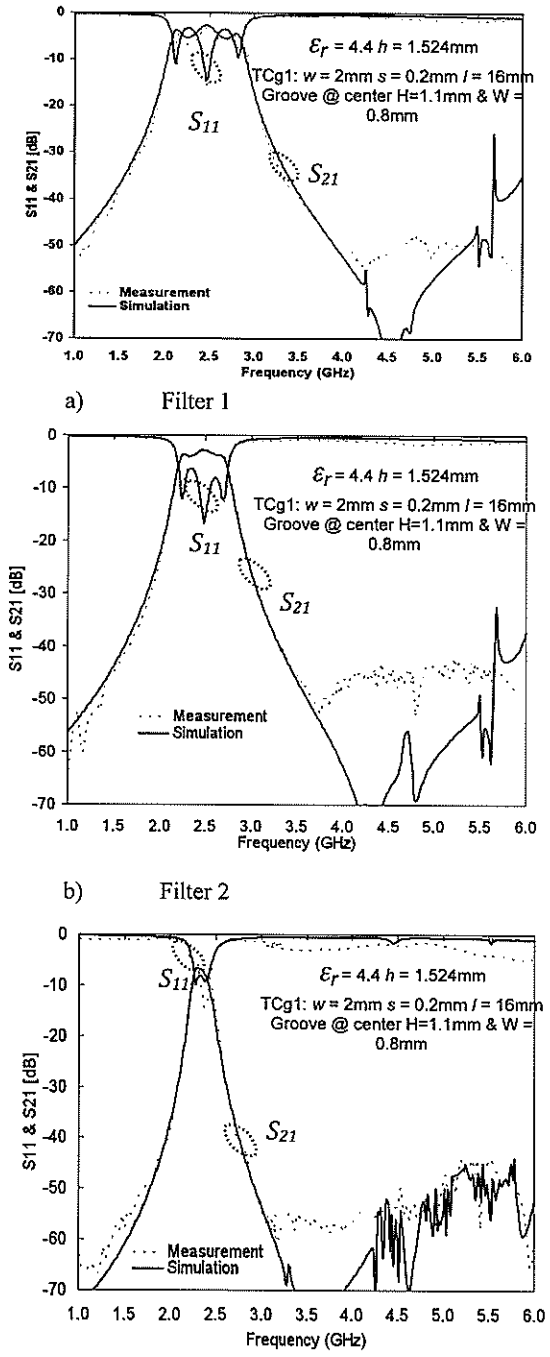

Figure 11. Response of two-stage PCMBFs with optimized groove.

for various operating bandwidth. The measured results shows full suppression of harmonic response and for Filter 1 with wideband response of more than 40%, Filter 2 with moderate wideband response of 28% while Filter 3 with narrowband response of 12%. Overall it shows for various operating bandwidth harmonic suppression and sharp rejection slopes can be achieved with optimized single grove at centre of PCML structure for PCMBF with low cost high loss laminate boards.

CONCLUSION

Detailed investigations done for various operating bandwidth on harmonics cancellation by using transmission zero frequency realign method on low cost high loss laminate board and have been presented. The harmonic suppression can be done by using specific single groove located at the center of the PCML structure. Then, a simple two–stage PCMBF is demonstrated for the first time for various operating bandwidths on low cost high loss laminate board. It shows that, various operating filter bands with sharp-rejection stopbands and excellent rejection of first harmonic spurious response can be achieved. For validation, three 2.45 GHz of various operating bands in a two-stage PCMBF prototype, useful in full-duplex Local Area Network (LAN) communication, have been demonstrated. The resulting agreement between measurements and simulations has confirmed the experimental viability of the single groove filter topology for various operating bandwidth fabricated on low cost high loss laminate board.

REFERENCES

1. Pozar D.M (2005) *Microwave Engineering* 3rd Edition. Wiley, New York.
2. Hong J.S. and Lancaster M.J. (2001) *Microstrip Filters for RF/Microwave Applications*. Wiley, New York.
3. Chang Chi-Yang and Itoh Tatsuo (1991) A Modified Parallel – Coupled Filter Structure That Improve The Upper Stopband Rejection and Response Symmetry. *IEEE Trans. On Microwave Theory and*

Techniques **39**(2): 31-314.

4. Ester B. and Merze K.A. (1981) Parallel – Coupled – Line Filters for inverted – Microstrip and Suspended – Substrate MICs. *11th Eur. Microwave Conf. Dig.* pp 164-167.
5. Marimuthu Jayaseelan and Esa Mazlina (2005) Novel Parallel-Coupled Grooved Chebyshev Response Microstrip Bandpass Filter for ISM Band Application. *Proceedings of 2005 Malaysia Science and Technology Congress* (MSTC 2005).
6. Marimuthu Jayaseelan and Esa Mazlina (2005) Second Harmonic Suppression Characteristic of a Grooved Bandpass Filter. *IEEE Proceedings of Asia-Pacific Conference on Applied Electromagnetics* 2005: 264-268.
7. Sun Sheng and Zhu Lei. (2005) Periodically Nonuniform Coupled Microstrip-Line Filters With Harmonic Suppression using Transmission Zero Reallocation. *IEEE Trans. On Microwave Theory and Techniques* **53**(5): 1817-1822.
8. Kuo Jen-Tsai, Hsu Wei and Ting Huang Wie (2002) Parallel Coupled Microstrip Filters with Suppression of Harmonic Response. *IEEE Microwave and Wireless comp. Lett. 12*: 383-385.
9. Kim Bong S., Lee Jae W. and Song Myung S. (2003) Modified Microstrip Filters Improving The Suppression Performance of Harmonic Signals. *IEEE MTT-S Digest*: 539-542.
10. Kim Bong S., Lee Jae W. and Song Myung S. (2004) An Implementation of Harmonic-Suppression Microstrip Filters with Periodic Grooves. *IEEE Microwave and Wireless Communication Letters* **9**: 413-415.
11. Marimuthu Jayaseelan and Esa Mazlina (2005) Harmonic Cancellation of Parallel - Coupled Bandpass Filter with Transmission Zero Realign Method. *IEEE Proceedings of Asia-Pacific Conference on Applied Electromagnetics 2005*: 227-231.
12. Marimuthu Jayaseelan and Esa Mazlina (2006) Equivalent J – Inverter Network Parameters Analysis and Cancellation of Spurious Response of Parallel Coupled Microstrip Line. *IEEE Proceedings of 2006 International RF and Microwave Conference*: 247-252
13. Marimuthu Jayaseelan and Esa Mazlina (2005) Modified Design Equations for Improved Accuracies of Microwave Parallel-Coupled Bandpass Filter. *Proceedings of 2005 Malaysia Science and Technology Congress* (MSTC2005).
14. Marimuthu Jayaseelan and Esa Mazlina (2007) Wideband and Harmonic Suppressed Method of Parallel Coupled Microstrip Bandpass Filter using Centered Single Groove. *IEEE Proceedings of 2007 14th International Conference on Telecommunication.*
15. Marimuthu Jayaseelan and Esa Mazlina (2007) Experimental Performance of Harmonic Suppressed Bandpass Filter. *IEEE Proceedings of Asia-Pacific Conference on Applied Electromagnetics 2007.*

Journal of Science and Technology in the Tropics **5**: 79-81

Horticultural carbon, terra preta, and high-performance horticulture in the humid tropics

F. S. P. Ng
C/o Forest Research Institute Malaysia, Kepong, Kuala Lumpur, Malaysia
(E-mail: fng@pc.jaring.my)

Abstract A horticultural carbon has been developed using charcoal briquette manufactured from sawdust. It has been used successfully with different proportions of clay soil to grow a variety of plants to create a rooftop garden and an indoor tropical rain forest at a shopping mall in Petaling Jaya, Malaysia.

Keywords horticultural carbon – roof-top garden – in-door rain forest

INTRODUCTION

Soils in the humid tropics tend to be highly clayey. Clay particles stick together to impede passage of water and air, and this is detrimental to root growth. Without sustained effort to keep clay soils open and porous, tropical soils rapidly become unproductive. Growers resort to many different methods of farming on clayey soils. For example, vegetable growers till the soil after each harvest and pile up the loosened soil to form raised beds. During each watering session, water soaks in and drains out easily, thereby simultaneously renewing the supply of water and air in the soil. A good soil is analogous to lung tissue in that both have large internal surfaces to hold moisture and air. Unfortunately the effect of tilling lasts only for a few months.

Clay soil may be burnt over a hot fire, in the process of which it becomes crumbly [1]. Burnt soil maintains its crumbly structure for up to one year, and such soil is often used for container gardening.

However, the most favoured soil for horticulture is garden black soil, which goes by the Malay name of *tanah hitam* (black soil). Black soil originated in household backyards where domestic waste was dumped and periodically burnt. The black colour was due to the accumulation of charcoal and soot in the soil over time.

Tanah hitam in Malaysia seems to be very similar to the soil in the Amazon known in Portuguese as *terra preta* (black earth). *Terra preta* soils are very fertile and contain a high content of carbon (about 10%). They occur on sites that appear to have had permanent native settlements for centuries before their populations were wiped out by diseases brought in by the Europeans. It would have taken centuries of firewood burning on the same sites to have produced black soil in the vast quantities, to 2 m deep in some sites. The discovery of *terra preta* sites has created a lot of discussion in the Internet about its origin.

THE DEVELOPMENT OF HORTICULTURAL CARBON

Open burning has been prohibited for many years in Malaysia, hence black soil is no longer available. Needing a large volume of good soil to establish a rain forest in the '1 Utama' shopping mall in Petaling Jaya, Selangor, Malaysia, I decided to make such a soil by mixing charcoal particles with soil. We made this soil by mixing normal clayey soil (mostly subsoil) with charcoal and coconut fibre in equal proportions by volume. The charcoal was conventional charcoal produced by the kilning of mangrove wood. This came in large hard pieces that had to be broken up mechanically. The resulting particles were irregular in size and difficult to mix with the clay and fibre. I then found a much better source of charcoal in the factory of a charcoal briquette manufacturer. Charcoal briquettes are made by compressing sawdust into standard-size briquettes for kilning. The briquettes, meant for the barbecue market, can be easily broken into particles, sieved to remove dust and graded into the desired sizes. We refer to the product as horticultural

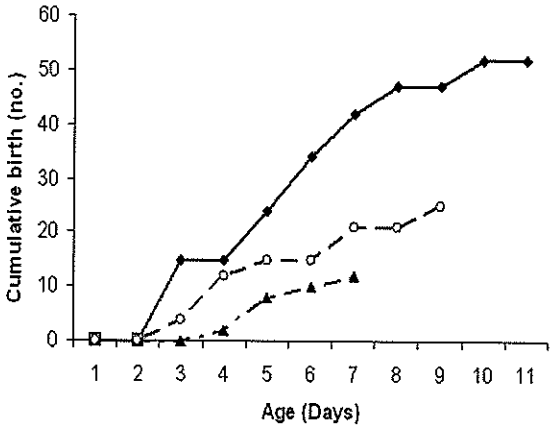

Figure 4. Cumulative birth of *Moina macrocopa* under different treatments. –□– control; –▲– *Spirulina* sp.; –○– *Chlorella* sp.; –◆– fish faeces.

with *Chlorella* and *Spirulina* (Fig. 3). Females in the control experiments did not produce any neonates. *M. macrocopa* fed with fish faeces and *Chlorella* started to reproduce from day 3 while those under *Spirulina* treatment produced offspring one day later (Table 1, Fig. 4). The peak population was reached on day 7, 9 and 11, for *Spirulina*, *Chlorella* and fish faeces, respectively. *M. macrocopa*, fed with fish faeces, gave higher reproductive rates and produced a greater number of neonates within a shorter generation time.

Under natural conditions, water fleas, rotifers and other zooplankton species generally feed on fine organic particles, bacteria, phytoplankton, fungi and protozoans that are suspended in water [20]. Mass cultivation of zooplankton for larviculture is widely carried out using baker's yeast, fish meal and ground trash fish [21]. The use of these foods is more convenient for large-scale production, but the production costs would be higher as zooplankton reared on yeasts and trash fish have inconsistent nutritional value and may be deficient in essential fatty acids (EFAs). This would lead to additional costs for enriching the zooplankton with microalgae or artificial feeds high in EFAs prior to feeding to fish and crustacean larvae [11-13, 21].

In the present study, completely or partially digested and totally undigested fish feed, which had passed through the gastro-intestinal system of the Nile tilapia, were excreted as faecal materials. The latter constituted a substantial proportion of total suspended solids in the rearing and treatment tanks of our freshwater RAS system. Burns [22] reported that suspended particles, with an upper size limit of 50 μm, were filtered from the water by cladocerans using their setae and body movements, and utilized as a source of food. It is speculated that these faecal materials might also induce the growth of heterotrophic and autotrophic bacteria, which are, in turn, ingested by *M. macrocopa* and other cladoceran species [23, 24].

Microbial degradation of organic and inorganic wastes depends on the amount of carbon, nitrogen and phosphorous available for their activity [25]. According to Fivlstad *et al.* [2] and Hakanson *et al.* [26], approximately 70% of total phosphorus and 15% of total nitrogen fed to cultured fishes are lost through faeces and subsequently utilized by bacteria. Some bacteria, for instance, nitrogen-fixing species of the genus *Nitrosomonas* and *Nitrobacter*, are able to obtain nitrogen, phosphorus and carbon from organic sources for optimal biomass production, and convert ammonia to nitrites and nitrates through the nitrification process [24, 27]. These bacteria provide energy for the dietary requirements of *M. macrocopa* as well as essential vitamins and amino acids, by decomposing dissolved organic compounds [28].

In conclusion, the application of fish faeces for cultivating *M. macrocopa* appears to show a promising potential for the larviculture industry, especially for freshwater recirculating aquaculture systems (RAS) where fish wastes can be easily harvested and recycled as a natural food source.

Acknowledgements – This study was funded by the UTAR postgraduate research fund (6202/L10). The authors would like to express their gratitude to Professor Dr. Thomas J. Smith of Sheffield Hallam University for his valuable comments on this manuscript and UTAR Bioscience laboratory staff for their cooperation and help throughout the study.

REFERENCES

1. Kibria G., Nugegoda D., Fairclough R. and Lam P. (1997). The nutrient content and the release of nutrients from fish food and faeces. *Hydrobiologia* **357:** 165-171.

2. Fivlstad S., Thomassen J.M., Smith M.J., Kjartansson H. and Anderson A.B. (1990). Metabolic production rates from Atlantic salmon (*Salmo salar* L.) and Arctic char (*Salvelinus alpinus* L.) reared in single

carbon (Fig. 1) [2]. We use two sizes: 1-4 mm particles for potting mixtures and 5-12 mm for garden beds.

We have found that a mixture of equal parts horticultural carbon and clay soil is good for general purpose horticulture. A mixture of three parts carbon to one part soil is better for cacti and succulents that need exceptionally well-drained soil.

Horticultural carbon is half the weight of soil, so the mixtures we make are lighter and more porous than ordinary garden soil. The reduction in weight was an important factor in my next project, a garden on the roof of the same shopping mall, seven floors above the ground. This garden, known as the Secret Garden of 1 Utama is now open to the public at weekends.

The porosity of soil mixed with horticultural carbon greatly reduces the labour of weeding because the weeds can be pulled out easily. However horticultural carbon only holds half the amount of water that an equivalent mass of clay soil will hold. Its lower water-holding capacity, together with its porosity, means that horticultural carbon dries out much faster than clay soils. The drying of the soil medium can be very damaging to the roots of plants, hence we find it necessary to keep our medium moist all the time. This can be arranged in various ways, for example, by watering twice a day. In pots, we would recommend placing the pots on shallow trays to hold water.

Horticultural carbon does not contain nutrients, hence fertilizers have to be applied regularly.

Initially the carbon and clay particles remain separate though mixed. Gradually the carbon wears down and becomes integrated with the clay, with consequent settling of the soil mixture. The soil level drops and is topped up with pure carbon.

Figure 1. Horticultural carbon.

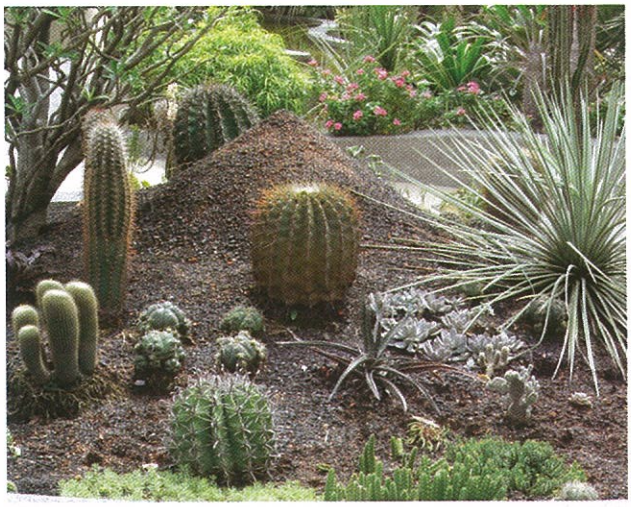

Figure 2. Cactus bed at the Secret Garden of 1 Utama.

Figure 3. Secret Garden of 1 Utama.

Figure 4. Rain Forest at 1 Utama.

THE PERFORMANCE OF PLANTS ON HORTICULTURAL CARBON

Our most extreme experiment was to grow rice on 100% horticultural carbon in plastic basins. The basins, about 20 cm deep, were three-quarters filled with carbon particles and topped up with water. Rice seeds were sown direct on the surface. Our Indonesian workers, rice-growers in their former lives, all had a good laugh because "everybody knows that rice only grows on *tanah liat* (sticky clay soil)". Well, our rice grew and produced a heavy crop of grains. We have now grown three successive crops. The roots form very dense mats. After each crop, the roots have to be dried out before the carbon particles can be shaken out and recovered.

For cacti and succulents, we use a mix of 75% carbon to 25% burnt soil in elevated beds. Some species thrive, but some still find it too wet, and rot when it rains daily. Nevertheless ours is a decent-looking cactus bed (Fig. 2) considering that it is fully exposed to tropical rain.

Begonias, calatheas, and aglaonemas grow well in 50:50 mixes on raised beds provided 50-75% of the sunlight is cut off using shade-nets.

Of temperate plants and montane plants, we have managed to grow apple, peach, plum, *Magnolia grandiflora*, *Magnolia liliiflora*, arabica coffee, azalea, camellia, day lilies and *Platanus*. It has been hypothesized that in the tropics, the high night-time temperatures raise the night-time respiration rate to a level that temperate plants cannot adapt to. We think a high carbon mix allows air (oxygen) to get to the roots more easily, making it easier for temperate plants to adapt. However the flowering patterns of temperate plants are disrupted by the lack of seasons. Some species do not flower at all (e.g. day lilies), some flower infrequently and sparingly (e.g. apple and plum), and some flower all through the year (e.g. *Magnolia liliiflora* and arabica coffee).

WHERE TO SEE HORTICULTURAL CARBON IN USE

In Malaysia, the Secret Garden of 1 Utama (Fig. 3) in Petaling Jaya, occupying 0.25 ha of flat roof top 7 floors above the ground, is the largest display open to public view. Here are grown over 500 species of plants, including palms, orchids, temperate plants, flowers, spices, rice, cacti, climbers and grasses. Also in 1 Utama but on the lower ground floor, is a rainforest (Fig. 4) with some 50 species of timber trees growing on a horticultural carbon mixture. In Sarawak, the Laila Taib Ethno Garden of the Sarawak Biodiversity Centre at Semengoh, Kuching, displays a good range of native herbs grown on horticultural carbon, most of them larger and healthier than in their original rain forest habitats.

HORTICULTURAL CARBON IN CARBON SEQUESTRATION

Since the Industrial Revolution, the amount of carbon dioxide in the atmosphere has increased significantly, to bring about global warming. The increase in carbon dioxide in the atmosphere is due partly to the extraction and burning of coal and petroleum and partly to the clearing of forests, which reduces the amount of organic carbon stored in forests.

Proposed measures to control global warming include reduction in consumption of coal and petroleum and the planting of trees and forests to convert atmospheric carbon dioxide into organic carbon. However, reduction in consumption has proven to be difficult, and trees and forests fix carbon efficiently only when they are in active growth, i.e. during their juvenile phase. When trees die, organic carbon is converted back to carbon dioxide through the normal processes of decay.

The conversion of wood to charcoal fixes carbon more permanently and the use of such carbon as a horticultural medium kills two birds with one stone. Horticultural carbon acts as a carbon store but instead of being just a passive store, its use as a high performance horticultural medium helps to solve the other global problem, of increasing food production in the world. On our roof top garden the average use of horticultural carbon is 1 tonne (equivalent to a volume of 2 m^3) to cover 6 m^2 of floor area. Our manufacturer of horticultural carbon is yoltan@tm.net.my.

REFERENCES

1. Holttum R.E. (1953) *Gardening in the Lowlands of Malaya*. Straits Times Press, Singapore.
2. Ng F.S.P. (2006) *Tropical Horticulture and Gardening*. Clearwater Publications, Kuala Lumpur.

pass land based brackish water and sea water system. *Aquacult. Eng.* **9:** 1-21.

3. Metcalfe M.R. (1995). Investing in aquacultural wastewater techniques for improved water quality: a coastal community case study. *Coast. Manage.* **23:** 327-335.
4. Thouvenot A., Richardot M., Debroas D. and Devaux J. (1999). Bacterivory of metazooplankton, ciliates and flagellates in a newly flooded reservoir. *J. Plankton Res.* **21:** 1659-1679.
5. Jhingran V.G. (1991). *Fish and Fisheries of India.* Hindustan Pub. Corp., New Delhi, India.
6. Cauchie H.M., Hoffmann L., Jasper-Versali M.F., Salvia M. and Thomé J.P. (1995). *Daphnia magna* Straus living in an aerated sewage lagoon as a source of chitin: ecological aspects. *Belgian J. Zoology* **125:** 67-78.
7. Balasubramaniam P.R. and Kasturi Bai R. (1994). Utilization of an aerobically digested cattle dung slurry for the culture of zooplankton, *Daphnia similis* Claus (Crustacea: Cladocera). *Asian Fish. Sci.* **7:** 67-76.
8. Roche K.F. (1995). Growth of the rotifer *Brachionus calyciflorus* Pallas in dairy waste stabilization ponds. *Water Res.* **29:** 2255-2260.
9. Golder D., Rana S., Sarkar (Paria) D. and Jana B.B. (2007). Human urine is an excellent liquid waste for the culture of fish food organism, *Moina micrura. Eco. Eng.* **30:** 326-332.
10. Alam M.J., Ang K.J. and Cheah S.H. (1993). Use of *Moina micrura* (Kurz) as an *Artemia* substitute in the production of *Macrobrachium rosenbergii* (de Man) post-larvae. *Aquaculture* **109:** 337-349.
11. He Z.H., Qin J.G., Wang Y., Jiang H. and Wen Z. (2001). Biology of *Moina mongolica* (Moinidae, Cladocera) and perspective as live food for marine fish larvae: review. *Hydrobiologia* **457:** 25-37.
12. Sorgeloos P. and Lavens P. (1996). *Manual on the production and use of live food for aquaculture. FAO Fisheries Technical Paper 361.* Laboratory of Aquaculture and *Artemia* Reference Center, University of Ghent, Belgium.
13. Tamaru C.S., Lee C.S. and Ako H. (1991). Improving the larval rearing of striped mullet (*Mugil cephalus*) by manipulating quantity and quality of the rotifer, *Branchionus plicatilis*. In Fulks W. and Main K.L. (eds) *Rotifer and Microalgae Culture System* pp 89-103. Honolulu, Hawaii: Proceedings of a U.S.-Asia Workshop.
14. Nigawaba C., Nalubega M., Vinnerås B., Sundberg C. and Jönsson H. (2008). Bench-scale composting of source-separated human faeces for sanitation. *Waste Manage.* **29:** 585-589.
15. Sáenz Y., Zarazaga M., Briñas L., Lantero M., Larrea F.R. and Torres C. (2001). Antibiotic resistance in *Escherichia coli* isolates obtained from animals, foods and humans in Spain. *Int. J. Antimicrob. Agents* **18:** 353-358.
16. American Public Health Association (APHA) (1985). *Standard methods for the examination of water and wastewater*, 16th Ed. American Public Health Association, Washington, USA.
17. Chuah T.S., Loh J.Y. and Hii Y.S. (2007). Acute and chronic effects of the insecticide-endosulfan on freshwater cladoceran, *Moina macrocopa* Straus. *Bull. Environ. Contam. Toxicol.* **79:** 557-561.
18. Krebs D.J. (1985). *The Experimental Analysis of Distribution and Abundance.* Harper and Row, New York, USA.
19. Nandini S. and Sarma S.S.S. (2000). Lifetable demography of four cladoceran species in relation to algal food (*Chlorella vulgaris*) density. *Hydrobiologia* **435:** 117-126.
20. Rodolfo F.V. and Edmundo M.E. (1980). Preliminary studies on *Moina* sp. production in freshwater tanks. *Aquaculture* **21:** 93-96.
21. Rottmann R.W., Graves J.S., Watson C. and Yanong R.P.E. (1992). Culture techniques of *Moina*: the ideal *Daphnia* for feeding to freshwater fish fry. Institute of Food and Agricultural Sciences. University of Florida, IFAS Extension Circular 1054.
22. Burns C.W. (1968). The relationship between body sizes of filter feeding Cladocerans and the maximum size of particle ingested. *Limnol. Oceanogr.* **13:** 675-678.
23. Dodson S.I. and Frey D.G. (2000). Cladocera and other Branchiopoda. *In* Thorp J.H. and Covich A.P. (eds) *Ecology and Classification of North America Freshwater Invertebrates* pp 850-914. Academic Press, San Diego, USA.
24. Schneider O., Sereti V., Eding E. and Verreth J.A.J. (2007). Heterotrophic bacterial production on solid fish waste: TAN and nitrate as nitrogen source under practical RAS conditions. *Bioresource Technol.* **98:** 1924-1930.
25. Kim D., Kim T.S., Ryu H.D. and Lee S.I. (2008). Treatment of low carbon-to-nitrogen wastewater using two-stage sequencing batch reactor with independent nitrification. *Process Biochem.* **43:** 406-413.
26. Hakanson L., Ervik A., Makinen T. and Moller B. (1988). *Basic concepts concerning assessments of environmental effects of marine fish farms.* Nordic Council of Ministers, Copenhagen.
27. Lechevallier M.W., Schulz W. and Lee R.G. (1991). Bacterial nutrients in drinking-water. *Appl. Environ. Microbiol.* **57:** 857-862.
28. Langis R., Proulx D., Noüe D.J. and Couture P. (1988). Effects of a bacterial biofilm on intensive *Daphnia* culture. *Aquacult. Eng.* **7:** 21-38.